UNIVERSIDADE DE SÃO PAULO
INSTITUTO DE GEOCIÊNCIAS

Petrological and volcanological insights into acid lavas from the Paraná-Etendeka Magmatic Province on the surroundings of Guarapuava city, Paraná, Southern Brazil: A contribution of detailed textural characterization combined with *in situ* Sr isotopes in plagioclase phenocrysts

PEDRO GERALDI ANGELINI

Orientadora: Profª. Drª. Adriana Alves

Dissertação de Mestrado

Nº 799

COMISSÃO JULGADORA

Drª. Adriana Alves

Drª. Liza Angélica Polo

Dr. Antonio José Ranalli Nardy

SÃO PAULO
2018

Serviço de Biblioteca e Documentação do IGc/USP
Ficha catalográfica gerada automaticamente com dados fornecidos pelo(a) autor(a)
via programa desenvolvido pela Seção Técnica de Informática do ICMC/USP

Bibliotecários responsáveis pela estrutura de catalogação da publicação:
Sonia Regina Yole Guerra - CRB-8/4208 | Anderson de Santana - CRB-8/6658

Angelini, Pedro Geraldi
Petrological and volcanological insights into acid lavas from the Paraná-Etendeka Magmatic Province on the surroundings of Guarapuava city, Paraná, Southern Brazil: a contribution of detailed textural characterization combined with in situ Sr isotopes in plagioclase phenocrysts / Pedro Geraldi Angelini; orientador Adriana Alves. -- São Paulo, 2018.
88 p.

Dissertação (Mestrado - Programa de Pós-Graduação em Mineralogia e Petrologia) -- Instituto de Geociências, Universidade de São Paulo, 2018.

1. Vulcanologia. 2. Província magmática do Paraná. 3. Magmatismo ácido. 4. Rochas Chapecó. 5. Guarapuava. I. Alves, Adriana, orient. II. Título.

UNIVERSIDADE DE SÃO PAULO
INSTITUTO DE GEOCIÊNCIAS

Petrological and volcanological insights into acid lavas from the Paraná-Etendeka Magmatic Province on the surroundings of Guarapuava city, Paraná, Southern Brazil: A contribution of detailed textural characterization combined with *in situ* Sr isotopes in plagioclase phenocrysts

PEDRO GERALDI ANGELINI

Orientadora: Profª. Drª. Adriana Alves

Dissertação de Mestrado

Programa de Pós-Graduação em Mineralogia e Petrologia

SÃO PAULO
2018

RESUMO

Nos entornos da cidade de Guarapuava (Paraná, Brasil) afloram rochas vulcânicas ácidas do tipo Chapecó associadas ao magmatismo Eocretáceo da Formação Serra Geral. Tais rochas formam extensos corpos tabulares com dezenas de metros de espessura, sobrepondo-se aos derrames basálticos correlatos. Classificam-se como traquidacitos pobres em sílica (63-66% SiO_2). A textura porfirítica caracteriza-se por 10 - 20% de macrocristais de plagioclásio, piroxênio (augita, principalmente) e óxidos de Fe-Ti, em ordem decrescente de abundância; imersos em uma matriz microgranular a afanítica. Em escala de afloramento, os traquidacitos possuem um padrão zebrado, alternando bandas sinuosas claras e escuras dispostas de maneira sub-horizontal. Vesículas e amídalas, apesar de pouco abundantes, são recorrentes. Macrocristais de plagioclásio foram amplamente investigados do ponto de vista petrográfico e isotópico. Tais cristais caracterizam-se por hábitos tabulares euedrais atingindo comprimentos de até 2 cm. Menos comuns, mas presentes, são agregados deste mineral com piroxênio e óxidos de Fe-Ti, definindo textura glomeroporfirítica. Neste caso, o plagioclásio ocorre em menores tamanhos, com formas irregulares e contatos interdigitados. Independente da associação petrográfica, o plagioclásio é predominantemente homogêneo, com ausência de zoneamentos. Imagens de catodoluminescência e microscopia eletrônica de varredura em matriz de traquidacito revelaram que esta é composta por dois domínios petrograficamente distintos; um contínuo e maciço caracterizado por um fino intercrescimento de sanidina e quartzo, e outro irregular e esburacado dominado apenas por sanidina. As bandas escuras observadas nos respectivos afloramentos são enriquecidas no primeiro, enquanto as bandas claras são relativamente empobrecidas neste e dominadas pelo segundo tipo. Todas amostras apresentaram curvas *crystal size distribution* (CSD) côncavas para cima, possibilitando sua subdivisão em fenocristais (> 3mm) e microfenocristais (< 3mm). Tal divisão guarda relação com o período de residência e ambiente de cristalização, estimados da ordem de 40 anos em câmara magmática profunda (taxa de crescimento de 10^{-9} $mm.s^{-1}$), e 2 anos durante ascensão e erupção (taxa de crescimento de 10^{-8} $mm.s^{-1}$), respectivamente. Assinaturas de isótopos de Sr em plagioclásio revelam sutis flutuações intra e intercristalinas das razões de $^{87}Sr/^{86}Sr$, com média de 0.70566 ± 0.00004 (2σ). Tais razões de $^{87}Sr/^{86}Sr$ em plagioclásio sobrepõem-se às de rocha total, condizente com uma cristalização em equilíbrio e sua classificação como fenocristais *sensu stricto*. As altas temperaturas dos magmas traquidacíticos (~1000°C) associadas aos cristais sinuosos de plagioclásio nos agregados e às curvas CSD côncavas para cima indicam relevante ação de *coarsening* durante estágio de câmara magmática. A limitada variação de isótopos de Sr obtida em plagioclásio sugere sua cristalização em uma câmara magmática com contínua injeção de magmas cogenéticos capazes de interagir e homogeneizar todo o ambiente. Tais eventos de injeção magmática causaram

rompimento e remobilização de partes das paredes da câmara, redistribuindo os fragmentos cumuláticos, posteriormente preservados como os agregados (*clusters*). Tal magma ascendeu pela crosta com 10-15% de cristalinidade. As baixíssimas quantidades de água dissolvidas (<1.5% H_2O) foram exsolvidas apenas em profundidades muito rasas até a superfície. Tal exsolução magmática ocorreu de maneira heterogênea, gerando zonas discretas com reologias e propriedades diferentes numa escala centimétrica. Fraturas sub-horizontais finamente espaçadas condicionadas pela direção do fluxo e pelo padrão de resfriamento possibilitaram o escape de tais fluidos, que teriam interagido seletivamente com as porções imediatamente próximas, gerando as diferentes cores observadas nos afloramentos bandados. Relações estratigráficas, ausência de texturas/estruturas piroclásticas, imponente presença de cristais euedrais de plagioclásio e homogeneidade isotópica associadas às baixas concentrações de água e altas temperaturas magmáticas refutam uma origem piroclástica para tais depósitos. Sugere-se um modelo eruptivo predominantemente efusivo na forma de extensos derrames de lavas ácidas a partir de condutos na região de Guarapuava.

ABSTRACT

Acid volcanic rocks of Chapecó affinity crops out on the surroundings of Guarapuava city (Paraná, Brazil) associated with the Eocretaceous magmatism of the Serra Geral Formation. Such rocks constitute extensive tabular deposits up to tens of meters thick, resting directly above the correlate basaltic flows. They classify as low-silica trachydacites (63-66% SiO_2). Their porphyritic texture is characterized by 10-20% of macrocrysts of plagioclase, pyroxene (augite, chiefly) and Fe-Ti oxides, in decreasing order of abundance; these are set in a microgranular fine to aphanytic groundmass. Trachydacite outcrops show a zebra-like pattern characterized by a rhythmic alternation of sub-horizontal light and dark bands in a sub-horizontal fashion. Vesicles and amygdales, although rare, are ubiquitous in these outcrops. Plagioclase macrocrysts were thoroughly investigated via petrography and isotopy. Crystals typically exhibit tabular euhedral habits up to 2 cm long. Less frequent, but ubiquitous, are clusters composed of plagioclase + pyroxene ± Fe-Ti oxides, that define a glomeroporphyritic texture. In this case, plagioclase is smaller and show irregular, interfingered contacts. Regardless of the petrographic association, the plagioclase is predominantly unzoned. Cathodoluminescence and scanning electron microscopy reveal the trachydacite groundmass to be composed of two petrographically distinct domains; one massive and continuous composed of a fine intergrowth of sanidine and quartz, and another one irregular and porous dominated only by sanidine. The dark bands observed on the respective outcrops are enriched in the former, whereas the light bands are relatively depleted in this and dominated by the latter type. All samples show concave-up crystal size distribution (CSD) curves, allowing sub-division in two groups: phenocrysts (> 3mm) and microphenocrysts (< 3mm). Such division bears relation with residence times and crystallization environment, estimated about 40 years in a deep-seated magmatic chamber (growth rate of 10^{-9} mm.s^{-1}) and 2 years during ascent and eruption (growth rate of 10^{-8} mm.s^{-1}), respectively. Plagioclase Sr isotopes signatures reveal subtle intra and intercrystalline fluctuations in $^{87}Sr/^{86}Sr$ ratios with a mean value of 0.70566 ± 0.00004 (2σ). These signatures overlap with the whole-rock Sr isotopes, implying equilibrium crystallization and their classification as phenocrysts *sensu stricto*. The high magmatic temperatures of trachydacite magmas (~1000°C) associated with the irregular plagioclase crystals in the clusters and the concave-up CSD curves indicate the importance of coarsening during the magmatic chamber stage. The restricted variation of Sr isotopes obtained in plagioclase suggest their crystallization in a magmatic chamber protractedly supplied by cogenetic magmas capable to interact and homogenize the entire environment. These injection events promoted disruption and remobilization of parts of the chamber walls, redistributing the observed cumulate fragments that form the glomerocrysts. The magmas ascended through the crust bearing 10-15% crystallinity. The very

low water contents dissolved (< 1.5% H_2O) were exsolved in very shallow depths up to the surface. Such exsolution was heterogeneous through the magma, generating discrete zones with different rheology and properties up to the centimeter scale. Finely spaced sub-horizontal fractures enabled the exsolved fluids to escape and these would have interacted selectively with the immediately adjacent portions, generating the different colors observed on the banded outcrops. Stratigraphic relationships together with the lack of pyroclastic textures/structures, ubiquitous presence of euhedral plagioclase crystals and isotopic homogeneity associated with the low water contents and high magmatic temperatures refutes a pyroclastic origin for such deposits. Otherwise, it is suggested a mainly effusive eruption style as vast acid lava flows fed by discrete conduits on the neighborhoods of Guarapuava.

AGRADECIMENTOS

Ninguém conquista nada e nem chega a lugar algum sozinho. A caminhada deste mestrado não foi diferente. Ele só foi possível graças a pessoas muito especiais que tenho a sorte de ter em minha vida e que mesmo diante dos momentos de desânimo, da falta de perspectiva, da grave crise financeira e política que o Brasil atravessa, nunca me deixaram pra baixo. Este trabalho é dedicado aos meus pais, Pedro e Nair. Muito obrigado por tudo. Ao meu irmão Bruno, ao meu avô Fabiano e meu tio Binho que na maior parte do tempo estiveram distantes fisicamente, mas sempre me apoiaram e torceram muito por mim. Também gostaria de ressaltar o quanto toda minha família que está espalhada em São Paulo, Ribeirão Preto e Varginha foi importante durante esta etapa. Tia Lívia, Tio Beto, Edi, Isadora, Sofia, Mariangela, tia Verinha, Deja, tia Gilda, Fernando, Lucas, Léo, Gerusa, vocês são incríveis. Gostaria de agradecer especialmente a uma pessoa que se foi tragicamente há não muito tempo, o Zé de Varginha. Sua partida foi triste e dolorosa, mas tenho certeza que seu neto, José, nasceu para trazer toda a felicidade que a família Avelar merece. Por fim, gostaria de agradecer a uma pessoa que conheci pouco antes de ingressar no mestrado e que me acompanhou de perto e sempre me ajudou em todos os momentos. Hoje simplesmente não me vejo sem você, minha namorada, Thaiz.

Este mestrado foi financiado e viabilizado pelo projeto temático 2012/06082-6 da FAPESP. Além, agradeço à CAPES pela bolsa de mestrado concedida pelo período de 2 anos.

Agradeço a minha orientadora, Adriana Alves. Desde o começo, quando ainda não nos conhecíamos muito bem, foi muito receptiva, propôs uma nova temática de mestrado, me proporcionou um intercâmbio acadêmico no Canadá e me fez evoluir como geólogo e pesquisador. Obrigado pela paciência, dedicação e pelas dicas valiosas. Agradeço também aos demais mestres da geologia que me acompanharam nesta jornada. Que honra conviver e fazer trabalho de campo com os professores Fábio Dias e Gergely Szabó. Vocês foram fundamentais. À amiga (quase) geóloga Ana Paula que nos acompanhou em um dos trabalhos de campo, obrigado. Vale prezar a enorme colaboração do professor Archanjo que, durante o período de licença da Adriana, me ajudou enormemente com a CSD, sempre com muito boa vontade. Este trabalho também só foi possível graças aos funcionários e funcionárias do IGc - USP, especialmente o Samuca, Paulo e Renato (seção de laminação), Zé Paulo, Vinícius e Jordana. Além, vale destacar a constante disposição dos professores Patrício, Valdecir, Rogério e Excelso, e a grande ajuda da colega Maria Isabel. Apesar de rápida, minha passagem por Chicoutimi (Canadá) foi bastante proveitosa. O professor Michael Higgins e sua esposa, Judith, foram extremamente acolhedores e educados. Eduardo e Carlos, os brasileiros da UQAC que me receberam assim que cheguei, muito obrigado. E, por fim, Christiane -a

vovó de Chicoutimi- que me abrigou em sua casa e, apesar das dificuldades de comunicação, nos tornamos bons amigos e tivemos uma ótima convivência.

Por último, mas não menos importantes, este parágrafo é dedicado a todos meus amigos e amigas. Ano passado tive a honra de ser padrinho de dois casamentos, Juliana e Leandro e Lucas (Shun-Lee) e Asdra, sou muito grato pelo convite e mais uma vez desejo toda felicidade do mundo aos casais. Contem comigo pra tudo. Pra variar, amigos da Geologia, Santandreia F. R., vocês tornam tudo mais fácil e divertido, mesmo depois de quase 10 anos estamos firmes e fortes. Aliás, esse ano tem Cambury edição especial. Grandes amigos do Ofélia: Pará, Alê, Waldyr, Nico, Trick, Du, Caio, André, Secolin, Lucão, Pizzo, Flávio, Sylvio, valeu por tudo, é bom demais ter vocês como amigos. E, por fim, agradeço ao time de basquete da Geologia - USP. Que incrível descobrir um novo esporte depois de velho e aprender com alguns dos melhores jogadores da USP, muito obrigado e rumo ao tetra do BIFE.

Tenho certeza que estou saindo deste mestrado uma pessoa melhor, um pesquisador mais crítico e um geólogo mais completo que quando entrei. Valeu a pena.

INDEX

CONTINENTAL FLOOD BASALTS: A BRIEF REVIEW AND INSIGHTS INTO THE PARANÁ-ETENDEKA MAGMATIC PROVINCE

Since the seminal papers of Wilson (1963, 1965) about ocean island chains and plate movements, a great effort has been demanded on hot-spots. Morgan (1972) suggested that hot-spots are surface expressions of deep mantle plumes; hot upwelling solid material ascending through the mantle that remain relatively stationary whilst tectonic plates ride over and are stippled by volcanic islands and forming a track along its path, the Hawaiian islands the most conspicuous example. The same author warned about the apparent link between giant basaltic provinces on continents with the opening of ocean basins. Later, White & Mckenzie (1989) proposed that the volcanism on rift zones is triggered by a combination of temperature rise and decompression in the upper mantle induced by plumes. This rift-related volcanism is potentially preserved along passive margins following continental breakup and ocean opening. In the same year, Richards et al. (1989) assigned the earliest basaltic volcanism over continental hot-spots to the melting of a plume "head" which is eventually followed by the opening of an ocean basin, with a continuing magmatism tracking linear and symmetric submarine chains on both sides of the new tectonic plates by the melting of a plume "tail". Despite the lack of compulsory of continental breakup, it normally follows basaltic floods being a natural consequence of the plume influence. This seeming connection between plumes, volcanism and continental splitting was further endorsed (e.g. Hill; 1991; White & Mckenzie, 1995; Courtillot et al., 1999). Noting the worldwide occurrence of huge basaltic provinces of different ages, Coffin & Eldholm (1992, 1993,1994) proposed the collective term Large Igneous Provinces (LIP) to describe very intense and short-lived volcanic events not related to subduction zones. A more strict definition of LIP was suggested by Bryan & Ernst (2008) as giant intraplate magma volumes (>0.1 MKm^3), mostly basaltic, erupted in geological short time intervals < 50 m.y., usually much less. Continental Flood Basalts (CFB) and Ocean Plateaus are the equivalents of LIPs on continental and oceanic crust, respectively.

There are many well-preserved CFBs around the world, chiefly the Mesozoic ones. The breaking of Gondwana and opening of the South Atlantic Ocean in the Early Cretaceous is linked with one of the largest CFBs preserved in the world, widespread on South America and, to a lesser extent, on the African counterpart, in Namibia (Bryan et al. 2010). Once continuous, this CFB is known as the Paraná-Etendeka Magmatic Province (PEMP) (Peate, 1997). Both sides of the PEMP seem to have a bathymetric continuity into the ocean by linear and symmetric submarine chains in latitudes between 25° and 35°S, the Walvis Ridge on the African Plate and the Rio Grande Rise on the South American Plate; which come together on the active volcanic island of Tristan da Cunha, located close to the South Atlantic mid-ocean ridge. The clear progressive aging of the respective chains away from Tristan da Cunha island (e.g. O'Connor et al., 2012; O'Connor & Jokat, 2015; Rohde et al., 2013),

meeting the ages of the continental PEMP (e.g. Renne et al., 1992, 1996; Thiede & Vasconcelos, 2010), enables us to trace back the plates configurations and infer similarities in the magmatic history for both on- and off-land volcanism. A reasonable assumption is the presence of a major mantle plume beneath the Tristan da Cunha Island responsible for the onset of the PEMP magmatism on continents and followed by the ocean floors (O'Connor & Duncan, 1990; Hawkesworth et al., 1992). Recent upper mantle tomography confirms the existence of a plume beneath Tristan da Cunha Island, but the shallow depths of the low velocity zone, with a main conduit extending about 250 Km and branching downwards, puts doubt on the deep-seated origin of the plume, otherwise indicating that it is dying out (Schlomer et al., 2017).

In this context, it is discussed the genesis and relative contributions of potential distinct sources to the PEMP. Gibson (1995; 1999; 2005) and Ewart et al. (1998) suggested that the PEMP basalts reflect a main deep asthenospheric source, the Tristan da Cunha plume in the case. However, Hawkesworth et al. (1988), Peate et al. (1999), Marques (1999) proposes the PEMP basalts are products of heterogeneous melts with a substantial sub-continental lithospheric mantle (SCLM) contribution. Combining geoid and seismic tomography data, Ernesto et al. (2002) advocated for a non-plume model related to the PEMP magmatism. Rocha-Júnior et al. (2012) showed that the exclusive melting of either asthenosphere or SCLM cannot satisfactorily explain the overall geochemical and isotopic features of the PEMP. Using Re-Os isotopy combined with highly siderophile elements, the latter authors attributed the PEMP generation to the partial melting of a metassomatized asthenosphere followed by variable mixing with enriched mantle portions, probably in the SCLM. In this model, the regionally distinct basalts in the PEMP are products of different amounts of mixing with these enriched mantle components. The same authors points to notable isotopic differences between the PEMP basalts and ocean islands along the Tristan da Cunha track, indicating a minor role of the plume. Recent geophysical investigation points to a high-density lithosphere underlying the PMP, attributed to a highly altered and fertile lithosphere (Chaves et al., 2016).

REFERENCES

BRYAN, S. E.; ERNST, R. E. Revised definition of Large Igneous Provinces (LIPs). **Earth-Science Reviews**, v. 86, n. 1–4, p. 175–202, 2008.

BRYAN, S. E.; PEATE, I. U.; PEATE, D. W.; SELF, S.; JERRAM, D. A.; MAWBY, M.R.; MARSH, J. S.; MILLER, J. A. The largest volcanic eruption on earth. **Earth-Science Reviews**, v. 102, p. 207-229, 2010.

CHAVES, C.; USSAMI, N.; RITSEMA, J. Density and P-wave velocity structure beneath the Parana Magmatic Province: Refertilization of an ancient lithospheric mantle. **Geochemistry Geophysics Geosystems**, v. 17, p. 2825–2834, 2016.

COFFIN, M. F. & ELDHOLM, O. Volcanism and continental break-up: a global compilation of large igneous provinces. **Geological Society, London, Special Publications**, v. 68, n. 1, p. 17–30, 1992.

COFFIN, M. F. & ELDHOM, O. Scratching the surface: Estimating dimensions of Large Igneous Provinces. **Geology**, v. 21, n. 6, p. 515-518, 1993.

COFFIN, M. F. & ELDHOM, O. Large Igneous Provinces: Crustal structure, dimensions, and external consequences. **Reviews of Geophysics**, v. 32, n. 1, p. 1-36, 1994.

COURTILLOT, V.; JAUPAT, C.; MANIGHETTI, P.; TAPPONIER, P.; BESSE, J. On causal links between flood basalts and continental breakup. **Earth and Planetary Science Letters**, v. 166, n. 3–4, p. 177–195, 1999.

ERNESTO, M.; MARQUES, L. S.; PICCIRILLO E. M.; MOLINA, E. C.; USSAMI, N.; COMIN-CHIARAMONTI, P.; BELLIENI, G. Paraná Magmatic Province-Tristan da Cunha plume system: Fixed versus mobile plume, petrogenetic considerations and alternative heat sources. **Journal of Volcanology and Geothermal Research**, v. 118, n. 1–2, p. 15–36, 2002.

EWART, A.; MILNER, S. C.; ARMSTRONG, R. A.. DUNCAN, A.R. Etendeka volcanism on te Gobboseb mountains and Messum igneous complex, Namibia, part I: Geochemical evidence of early Cretaceous Tristan plume melts and the role of crustal contamination in the Paraná-Etendeka CFB. **Journal of Petrology**, v.39, n.2, p. 191-225. 1998.

GIBSON, S. A.; THOMPSON, R. N.; LEONARDOS, O. H.; DICKIN, A. P.; MITCHELL, J. G. The late Cretaceous impact of the Trindade mantle plume: Evidence from large volume, mafic, potassic magmatism in SE Brazil. **Journal of Petrology**, v. 36, n. 1, p. 189-229. 1995.

GIBSON, S. A.; THOMPSON, R. N.; LEONARDOS, O. H.; DICKIN, A. P.; MITCHELL, J. G. The limited extent of plume-lithosphere interactions during continental flood-basalt genesis: geochemical evidence from Cretaceous magmatism in southern Brazil. **Contributions to Mineralogy and Petrology**, v. 137, p. 147-169. 1999.

GIBSON, S. A.; THOMPSON, R. N.; DAY, J. A.; HUMPHRIS, S. E.; DICKIN, A. P. Melt-generation processes associated with the Tristan mantle plume: Constraints on the origin of EM-1. **Earth and Planetary Science Letters,** v. 237, p. 744-767. 2005.

HAWKESWORTH, C. J.; MANTOVANI, M.; PEATE, D. Lithosphere remobilization during Paraná CFB magmatism. **Journal of Petrology**, Special Lithosphere Edition, issue 1, p. 205-223. 1988.

HILL, R. I. Starting plumes and continental break-up. **Earth and Planetary Science Letters**, v. 104, n. 2–4, p. 398–416, 1991.

MARQUES, L. S.; DUPRÉ, B.; PICCIRILLO, E. M. Mantle source compositions of the Parana Magmatic Province (southern Brazil): Evidence from trace element and Sr-Nd-Pb isotope geochemistry. **Journal of Geodynamics**, v. 28, n. 4–5, p. 439–458, 1999.

MORGAN, W. J. Deep Mantle Convection Plumes and Plate Motions. **The American Association of Petroleum Geologists Bulletin**, v. 56, n. 2, 1972.

O'CONNOR, J. M.; DUNCAN, R. A. Evolution of the Walvis Ridge-Rio Grande Rise Hot Spot System: Implications for African and South American Plate motions over plumes. **Journal of Geophysical Research**, v. 95, n. B11, p. 17475, 1990.

O'CONNOR, J. M.; JOKAT, W.; LE ROEX, A. P.; CLASS, C.; WIJBRASN, J. R.; KEBLING, S.; KUIPER, K. F.; NEBEL, O. Hotspot trails in the South Atlantic controlled by plume and plate tectonic processes. **Nature Geoscience**, v. 5, n. 10, p. 735–738, 2012.

O'CONNOR, J. M. & JOKAT, W. Tracking the Tristan-Gough mantle plume using discrete chains of intraplate volcanic centers buried in the Walvis Ridge. **Geology**, v. 43, n. 8, p. 715-718. 2015.

PEATE, D. W. The Parana-Etendeka Province. In: Large Igneous Provinces: continental, oceanic, planetay flood volcanism. Geophysical Monography, 100, American Geophysical Union, 438 p., 1997.

PEATE, D. W.; HAWKESWORTH, C. J.; MANTOVANI, M. M. S.; ROGERS, N. W.; TURNER, S. P. Petrogenesis and stratigraphy of the high-Ti/Y Urubici magma type in the Parana Flood Basalt Province and implications for the nature of "Dupal"-type mantle in the South Atlantic Region. **Journal of Petrology**, v. 40, n. 3, p. 451–473, 1999.

RENNE, P.; ERNESTO, M;, PACCA, I. G; COE, R. S.; GLEN, J. M., PREVÓT, M., PERRIN, M. The age of the Paraná flood volcanism, rifting and Gondwanaland, and the Jurassic-Cretaceous boundary. **Science**, v. 258, p. 975-979, 1992.

RENNE, P. R.; DECKART, K.; ERNESTO, M.; FÉRAUD, G.; PICCIRILLO, E.M. Age of the Ponta Grossa dike swarm (Brazil), and implications to Paraná flood volcanism. **Earth and Planetary Science Letters**, v. 144, n. 1–2, p. 199–211, 1996.

RICHARDS, M. A.; DUNCAN, R. A.; COURTILLOT, V. E. Flood Basalts and Hot-Spot Tracks: Plume Heads and Tails. **Science**, v. 246, n. 4926, p. 103–107, 1989.

ROCHA-JÚNIOR, E. R. V.; PUCHTEL, I. S.; MARQUES, L. S.; WALKER, R. J.; MACHADO, F. B.; NARDY, A. J. R.; BABINSKI, M.; FIGUEIREDO, A. M. G. Re-Os isotope and highly siderophile element systematics of the Paraná continental flood basalts (Brazil). **Earth and Planetary Science Letters**, v. 337–338, p. 164–173, 2012.

ROHDE, J. K.; BOGAARD, P. V. D.; HOERNLE, K.; HAUFF, F.; WERNER, R. Evidence for an age progression along the Tristan-Gough volcanic track for new $^{40}Ar/^{39}Ar$ ages on phenocryst phases. **Tectonophysics**, v. 604, n. 24, p. 60-71.

SCHLÖMER, A.; GEISSLER, W. H.; JOKAT, W.; JEGEN, M. Hunting for the Tristan mantle plume – An upper mantle tomography around the volcanic island of Tristan da Cunha. **Earth and Planetary Science Letters**, v. 462, p. 122–131, 2017.

THIEDE, D. S. & VASCONCELOS, P. M. Paraná flood basalts: Rapid extrusion hypothesis confirmed by new $^{40}Ar/^{39}Ar$ results. **Geology**, v. 38, p. 747-750, 2010.

WHITE, R.; MCKENZIE, D. Magmatism at rift zones: The generation of volcanic continental margins and flood basalts. **Journal of Geophysical Research**, v. 94, n. B6, p. 7685, 1989.

WHITE, R. S.; MCKENZIE, D. Mantle plumes and flood basalts. **Journal of Geophysical Research**, v. 100, n. B9, p. 17,543-17,585, 1995.

WILSON, J. T. A possible origin of the Hawaaian islands. **Canadian Journal of Physics**, v. 41, n. 6, p. 863-870. 1963.

WILSON, J. T. A new class of faults and their bearing on continental drift. **Nature**, v. 207, p. 343-347. 1965.

METHODOLOGY

1 Crystal Size Distribution (CSD)

The CSD theory was initially developed for chemical engineering purposes (Randolph & Larson, 1971) and later adapted for igneous petrology (Marsh,1988). The CSD enables direct assessment of residence timescales of crystallization without the necessity of further sophisticated thermodynamic approaches.

The CSD theory is based on a crystal population balance that relates the change in the number of crystals whilst these nucleate and grow in a liquid environment (Marsh, 1988). This equation reports the change of the number and size of crystals as a function of their respective magmatic residence times and inflow and outflow of the size intervals. Such balance requires a parameter that determines the number of crystals within a specific size range in a particular volume of rock/magma, called *population density* (n; mm^{-4})

According to Cashman & Marsh (1988), in summary, the balance equation of a population of growing crystals in a steady-state system within a specific size range (dL) can be described as:

$$(1) \qquad d(Gn)/dL = -n/\tau$$

where G is the linear growth rate of the crystal ($mm.s^{-1}$) and τ is the residence time (s). Assuming G as constant, equation (1) can be integrated to:

$$(2) \qquad n = n^0 \exp(-L/G\tau)$$

$$(3) \quad \ln(n) = \ln(n^0) - (1/G\tau)\, L$$

In which n^0 is a constant that represents the population density at the moment that crystals size approach zero ($L \rightarrow 0$), or the nucleation density. A diagram relating ln(n) and L of a system following such requirements is shown in Figure 1a.

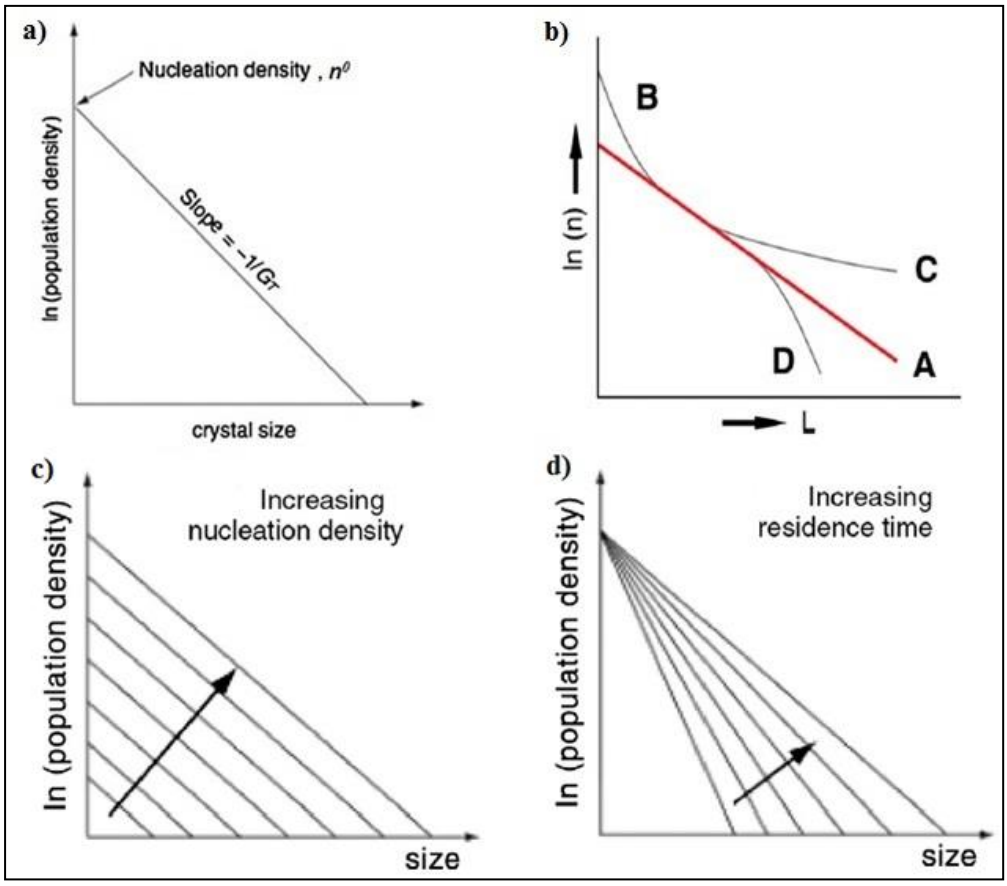

Figure 1. A) Representation of a typical CSD graph. B) Examples of different CSD curves and their respective interpretations. Line a (red): Straight CSD formed by purely kinetic reasons in a steady-state crystallizing igneous system. Line b: Concave-up CSD along the smaller crystal sizes caused by a rapid cooling in the system. Line c: Concave-up CSD along the larger crystal sizes promoted by crystal accumulation. Line d: Concave-down CSD along the smaller crystal sizes induced by crystal removal. C) Keeping the residence time constant the CSDs are displaced parallel by changing their nucleation density. D) Otherwise, keeping the nucleation density constant, the CSD slopes change according to different residence times (the quicker the crystallization interval, the steeper the CSD). Image withdrawn from Higgins (2006).

From Figure 1a we conclude that (1) The slope of the CSD curve is inversely proportional to G$\mathcal{T}$ (2) The intersection of the CSD with the *y* axis is equivalent to the nucleation density, n^0 (L→0).

However, natural CSDs are rather curved than straight (Fig. 1b). Higgins (2006) attributed this to additional mechanical processes (ex: crystal removal and accumulation, compaction, magma mixing, mingling, and others) and kinetic effects (ex: rapid undercooling) operating during and even post-crystallization (ex: coarsening). The participation of these mechanisms that are able to deviate the CSD from the predicted straight line are likely to be recorded by the different shapes of the CSD curves (Fig. 1b). The evaluation of the CSD from a set of samples reveals trends on the nucleation density (Fig. 1c) and residence time (Fig. 1d) and, consequently, on the crystallization pathways.

CSD curves requires the tridimensional knowledge of the crystals sizes. However, this is not an easy task due to the difficulty in isolating the individual crystals from their hosting rocks. This

problem can be circumvented by an indirect approach in which intersection planes (petrographic thin sections, rocks slabs, outcrop surfaces) are investigated to obtain morphological parameters of the crystals (length, area, shape, orientation; Figure 2a). These two-dimensional data are converted to three dimensions via stereology corrections (e.g. Sahagian & Proussevitch, 1998). Other methods also permit assessment of crystal parameters (serial sectioning and tomography, for example), however, stereology is easier, faster, and cheaper than these ones and was preferred for this study.

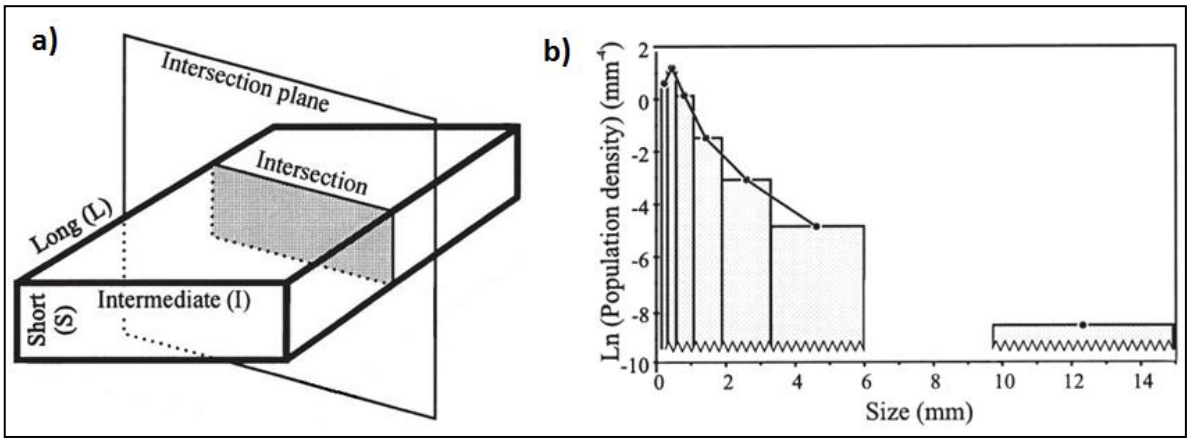

Figure 2. A) Parallelepiped representing a natural crystal. Ideally, the volume of the parallelepiped encloses the crystal. The intersection of this shape with a random plane gives an intersection area (grey area). B) CSD graph displaying the method developed by Higgins (2000) in which the crystals are distributed along specific size ranges (bins) with different widths. The bins are progressively wider in order to compensate the underrepresentation of the larger crystals in bi-dimensional sections. Thus, the CSD graph is a histogram in which the center of the bins are connected by a simple line. Both images were withdrawn from Higgins (2000).

Higgins (2000) developed an algorithm, which performs crystal stereology in natural rocks, *CSDCorrections Program*. The analyzed crystals are approximated to rectangular parallelepipeds with three perpendicular axis, long : intermediate : short (Fig. 2a). This ratio must be defined by empirical observations in the intersection planes and informed to the program for stereological conversion. Crystals are then divided in different size ranges that are progressively wider in order to compensate the underrepresentation of larger crystals in the intersection planes (Fig. 2b). The horizontal axis of the CSD graph, size (mm), refers to the long axis of the bestfit ellipses enclosing the parallelepipeds.

2 Cathodoluminescence

The interaction of a solid phase with a focused beam of electrons promotes ionization of the former and produces a set of products (Pagel et al., 2000): 1) Characteristic X-ray emission from the inner layers of the atoms 2) A continuous radiation 3) High and low energy electron scattering 4) Electrons ejected from the outer layers of the atoms (Auger electrons) and 5) Cathodoluminescence (CL). The CL is characterized by photons with large wavelengths, from the ultraviolet to the visible

spectra and infrared. The latter is activated by a series of trace elements (rare earth elements REE, actinides and transition elements, chiefly) present in specific crystal sites. The excited valence electrons generates a photon with specific wavelength when these return to their original positions. Such phenomenon is observed as different CL colors. These colors are a function of the respective activator element, valence state, and crystal site among others.

In this study, polished thin sections of selected samples were investigated under cold CL. In this method, electrons are produced by applying an electrical charge between two electrodes under low gas pressure (Pagel et al., 2000). The main advantages of the cold CL are the possibility coupling it to an optical microscope and the relatively simple vacuum system, which combined permits the observation of large fields without need of carbon coating. However, the wide electron beam implies an inferior spatial resolution relatively to the hot CL. The cold CL images in this study were obtained at the Université du Québec à Chicoutimi (Canada) under analytical conditions of 10 Kv and electrical current of 185 µÅ.

3 Powder X-ray Diffraction

The X-ray diffraction is a physical phenomenon embracing a series of departures of wave paths after hitting the crystalline structure of solid phases in mono or polycrystalline aggregates. This is possible due to the size equivalency between the X-rays wavelength (0.1 to 100 Å) and the spacing between interatomic planes.

The crystalline structure of any solid (*sensu stricto*) consists of a regular array of atoms that repeat themselves three dimensionally. This array results in atomic planes with different orientations, spacing, and densities (Figure 3a). The atoms promote X-rays scattering, which, in special conditions, will interact constructively and produce a peak of intensity in an X-ray diffraction graph.

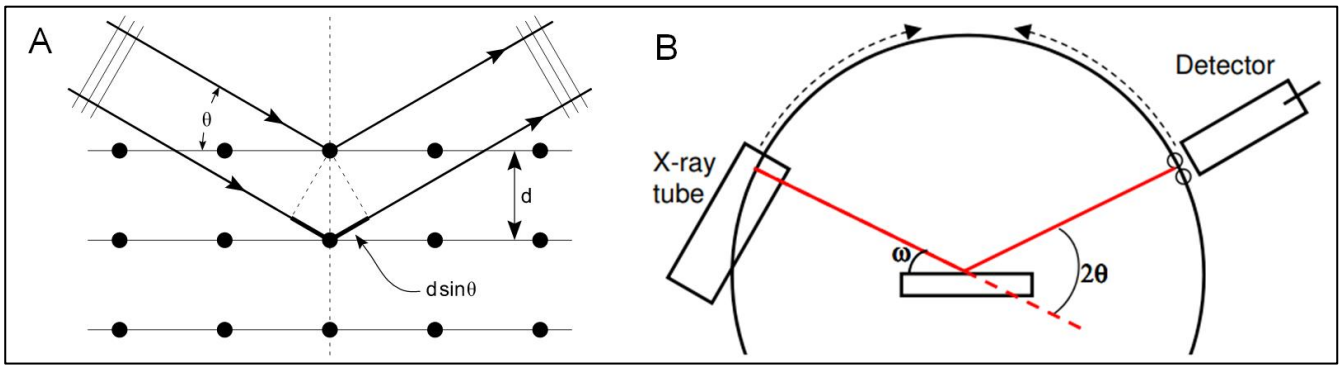

Figure 3. A) Bi-dimensional example of a set of atomic planes (thin straight lines) spaced by *d*. The atoms (black balls) diffract the incident X-rays according the Bragg's law. B) Sketch representing how a typical diffractometer operates.

The geometric relationships between the X-rays incident angle and the spacing of the atomic planes are described by the Bragg's law:

$$(4)\quad n\lambda = 2\,d\,\mathrm{sen}\theta$$

in which *n* is an integer number, λ is the X-ray wavelength, *d* is the spacing between the atomic planes and θ is the incident angle (Figure 3a). The constructive diffraction pattern will only occur in particular incident angles. In polycrystalline aggregates, like rock powder, the sample must be prepared in a way to ensure the random disposition of their particles. Following this premise, for each set of atomic planes, a small but important number of particles will be oriented in an optimal angle favorable to diffract the X-rays and promote a peak intensity. Multiple peaks from the same phase and other ones will be displayed in the same graph and can be overlapped depending on the phases present. The identification of each phase is performed by direct comparison with an X-ray diffraction database (e.g. CIF; Crystallographic Information File) and by considering the geological context and rock composition.

In most cases, the X-rays source is a tube containing a cathode and an anode under vacuum. The electrons emitted by the cathode are accelerated under 30-60 Kv and collide with the anode, producing the X-rays. These leave the tube by a small beryl window. As they hit the sample, the diffracted rays produced by this interaction are captured in the opposite symmetrical detector. This set moves slowly by increasing gradually the incident and diffracted angles (Figure 3b). The rock powders used in the X-ray diffraction analyzes in this study were obtained following the same procedure described in item 1.

4 Laser Ablation Inductively Coupled Plasma Mass Spectrometry (LA-ICP-MS)

Following Sylvester (2008), the LA-ICP-MS is used for *in-situ* elemental and/or isotopic analyzes of minerals and matrices (glass, fine grained groundmass). The technique does not requires powdering on the sample, and permits textural control of the analyzed spots by using standard polished section. The LA-ICP-MS is made of three distinct portions represented in the acronym. The first, *laser ablation* (LA), performs the microsampling of the polished section by a laser beam up to a few hundreds μm in diameter. Once the laser beam hits the sample, the latter is pulverized and transformed into an aerosol composed of very fine particles. This aerosol is transported through a gas, commonly Ar, up to the next stage, the *ion coupled plasma* (ICP), where the aerosol interacts with an extremely hot plasma made by a mixture of Ar and He. The sample is vaporized and converted to ionized atoms. These ions are accelerated to the last part of the equipment, the *mass spectrometer* (MS) that operates under vacuum conditions. Once in the MS, a magnetic field applied to the ions forces them to follow different curved pathways depending on the mass to charge ratio of the deflected ions. A range of voltages can be applied in order to record from the lightest (e.g. Li^+) to the heaviest

(e.g. U^+) ions. The frequency of the ionic impacts (counts per second, cps) on the detectors are translated in electric pulses or potential (voltage) which are recorded in a computer. The absolute contents of the respective elements are obtained by comparing the acquired signals to the ones of an internal standard determined independently. The detector possesses many possible configurations used for different applications. The specific configuration used in this work is described next.

4.1 Multi-Collector

The multi-collector has a configuration that allows simultaneous measurements of several masses. The employed system has 12 Faraday cups and 5 ion counters that can be moved to detect specific isotopes of interest. This was the configuration used to measure the Sr isotopic ratios in the plagioclase crystals. Such analyzes were performed in two stages. One at the Radiogenic Isotope Facility (RIF, University of Alberta, Canada) in 2009 (sample FP-15-15), and another at the MidWest Isotope and Trace Element Research Analytical Center (MITERAC) of the University of Notre Dame in 2017 (samples PA-16-01 and -21). The analyzes at RIF were conducted using a NuPlasma MC-ICP-MS coupled with a Laser Ablation system UP213 under analytical conditions of laser beam diameter of 160 µm and 10 Hz frequency and output energy of approximately 11 J/cm^3. Otherwise, the analyzes at MITERAC were conducted with a NuPlasma II MC-ICP-MS coupled with an Excimer NWR-193 nm LA system, under analytical conditions of laser beam diameter of 150 µm and 10 Hz frequency and output energy of approximately 14 J/cm^3.

5 Scanning Electronic Microscope (SEM)

In this method, the interaction of a geological material with a focused electron beam produces signals that translate into composition, morphology, and topography of the target. The SEM combines such phenomenon with the possibility of investigation under high magnification, which allows identification and imaging of nanometric phases and textures. In this study, SEM analyzes were performed at the Laboratório de Caracterização Tecnológica (LCT - EPUSP) of the Escola Politécnica of the Universidade de São Paulo, using a Quanta 600 FEG (FEI) coupled with an energy dispersive spectrometer (EDS; Quantax, Bruker). Phase association was characterized from backscattered images, EDS and digital mapping by X-rays for major elements (Si, Al, Fe, Mg, Na, K, Ca, Ti, P). The SEM analyzes were conducted in order to investigate the banded structure of the studied acid rocks.

6 References

HIGGINS, M. D. Measurement of crystal size distributions. **American Mineralogist**, v. 85, n. 9, p. 1105–1116, 2000.

HIGGINS, M.D. 2006. Quantitative textural measurements in igneous and metamorphic petrology. Cambridge University Press, 276 pages.

MARSH, B. D. Crystal Size Distribution (CSD) in rocks and the kinetics and dynamics of crystallization. **Contributions to Mineralogy and Petrology**, v. 99(3), p. 277 – 291, 1988.

PAGEL, M.; BARBIN, V.; BLANC, P.; OHNENSTETTER, D. 2000. Cathodoluminescence in Geosciences. Springer, 514 pages.

PECHARSKY, V. K. & ZAVALIJ, P. Y. 2005. Fundamentals of powder diffraction and structural characterization of materials. Springer, 713 pages.

SAHAGIAN, D. L.; PROUSSEVITCH, A. A. 3D particle size distributions from 2D observations: Stereology for natural applications. **Journal of Volcanology and Geothermal Research**, v. 84, n. 3–4, p. 173–196, 1998.

SYLVESTER, P. J. 2008. Laser ablation-ICP-MS in the earth sciences: Current practices and outstanding issues. Mineralogical Association of Canda, 348 pages.

1 INTRODUCTION

Continental Flood Basalts (CFBs) are giant magma volumes (>0.1 MKm^3) erupted in continental environments in geologically short time intervals < 50 m.y., usually much less (Bryan & Ernst, 2008). Although mainly composed by basalts, CFBs commonly have minor contributions of intermediate and acid rocks.

Brazil hosts one of the world's most expressive continental flood basalts (CFB) associated to the breakup of the Gondwana Supercontinent and the opening of the Atlantic Ocean. The Paraná-Etendeka Magmatic Province (PEMP) holds up to 5 x 10^5 km^3 of tholeiitic basalts exposed over an area about 1 million km^2 (Frank et al., 2009). This huge volume of lava is believed to have outpoured to surface in less than 4 M.y. (Renne et al., 1992, 1996, Pinto et al., 2011; Janasi et al., 2011; Thiede and Vasconcelos, 2010; Baksi, 2017), which in geological terms is almost instantaneous.

Knowledge about the province has increased in the last years thanks to systematic studies on the volcanic stratigraphy and eruptive style (Nardy et al., 2002, 2008; Polo et al., 2017; Rossetti et al., 2017). However, several key questions remain unanswered, especially those concerning the time it took for each individual flow to extrude to the surface, the characteristics of the hidden reservoir that fed the volcanic system, and the physical properties and the volatile budget of the magmas that form the PEMP.

The study of crystals might help answering some of these questions, since accurate *in situ* Sr analyzes are now routine in many laboratories (e.g. Davidson et al., 2007; Ramos & Tepley, 2008). Volcanic phenocrysts are archives of the chemical and physical evolution of a magma from the chamber stage through the ascent and eruption moment. Plagioclase, in particular, has gained increased attention due to several reasons: (1) it is present over most of the crystallization interval in typical magmatic systems; (2) it is stable over a wide range of crustal T, P, aH_2O and melt composition; (3) its chemical and isotopic composition might register subtle changes in intensive variables, which might help to elucidate magmatic processes; (4) the very slow coupled diffusion of CaAl-NaSi prevents plagioclase homogenization and favors preservation of distinct An-content zones (Grove et al., 1984); and (5) different shapes and sizes of plagioclase reflect distinct thermal and kinetic regimes operating during crystallization (e.g. Lofgren, 1974; Swanson, 1977; Kirkpatrick, 1979). Thus, plagioclase textural and chemical variations have been widely used to reconstruct chamber dynamics, petrological processes and emplacement style from many volcanic provinces (e.g. Anderson, 1984; Nixon & Pearce, 1987; Singer et al., 1995; Davidson & Tepley, 1997; Tepley et al., 2000; Ginibre et al., 2002; Browne et al., 2006; Humphreys et al., 2006; Ruprecht & Wörner, 2007; Ginibre & Wörner, 2007; Gagnevin et al., 2007; Andrews et al., 2008; Viccaro et al., 2010, 2016; Giacomini et al., 2014; Shane, 2015; Coote & Shane, 2016).

The crystal size distribution (CSD) theory provides support to evaluate how igneous textures evolve and allow quantification of magmatic residence timescales (Randolph & Larson, 1971;

Cashman & Marsh, 1988). The combination of plagioclase chemical and isotopic data with CSD results has been proved to be a successful approach to unravel petrological processes (e.g. Piochi et al., 2005; McCanta et al., 2007; Morgan et al., 2007; Salisbury et al., 2008; Fornaciai et al., 2015; Flaherty et al., 2018).

In this work, we investigate some acid volcanic rocks of the PEMP on the surroundings of the Guarapuava city, Paraná State, southern Brazil. These rocks present a tabular geometry up to tens of kilometers wide and a high silica content, which together foment a controversial debate about their origin and emplacement style; lava *vs* ignimbrite (Bellieni et al., 1986; Garland et al., 1995; Polo et al., 2017; Luchetti et al., 2018a, b). We combined cold-stage cathodoluminescence and scanning electron microprobe to select plagioclase crystal zones for the conduction of *in situ* Sr isotopes analyzes, which combined with CSD studies allowed placing time constraints to the identified magmatic processes. We compare the results with the data in the literature and, finally, propose some petrological insights to the emplacement style for the Guarapuava Acid Volcanics (GAV) rocks and their bearing on the evolution of the acid magmatism of the PEMP.

2 GEOLOGICAL BACKGROUND

The breaking of the Gondwana Supercontinent and opening of the South Atlantic Ocean in the Early Cretaceous was marked by a colossal magmatic event preserved as one of the world's largest Continental Flood Basalts (CFB) known as Paraná-Etendeka Magmatic Province (PEMP). Most of the volume of the PEMP outcrops in South America (Fig. 1), with minor amounts preserved on the African counterpart, in Namibia (Hawkesworth et al., 1992; Bryan et al. 2010).

On Brazil, the volcanic rocks of the PEMP occur as shallow intrusions and flows on the top of the Phanerozoic sediments of the Paraná Basin. The flows cover ~ 1 x 10^6 Km^2 and have thicknesses varying from tens of meters up to a kilometer (Frank et al., 2009). Dyke swarms and small alkaline intrusions associated in the nearby Pre-Cambrian basement are ubiquitous but much less abundant (Comin-Chiaramonti & Gomes, 2005). Accurate Ar^{40}/Ar^{39} dating of fresh plagioclase crystals and U-Pb dating of zircon (Pinto et al., 2011) and baddeleyite (Janasi te al., 2011) crystals separated from acid rocks indicate that the whole province formed in a time span of 3 to 5 M.y. in the Early Cretaceous around 135 M.y. (Renne et al. 1992, 1996; Thiede & Vasconcelos, 2010; Baksi, 2017).

The basalts represent over 90% of the lava volume and occur as flows and shallow intrusions (dykes and sills) reaching up 1500 m in the thickest portions (Frank et al., 2009). Intermediate rocks correspond to around 7% of the province, whereas silicic lavas represent less than 2.5% of the total PMP volume; albeit volumetrically less important, their volume overcomes what is commonly associated to CFBs worldwide (Nardy et al., 2002; Bryan et al., 2010). The tholeiitic magmatism is regionally distinctive in geochemistry, with high titanium basalts (HTiB) prevailing to the north, whereas low titanium basalts (LTiB) occur chiefly at the south of the PEMP. These were subsequently divided in other subtypes based on isotopic and trace element signatures (Peate et al., 1992; Peate, 1997; Nardy et al., 2002; Polo & Janasi, 2014) and are shown in Table 1.

The acid volcanics occurs as isolated plateaus restricted to the eastern edge of the Paraná sedimentary basin along the 25 - 35°S latitudes (Fig. 1). Based on textural and compositional contrasts, the acid rocks are divided in two major groups: Palmas, which comprises microporphyritic to aphyric, low-Ti dacites and rhyolites, and Chapecó, which is composed of porphyritic, high-Ti trachydacites and dacites. Both types were further subdivided into minor types on the basis of their isotopic and trace element signatures (Table 1; Peate et al., 1992; Peate, 1997; Garland et al., 1995 Nardy et al., 2008).

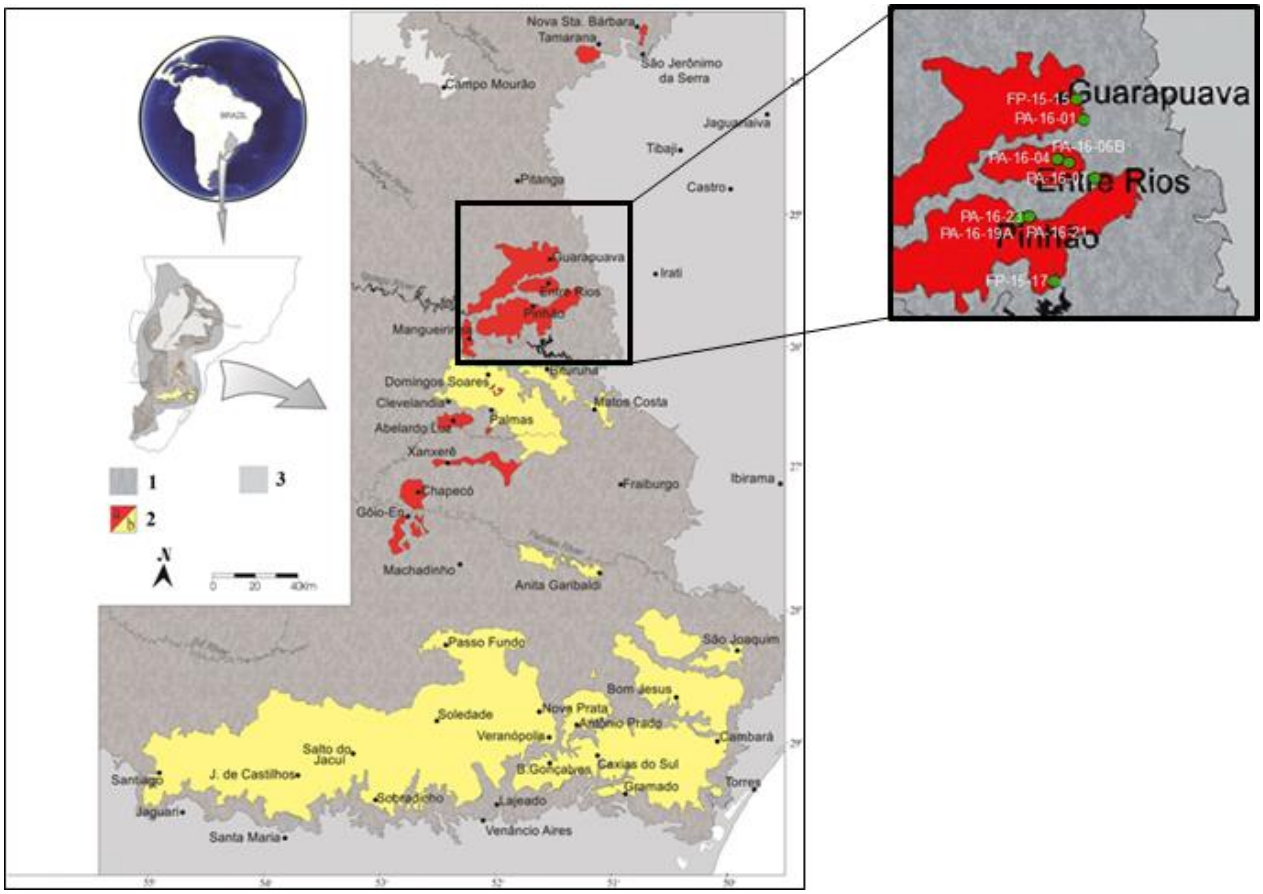

Figure 1 - Geological map focusing the south PMP in Brazil. Dark grey = Basalts; Light grey = Pre-Cambrian basemente; Red = Chapecó acid volcanics; Yellow = Palmas acid volcanics; Black square = Studied area. Map withdrawn from Luchetti et al. (2014). Sample locations are indicated on the inset on right portion of the image.

Table 1 - Geochemical characteristics of the PMP volcanic rocks. Data from: Peate et al., 1992; Peate, 1997; Garland et al., 1995; Nardy et al., 2008; Freitas, 2009; Rocha-Júnior et al., 2013; Polo & Janasi, 2014; Barreto et al., 2016. Polo et al., 2017.

		$SiO_{2\,(\%)}$	$TiO_{2\,(\%)}$	$P_2O_{5\,(\%)}$	Sr	Ba	Ti/Y
Low Ti basalts	Gramado	49-60	0.7 - 1.9	0.05 - 0.4	140-400	100 -700	< 330
	Esmeralda	48-55	1.1 - 2.3	0.1 - 0.35	< 250	90 - 400	< 330
	Ribeira	49-52	1.5 - 2.3	0.15 - 0.50	200-375	200 - 600	> 300
High Ti basalts	Paranapanema	48-53	1.7 - 3.2	0.2 - 0.8	200-450	200 - 650	> 350
	Pitanga	> 47	> 2.9	> 0.35	> 350	> 200	> 350
	Urubici	> 49	> 3.3	> 0.45	> 550	> 500	> 500
Chapecó Acid Volcanics	Ourinhos	65-69	1.1 - 1.3	0.3 - 0.4	300-360	1000-1300	120-180
	Guarapuava	63-66	1.4 - 1.6	0.4 - 0.5	350-400	900-1100	220-280
	Tamarana	63-65	1.3 - 1.5	0.4 - 0.47	350-400	1000-1150	150-200
Palmas Acid Volcanics	Santa Maria	68-72	0.7 - 0.8	0.20 - 0.25	90-110	600-650	50-150
	Anita Garibaldi	65-68	1.0 - 1.15	0.30 - 0.35	130-150	530-610	150-200
	Caxias do Sul	66-69	0.9 - 1.0	0.25 - 0.30	70-110	550-730	80-150
	Barros Cassal	64-66	1.2 - 1.8	0.28 - 0.35	140-180	600-900	110-150
	Jacuí	64-69	1.0 - 1.16	0.28 - 0.31	140-160	510-580	250-300
	Clevelândia	68-73	0.7 - 0.9	0.21 - 0.23	80-110	620-680	100-150

Irrespective of composition, high and low titanium compositions prevail roughly at the north and south of the province, respectively (Fig. 1). The sharing of common isotopic and geochemical features between the acid rocks and their associated basalts suggest an apparent petrogenetic relation (Fig. 2). The restricted occurrence of these rocks on the eastern edge of the basin suggest the role of a high heat flux close to the former rift axis on their genesis. The higher radiogenic signatures of the Palmas rocks would reflect processes of crustal contamination combined with fractional crystallization of the parental basaltic magma (Garland et al., 1995; Florisbal et al., 2018). Partial melting of middle/lower crust might be more relevant than suspected for the Palmas petrogenesis (Harris & Milner, 1997). Otherwise, partial melting of basaltic underplates with negligible crustal assimilation is evoked as the main processes responsible for the Chapecó petrogenesis (Bellieni et al., 1986; Garland et al., 1995).

The present work focuses on the Chapecó rocks of the Guarapuava Acid Volcanics (GAV) type that crops out on the transitional zone between the north and south domains of the PEMP (Fig. 1). The local geology is marked by intercalations of Pitanga (HTiB) and Esmeralda (LTiB) basalts, forming a mafic sequence reaching up 1 km in thickness overlying Paleozoic sediments from the Paraná Basin (Lopes, 2008). The GAV rocks cover this basaltic unit, forming tabular sequences with thicknesses up to 100 meters (Nardy et al., 2002). Literature data indicate that GAV whole-rock major element composition are remarkably similar, being classified as trachydacites (Bellieni et al., 1986; Garland et al., 1995; Nardy et al., 2008, 2011; Pinto et al., 2011; Luchetti et al., 2014; Table 2).

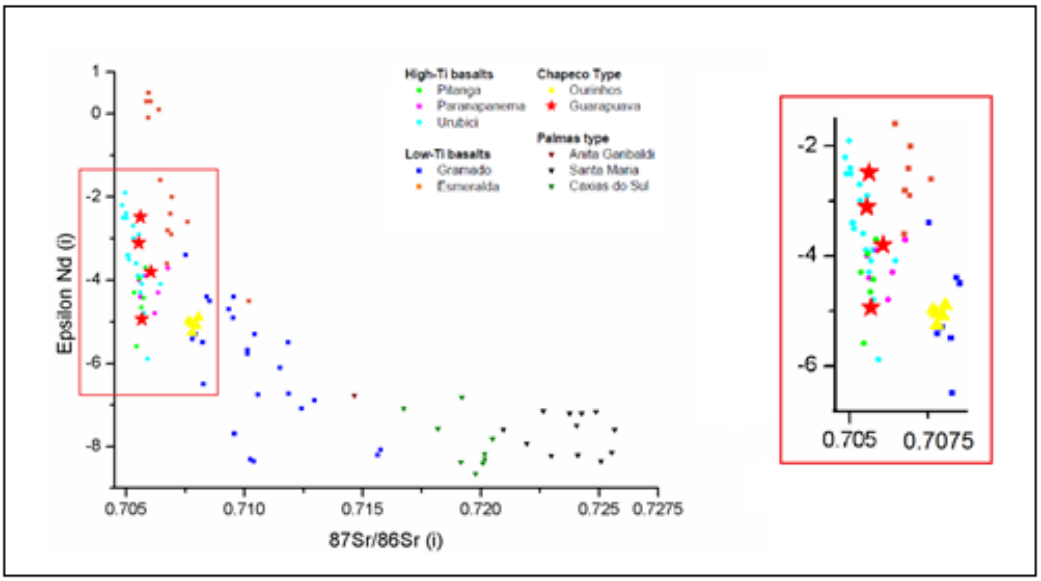

Figure 2 - a) εNd_{134} x $^{87}Sr/^{86}Sr_{134}$ graph exhibiting the sub-types of the basic and acid units of the PMP. The inset graph on the right corner represents the red rectangle that encloses the Chapecó rocks and their associated basalts. Data from: Peate et al., 1992; Peate, 1997; Garland et al., 1995; Nardy et al., 2008; Freitas, 2009; Rocha-Júnior et al., 2013; Barreto et al., 2016.

Table 2 - GAV whole-rock major element composition. a = Pinto et al. (2011); b = Luchetti et al. (2014); c = Nardy et al. (2011). LOI = Loss on ignition.

	a		b		c		
SiO_2	63,60	64,04	64,38	65,44	63,63	65,25	64,66
TiO_2	1,45	1,41	1,46	1,57	1,47	1,49	1,53
Al_2O_3	12,87	13,08	12,83	13,03	13,2	13,19	13,51
FeO total	7,84	7,86	7,01	7,57	7,75	7,62	7,34
MnO	0,14	0,15	0,16	0,12	0,16	0,12	0,12
MgO	1,44	1,30	1,36	1,28	1,28	1,32	1,42
CaO	3,18	3,22	2,91	2,94	2,99	2,99	3,1
Na_2O	3,15	3,36	3,32	3,61	3,65	3,61	3,59
K_2O	4,10	3,96	4,45	4,33	4,24	4,23	4,08
P_2O_5	0,48	0,46	0,48	0,46	0,45	0,45	0,47
LOI	1.50	0.90	1.05	0.61	0.83	0.67	0.80
Sum	99,75	99,75	99,41	100,96	99,64	100,93	100,62

3 METHODS

3.1 Textural Measurements

Plagioclase quantitative textural measurements were performed on nine GAV samples collected in the surroundings of Guarapuava city (Figure 1 and Table 3 for samples location). Six to seven 30µm-thick sections were obtained per sample. The serial sectioning was intended to improve the statistical representativeness of the results, rather than to reconstruct 3D crystal shapes. Optical microscopy and imaging were performed under uncrossed polarized light using a petrographic microscope (Leica M420) coupled to a regular digital camera. The photos were mosaicked in order to obtain images of the thin section as a whole (see Fig. 3). Plagioclase crystals were manually outlined using Adobe Photoshop, in order to prevent problems with the individualization of touching crystals (see appendix 8.1). The digitized images from different thin sections of the same sample were stacked together as a unique panel. Dimensions of the bestfit ellipses of the digitized crystals were obtained using ImageJ software, an open access image analysis program (Rasband, 2010). The results were imported into the *CSDCorrections* 1.51 software (Higgins, 2000) for stereological corrections and acquisition of the CSD curves.

Table 3 - Sample locations.

	Latitude (N)	Longitude (W)	Altitude (m)	Geographic Localization
FP-15-15	25° 31.09	51° 50.35	1025	Guarapuava - Palmeirinha road
FP-15-17	25° 85.01	51° 57.77	1171	Pinhão - Criciúma road
PA-16-01	25° 37.08	51° 47.85	1046	Fé square - Guarapuava
PA-16-04	25° 85.01	51° 56.75	974	Colônia waterfall - Entre Rios district
PA-16-06B	25° 49.96	51° 52.96	1010	Samambaia waterfall - Entre Rios district
PA-16-07	25° 54.67	51° 44.44	1145	Rapel waterfall - Entre Rios district
PA-16-19	25° 66.99	51° 69.43	1005	Zoraldo waterfall - Close to Pinhão
PA-16-21	25° 66.13	51° 68.97	1011	Osvado waterfall - Close to Pinhão
PA-16-23	25° 65.93	51° 65.87	1051	Pinhão - Guarapuava road

The stereological conversion requires the input of the mean crystal shape expressed in terms of the short(S) : intermediate(I) : long(L) axes. According to Higgins (1994), the S/I ratio is close to the intersection width/length mode calculated by the *CSDCorrections* software (constant at 0.59 for the analyzed samples). Assessment of the I/L ratio in randomly oriented rocks is more complicated. Higgins (1994) suggested using the skewness of the intersection rate distributions, whereas Higgins (2006a) proposed examining the (010) face of plagioclase crystals for direct evaluation of the I/L ratio. Suitably oriented plagioclase crystals resulted I/L ratio close to 0.7. Thus, the plagioclase aspect ratio chosen to represent all samples was 1.0 : 1.7 : 2.5. Most crystals have euhedral habits with angular shapes and were considered to have a roundness factor of 0.3 (on a scale of 0 to 1; 0=block;

1=ellipsoid). Logarithmic length intervals were defined in a way that the next bin is $10^{0.20}$ times larger than the previous one. All the CSDs were calculated on a vesicle free basis (tests varying the vesicle amount up to 3% produced no appreciable differences). Bins with less than 10 crystals per unit area or with large uncertainties were removed from the CSDs due to compromised measurement precision.

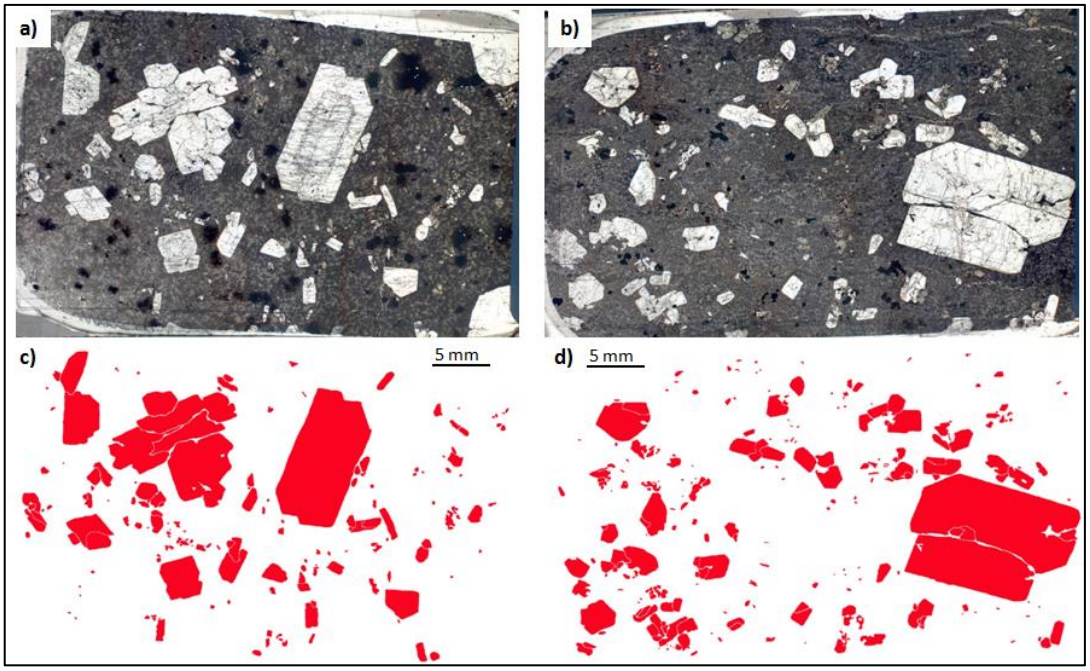

Figure 3 – Examples of thin section panels of the PA-16-04 (a) and PA-16-19 (b) samples with uncrossed polars. (c) and (d) are the respective digitized outlines of plagioclase crystals.

3.2 Cathodoluminescence Imaging

The bombardment of materials by electrons produces a wide range of secondary particles and radiations, including light, which is the phenomenon of cathodoluminescence (CL) (Pagel et al., 2000). Electrons lose their energy fast in minerals; hence, the CL light is produced close to the surface. CL light has a wide range of wavelengths, but usually only the visible light is used for geological purposes. The intensity and color of luminescence are highly variable and depend on several factors including the concentration of activator trace elements (Table 4). In plagioclase, the most important activators are Mn^{2+} and Fe^{3+}, but the elements Cu^{2+}, Ti^{4+}, Ce^{3+} and Eu^{2+} may also be important (Mora & Ramseyer, 1992).

Table 4 - Cathodoluminescence properties of the minerals found in the volcanic rocks imaged in this study.

Mineral	Color	Intensity	Important Acivators
Plagioclase	Dark green	Medium	Mn^{2+}
Alkali Feldspar	Bluish green	Medium	Al-O^{-}-Al
Quartz	Dark blue	Low	Lattice defects, Ti, etc.
Apatite	Bright green	High	Mn^{2+}
Mafics, Fe-Ti oxides	No CL	Zero	

In this study, CL images were obtained at the University of Québec at Chicoutimi, Canada, with a CITL CL8200 cold cathode instrument mounted on a regular petrographic microscope. In this equipment, a wide electron beam is directed towards a polished thin section, which is in a vacuum chamber attached to the microscope stage. An area about 3 mm in diameter is obliquely illuminated with electrons. Light from the section escapes through a window into the objective of the microscope and the system detects simultaneously both CL color and intensity. The images were acquired using a voltage of 10 Kv and an electric current of 185 μÅ. Multiple images were mosaicked to give a composite image covering the entire thin section.

3.3 Scanning Electron Microscope

One sample (FP-15-15) with well-defined banded structure was cut and separated in slices representing the macroscopic diversity of the GAV (lighter and darker bands). Each slice was separately crushed in millimeter-size pieces and mounted on polished epoxy sections. Scanning Electron Microscope (SEM) was performed using a Quanta 600 FEG (FEI) coupled with an energy disperse spectrometer (EDS; Quantax, Bruker) in the Laboratório de Caracterização Tecnológica (LCT) of the Escola Politécnica da Universidade de São Paulo. Phases associations were characterized through backscattered images, energy dispersive spectroscopy (EDS) and X-ray digital mapping for the major elements (Si, Al, Fe, Mg, Na, K, Ca, Ti, P).

3.4 X-ray Diffraction

X-ray diffraction patterns of powder samples from the lighter and darker bands of sample FP-15-15 were collected in a Bruker D8 Advanced Diffractometer at the Núcleo de Apoio à Pesquisa (NAP) Geoanalítica, Instituto de Geociências da Universidade de São Paulo (IGc-USP). Analyzes were performed in a step scan mode with angular range from 5° to 120° 2θ, step size 0.02°, 70s/step, Cu Kα, 40kV, 40mA, flat sample holders, fixed divergence slit and 0.1mm receiving slit. The samples were mixed with 10 wt% of high purity α-Al_2O_3. Ritveld refinements was performed using High Score Plus 3.0 Panalytical Software. The following crystallographic information files (CIF) were used: plagioclase An_{52} (Horst et al., 1981), quartz, sanidine and augite (Gualtieri, 2000). Magnetite,

pigeonite, enstatite and apatite occur as minor phases and were not included in quantitative phase analyzes due to their low weight fraction and, consequently, large intrinsic errors.

3.5 Plagioclase *in situ* analyzes

Plagioclase isotopic analyzes were conducted with in adjacent micrometric spots in order to sample material from the same mineral growth zones.

In situ Sr isotope analyzes in plagioclase were carried out at two stages. One at the Radiogenic Isotope Facility (RIF, University of Alberta, Canada) in 2009 (sample FP-15-15) and another one at the MidWest Isotope and Trace Element Research Analytical Center (MITERAC) of the University of Notre Dame in 2017 (samples PA-16-01 and -21). The analyses at the RIF were conducted using a NuPlasma MC-ICP-MS coupled with a *Laser Ablation* UP213 system under analytical conditions of laser beam diameter of 160 µm and 10 Hz frequency at energy output of approximately 11J/cm^2. Whereas, the analyses at the MITERAC were performed using a NuPlasma II MC-ICP-MS coupled with the Excimer NWR-193 nm LA system, under analytical conditions of laser beam diameter of 150 µm at a 10 Hz frequency at energy output of approximately 14J/cm^2. For Sr isotope determinations, a modern coral was used as external standard, whereas monitoring of the invariant $^{84}Sr/^{86}Sr$ ratio 0.056546 ± 0.00001 (2σ) allowed assessment of the effectiveness of the interference correction. Repeated measurements on the modern coral yielded an average $^{87}Sr/^{86}Sr$ value 0.709156 ± 0.00005 (2σ) which agree with the value for the modern sea water of 0.709168 (Hodell et al., 1990).

4 RESULTS

4.1 Field Aspects

GAV exposures are marked by a laterally discontinuous sub horizontal banding that alternates three-dimensional light- and dark-colored bands with anastomosed geometries with high aspect ratios (Figs. 4 a and b). As a purely descriptive term, this pattern will be referred as banding. There seems to be a close association between banding and fracturing. The light bands are composed predominantly by a very fine granular white material; whereas the dark bands have a prevailing massive appearance (Figs.4 c and d). In spite of the apparently sharp transition between bands, there is no evident petrographic difference and close inspection reveals the contacts to be of diffuse and gradational character (Figs. 4c and d). At outcrop scale, the internal fabric of the rock is massive and homogeneous showing no preferred orientation of crystals and major differences between both bands other than their colors. Spherical vesicles up to 5 mm are a common feature, but in small amounts and their distribution is apparently unrelated to banding. The samples have bimodal texture marked by very fine-grained matrix interspersed with plagioclase macrocrysts reaching up 1.5 cm (Figs. 4 c-f). Some single plagioclase crystals are common in both bands (Figs. 4 d and f). The precise stratigraphic control of the visited outcrops imposed a very challenging task due to extensive faulting and the presence of thick soil horizons.

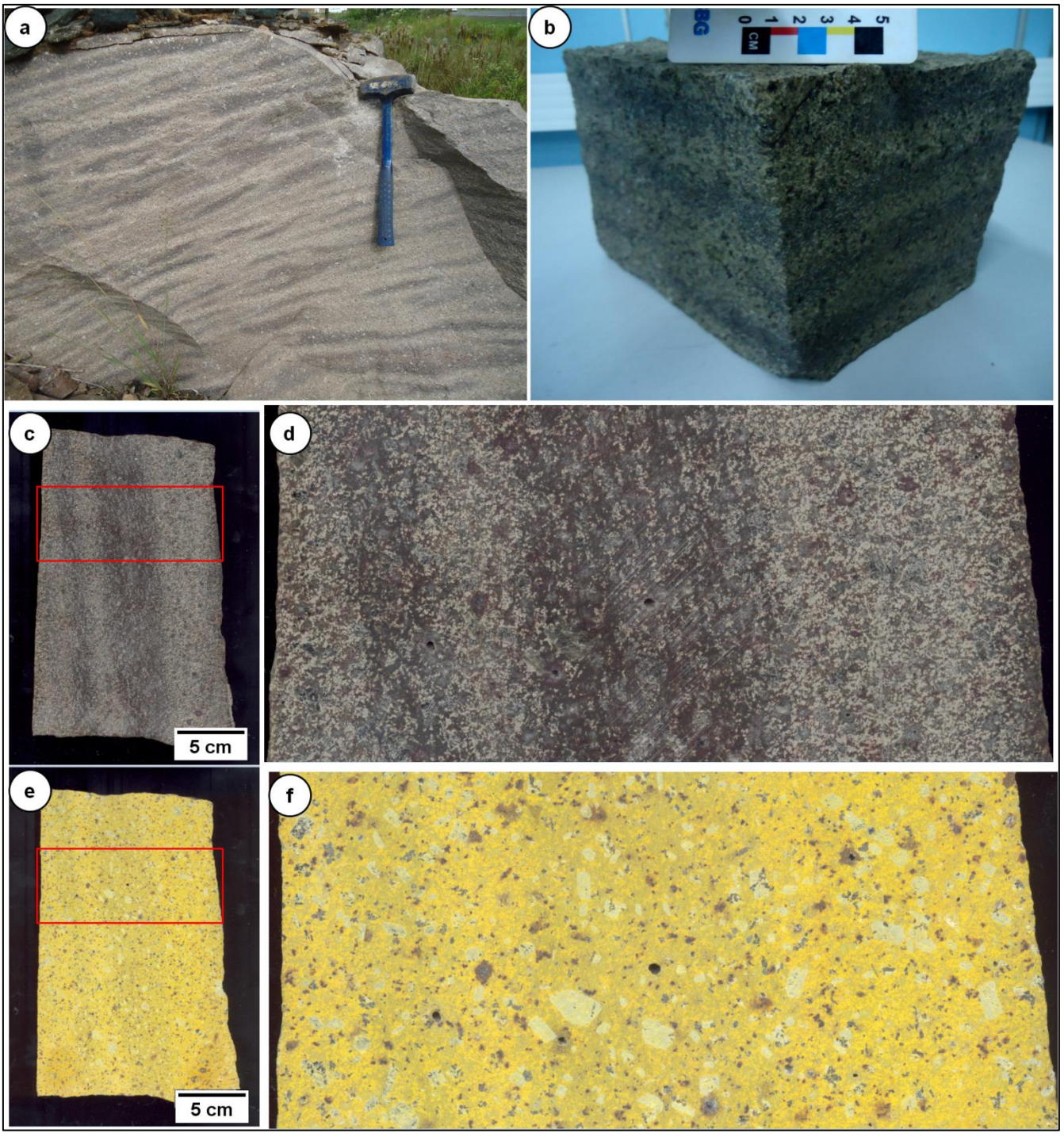

Figure 4 - a) Anastomosed pattern of the GAV trachydacites from Guarapuava region marked by alternation of light and dark bands. b) Sample from the respective outcrops showing the three-dimensional structure of the rock. c) Slice of a GAV displaying light and dark bands. d) Inset of the red rectangle in c) showing details of both bands. e) Same slice showed in c) after staining. f) Inset of the red rectangle in e). Plagioclase macrocrysts appear in pale colors, Fe-Ti oxides in red/brown color. Groundmass in yellow.

4.2 Petrography

4.2.1 Groundmass

The matrix represents 80 to 90% volume of the samples. It is defined by a framework of indiscernible crystallites and small crystals (< 0.2mm) of pyroxene and Ti-rich magnetite (Figs. 6a and b). Glass was not observed in optical or electron microscopy, neither was it detected in X-ray diffraction. Despite the relative homogeneity, the groundmass shows subtle size variations according to the sample stratigraphic position, with the finest sample observed just above the contact with the underlying basalts. Irrespective of band color, the matrices from different bands show no substantial differences under the petrographic microscope.

4.2.2 Plagioclase

Plagioclase is the most abundant macrocrystic phase, corresponding to 10-15% area in thin sections. Plagioclase occurs preferably as individual euhedral crystals (Figs. 6c and d) up to 1 cm or, less frequently, as mono or polymineralic clusters. Plagioclase crystals from the mineral clusters contrast with individual crystals in having rounded edges and sinuous contacts against each other. Regardless of the textural association, most crystals show no evident zoning under the petrographic microscope. The largest crystals commonly host irregular 0.2 to 2 mm wide patches filled with material that resemble the matrix of the rock, interpreted to represent devitrified melt inclusions.

4.2.3 Pyroxene

Pyroxene occurs either as widespread individual crystals set in the groundmass, as fine aggregates within and around plagioclase (Figs. 6c, d, g-m), or as rare monomineralic clusters (Fig. 6n). It has smaller sizes (0.1 to 1 mm) compared with plagioclase and show subeuhedral to anhedral habits, often exhibiting rounded shapes when clustered with plagioclase (Figs. 6i and j).

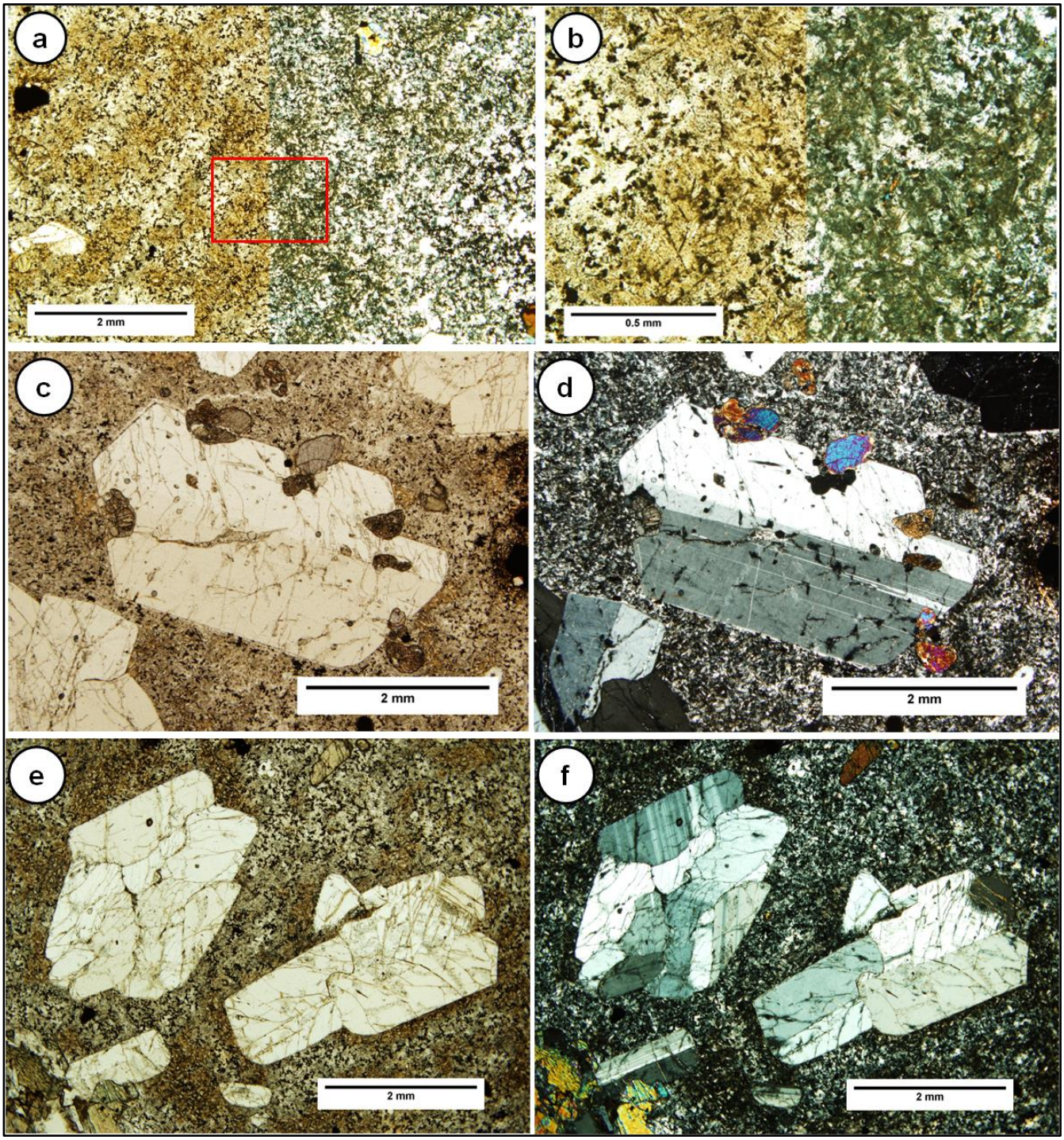

Figure 6 – Microphotographs under transmitted light showing the petrographic aspects of the GAV trachydacite samples. a) Groundmass from sample FP-15-15 with uncrossed and crossed polars on the left and right halves, respectively. b) Inset of the red rectangle displayed on a). c) Euhedral plagioclase from sample PA-16-04 with some pyroxene crystals around it. Uncrossed polars. d) Same as c) but with crossed polars. e) Monomineralic cluster of plagioclase crystals from sample FP-15-15 displaying rounded contacts against each other. Uncrossed polars. f) Same as e) but with crossed polars.

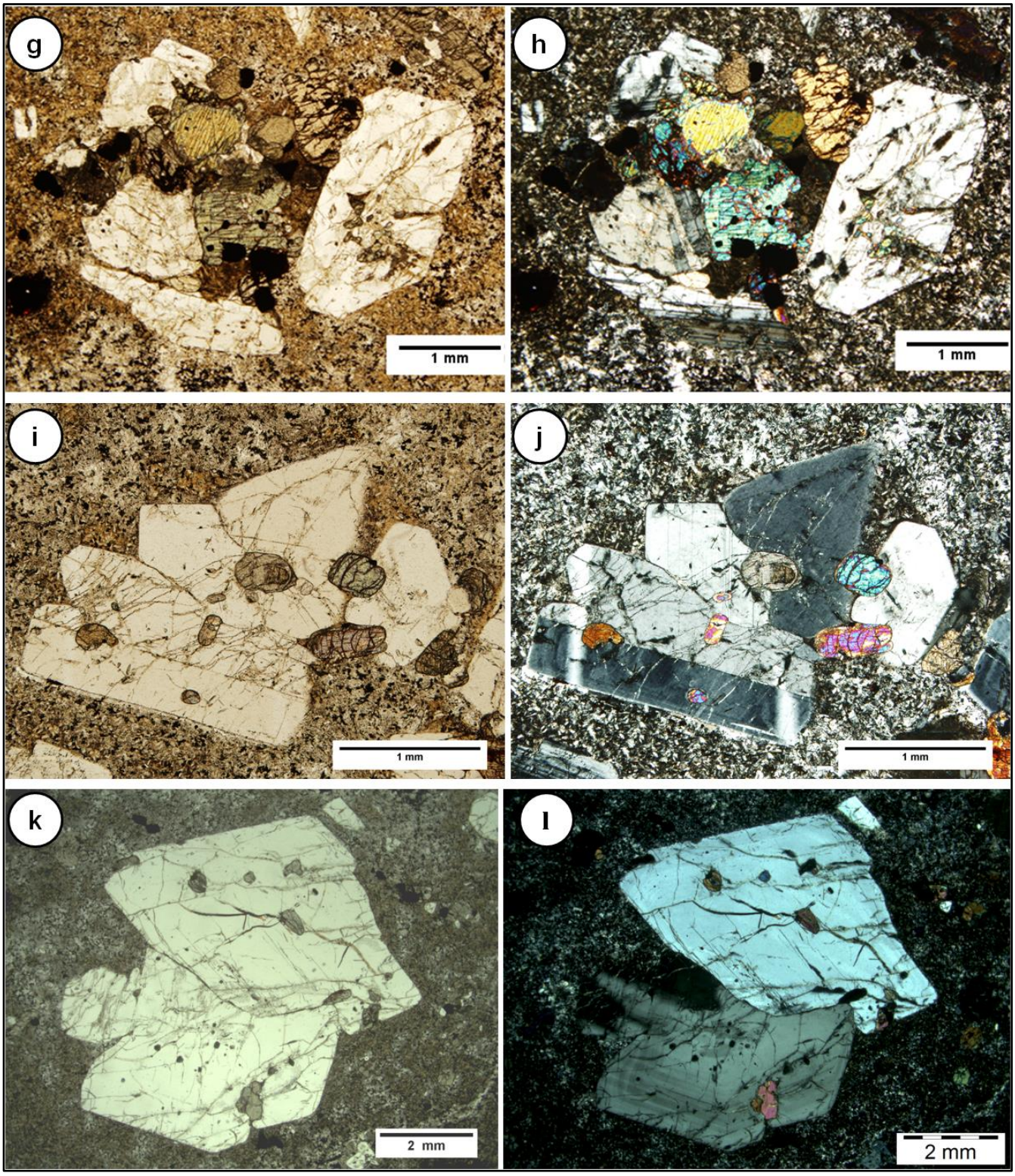

Figure 6 – cont. g) Typical aggregate of plagioclase and pyroxene crystals. Uncrossed polars. h) Same as g) but with crossed polars. i) Aggregate of plagioclase + pyroxene displaying rounded shapes and sinuous contacts. Uncrossed polars. j) Same as i) but with crossed polars. k) Two rounded plagioclase crystals with sinuous contacts against each other and hosting pyroxene inclusions. Uncrossed polars. l) Same as k) but with crossed polars.

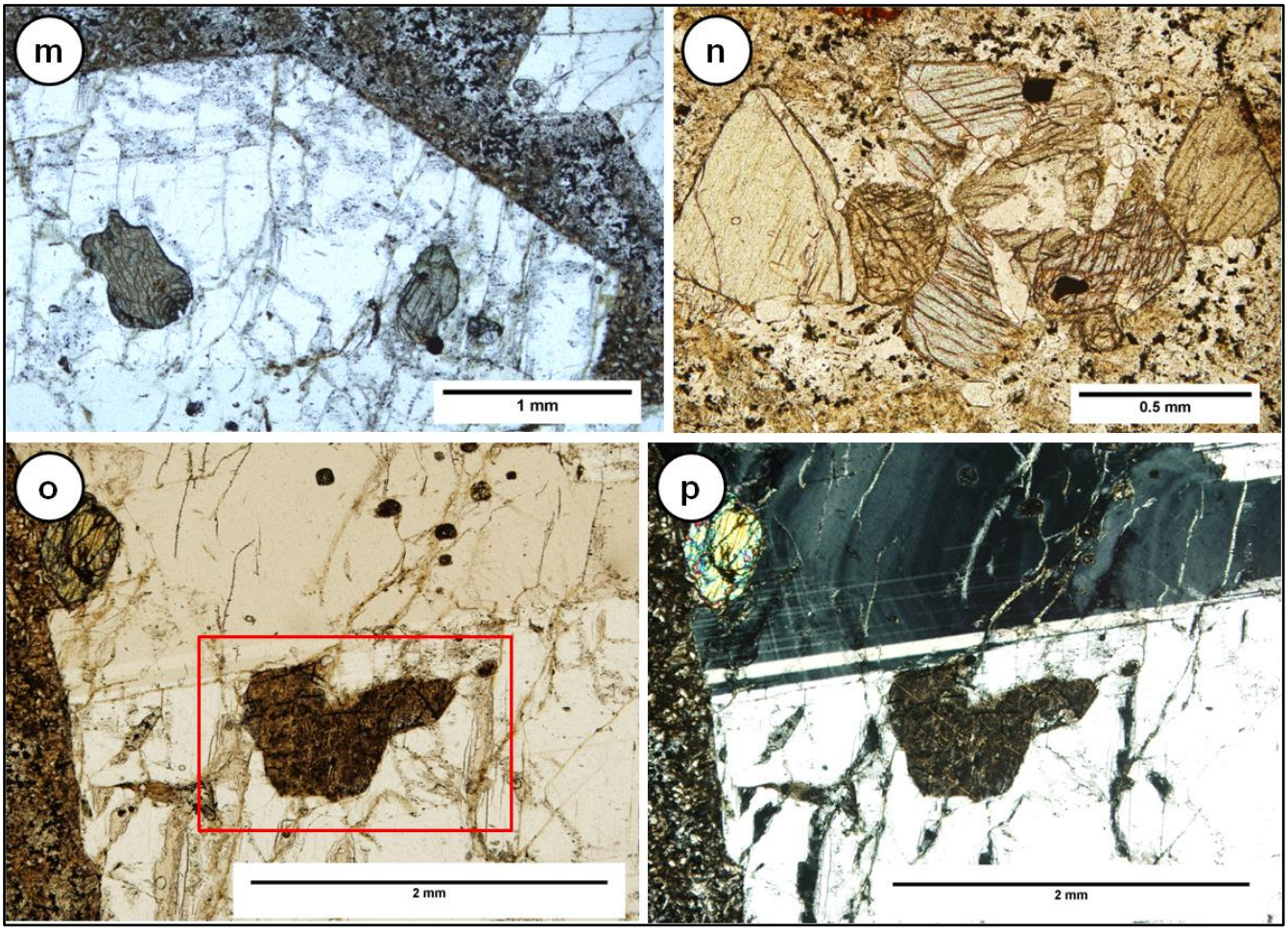

Fig. 6 – cont. m) Two pyroxene inclusions hosted within euhedral plagioclase. Uncrossed polars. n) A rare small monomineralic aggregate of pyroxene crystals. o) Melt inclusion (highlighted with a red rectangle) hosted within a plagioclase. Uncrossed polars. p) Same as o) but with crossed polars.

4.3 CL Images

CL images of nine 100 µm-thick polished sections (for sample locations, see Table 2) highlighted important details of the GAV trachydacite texture. The groundmass is composed by an irregular mixture of distinct patches in dark and bright shades of blue (Figs. 5 and 6a). The dark blue patches constitute a fine framework resembling touching feldspar microlites with interstices filled by quartz (Figs. 7a and b). The feldspar microlites have sizes up to 100µm, but are usually much smaller. They commonly show inner and outer portions in green and blue colors, respectively (Fig. 7b). The bright blue patches are monomineralic aggregates of feldspar crystals (Figs. 7c and d). Some samples show irregular fractures which are immediately surrounded by dark blue patches; whilst bright ones occur gradually further from it (Figs. 7e and f). One exception to the textural patterns described above is the sample taken at the contact with the basaltic substrate (PA-16-21). It shows a very fine, homogeneous groundmass with a regular CL response in dark blue color (Figs. 7g, h and i). Another striking feature from the groundmass observed on all the samples is a remarkable spatial association between tiny apatite crystals and pyroxene/Fe-Ti oxides (Fig. 7i). A similar texture has been described in the Palmas volcanic rocks (Dias et al., 2017).

Irrespective of shape and size, plagioclase macrocrysts show homogeneous CL responses both intra- and inter samples. Crystals appears always with dark green luminescence (Figs. 8a and b). Structures like zonation, growth and resorption zones are either lacking or are very rare and obliterated. Pockets filled with materials similar to the groundmass are interpreted as devitrified melt inclusions and appear in different shades of blue and varying shapes and sizes (Figs. 8c,d and e).

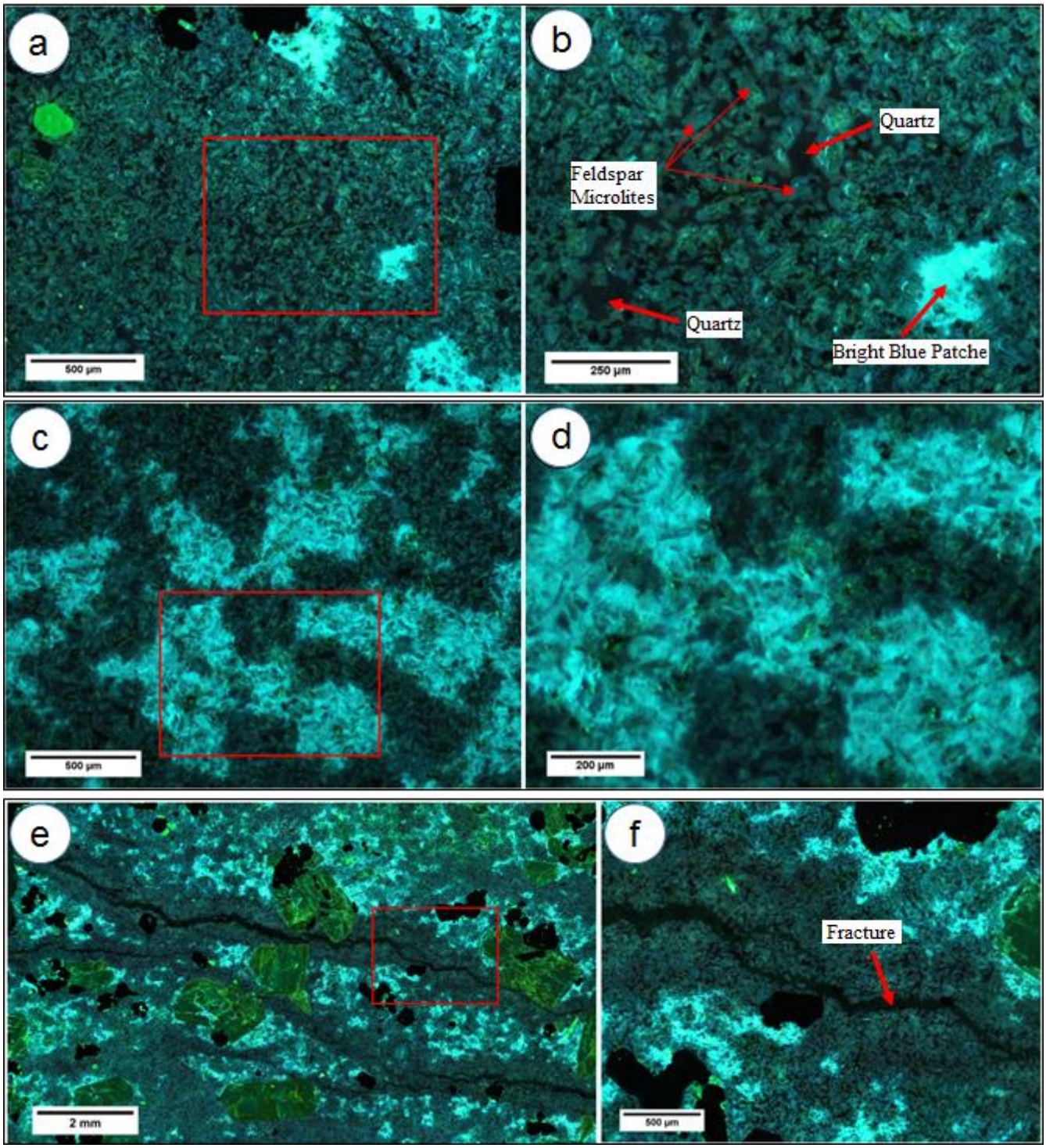

Figure 7 - CL images of the groundmass from distinct samples. The different colors represent different phases. Dark blue = Quartz; Intermediate blue = K-feldspar; Dark green = Plagioclase. Bright green = Apatite; Black = Pyroxene and Fe-Ti oxides. a) Dark blue patches from sample PA-16-23. b) Inset of the red rectangle shown in a). c) Mixture of dark and bright blue patches from sample FP-15-15. d) Inset of the red rectangle in c). e) Irregular fractures in sample PA-16-19. These are immediately surrounded by dark blue patches, whilst the bright ones occur further from it. f) Inset of the red rectangle in (e).

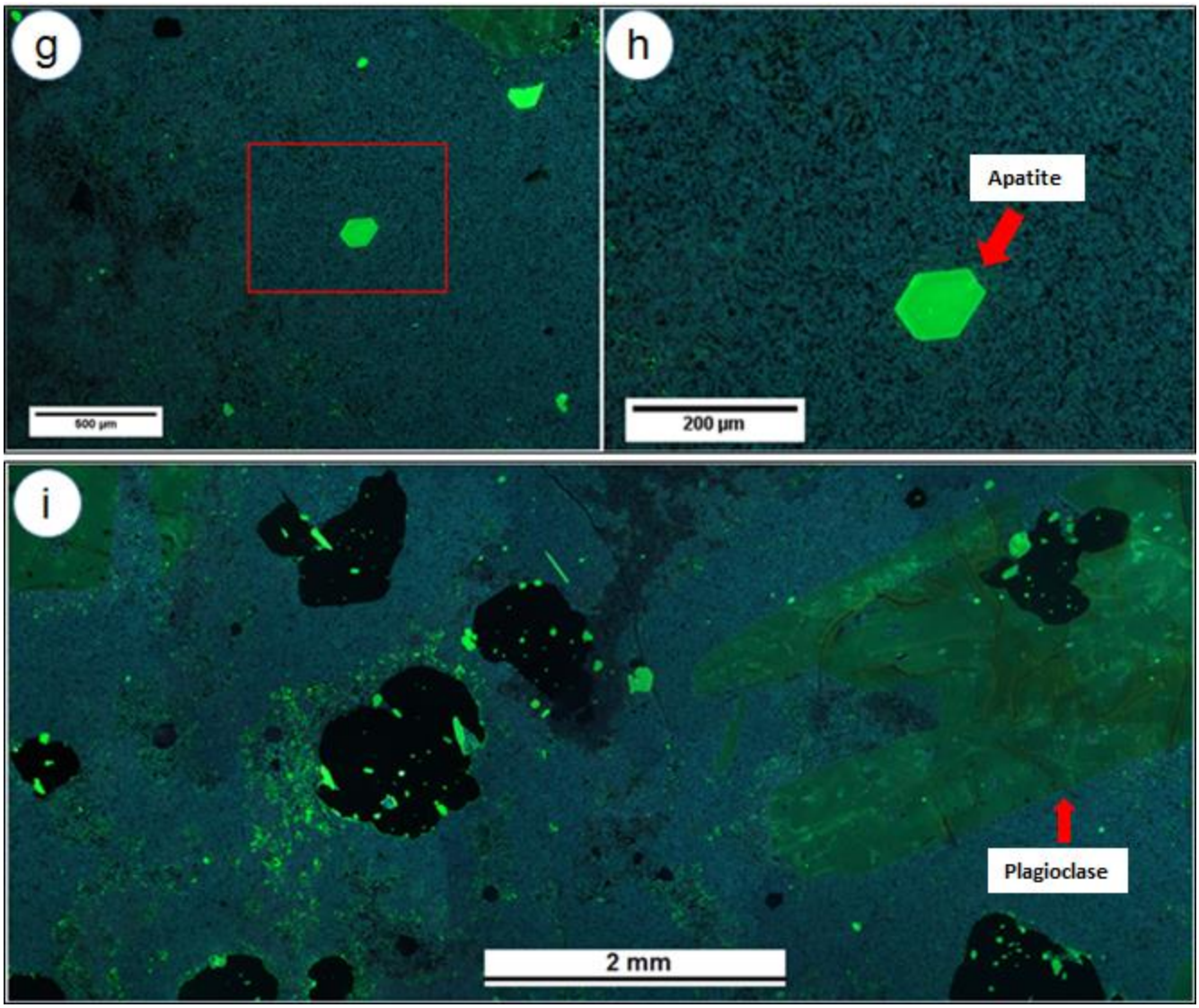

Figure 7 – cont. g) Homogeneous groundmass from sample PA-16-21. h) Inset of the red rectangle shown in g) showing the very fine character of this groundmass and an apatite crystal in the middle. i) Remarkable spatial association between tiny apatite crystals and pyroxene/Fe-Ti oxides in sample PA-16-21.

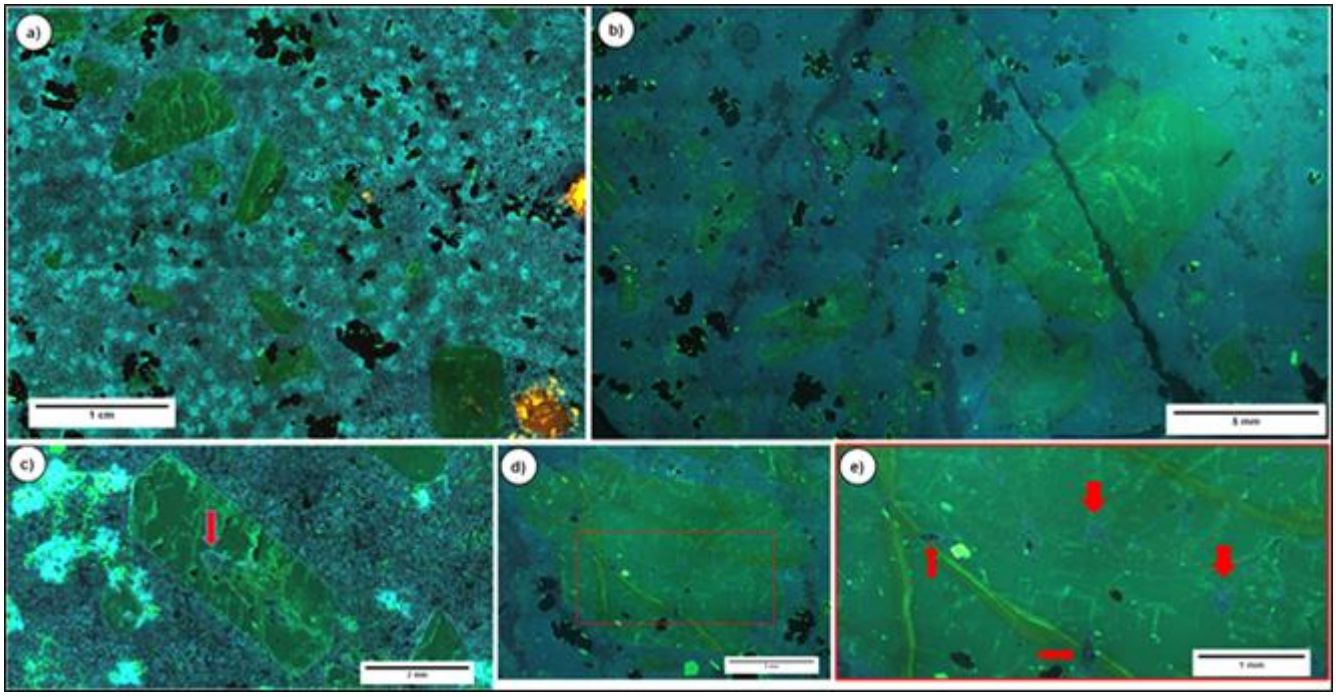

Figure 8 - CL images of plagioclase crystals. Part of a mosaic showing dispersed plagioclase macrocrysts from samples PA-16-07 a) and PA-16-21 b). c) Plagioclase crystal from sample PA-16-07 hosting a melt inclusion indicated by the arrow. d) Plagioclase crystal from sample PA-16-21 hosting several small melt inclusions. e) Inset of d) showing details of the melt inclusions indicated by the red arrows.

4.4 SEM Images and Major Element Characterization of the Groundmass

The matrices of the light and dark bands appear as relatively homogeneous, indistinct shades of grey with conspicuous presence of small crystals of apatite, pyroxene, and Fe-oxides (Figs. 9a and b). A closer inspection reveal both matrices to be defined by two petrographically distinct domains: one with a continuous backscattered signal (Massive Matrix – MM), and another one defined by a discontinuous backscattered signal speckled by varying amounts of tiny vugs (Porous Matrix – PM) (Figs. 9c and d). Both occur dispersed through the matrices composing irregular areas with diffuse contacts against each other (Figs. 9c-h).

4.4.1 Massive matrix (MM)

X-ray mapping of the MM domain reveals a mottled pattern that alternates dark and light tones of grey (Fig. 10a). Element maps reveal the former to be composed of Si, whereas the light areas have increased Na, K and Al contents, implying a quartz-feldspathic composition, respectively (Figs. 9 b-e). The inner portions of the feldspathic zones are enriched in Na, Ca and Al, whereas the outer parts contain enhanced K contents. All these findings are in agreement with EDS analyzes (Fig. 10a and in

appendix 8.2). A merged image of all the individual maps gives a clear view of how the compositional variability (Fig. 10i).

4.4.2 Porous matrix (PM)

Locally, tiny feldspar crystals with a "vuggy" aspect occur interspersed with the PM. A representative image comprehending both MM and PM is illustrated in Figure 11a. The same compositional trends described so far are also observed in the MM domain. However, the PM (on the right corner of Fig. 11) shows high responses of K, Al and Na and intermediate ones of Si compared with the contents observed in the MM, implying an alkali feldspar composition (Figs. 11b-e). Again, a merged image of all the individual maps clearly illustrates the distribution of the major elements (Fig. 11j), confirmed by EDS analyses as indicated in Figure 11a and in appendix 8.2.

Table 6 - Summary of the MM and PM features.

Massive Matrix (MM)	Porous Matrix (PM)
Well defined areas rich in silica and feldspathic components	Poor defined scattered areas with alkali feldspar composition
Framework of touching feldspar microlites with interstices filled by quartz	Only feldspathic zones
Small amount of vugs	Great amount of vugs
Greater abundance in the dark bands	Greater abundance in the ligth bands
Correspondence with the dark blue patches under CL	Correspondence with the bright blue patches under CL

The small black features seen in Figs. 10 and 11 are interpreted as vugs, once they did not present any chemical response, and correspond to areas with no CL signal. A summary of the features from both domains is presented in Table 6.

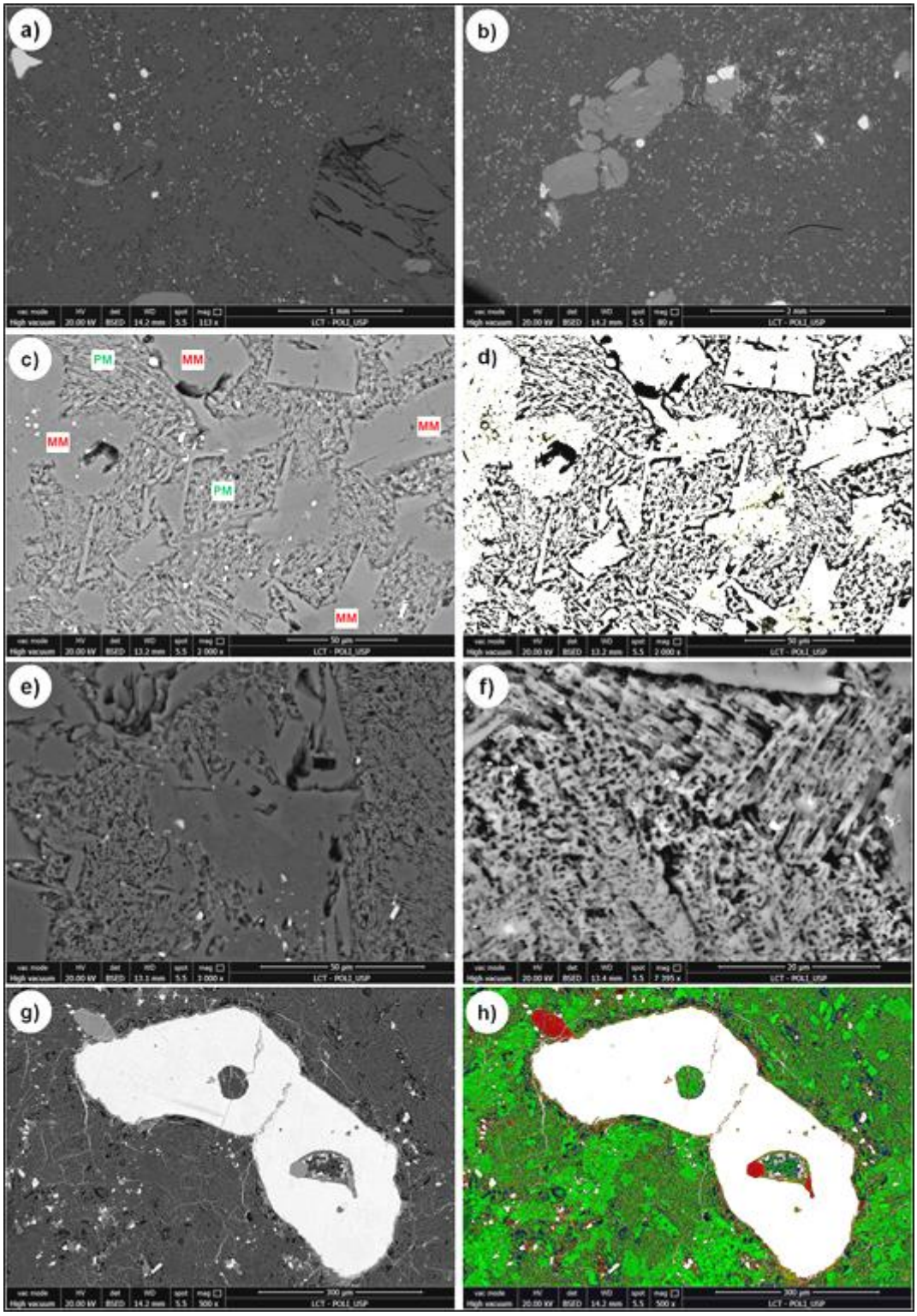

Figure 9 - a) Backscattered electron (BSE) image of the general appearance of the light (a) and dark (b) band samples. c) BSE encompassing MM and PM domains in detail. Both are indicated in the figure. d) False color of c) highlighting both domains. e) MM and PM domains. f) Detail of a PM domain. Vuggy feldspar. g) BSE of a Fe-oxide macrocryst (in bright color) set in a groundmass composed with both MM and PM domains in a dark band sample. The patches hosted within the macrocryst are interpreted as melt inclusions. h) False color of d) highlighting the MM and PM components in continuous bright and discontinuous dark green tones, respectively. The crystals in red are apatite.

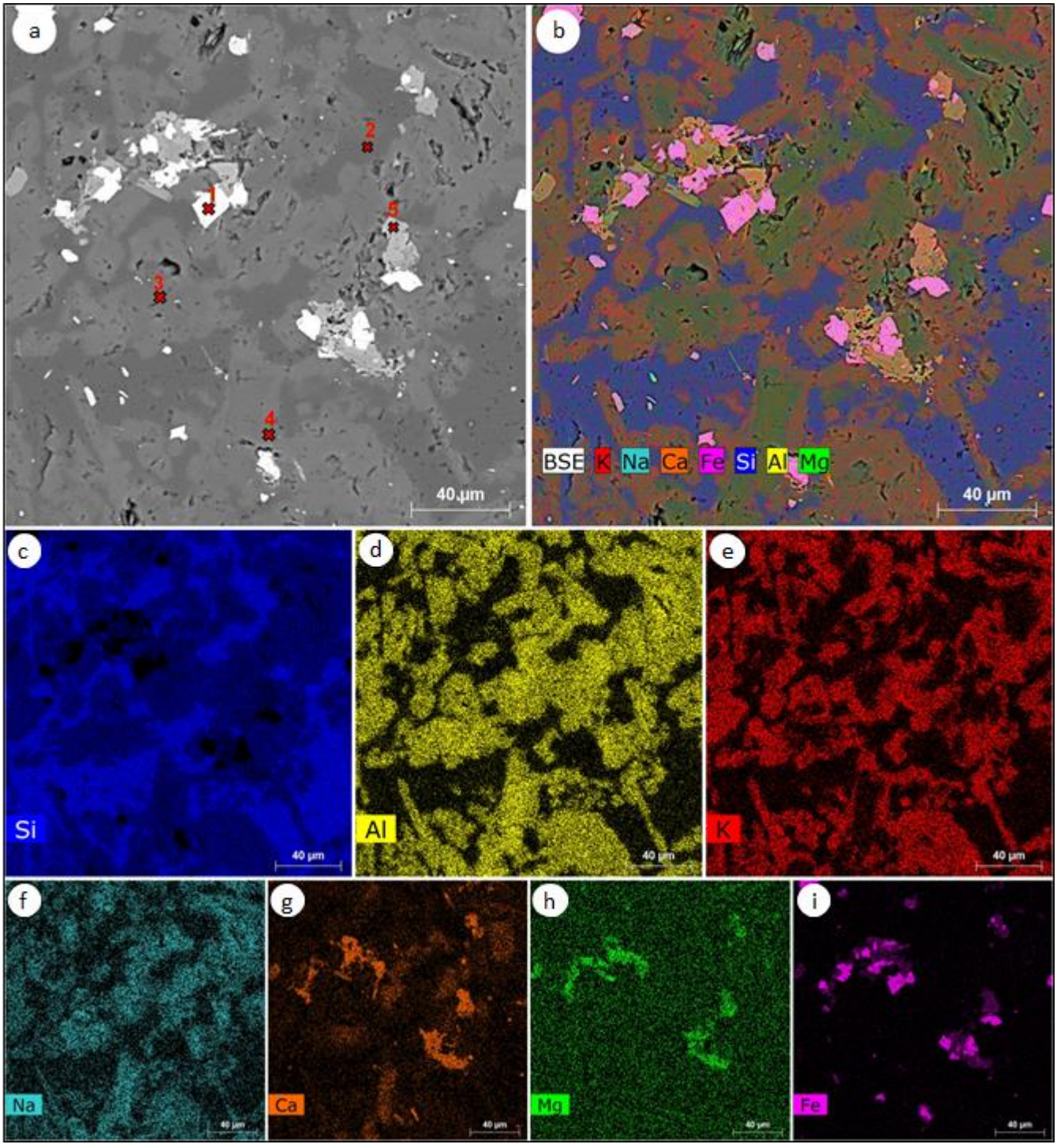

Figure 10 - a) BSE image from a MM domain. The red spots and numbers indicate the targets of EDS analyses. The respective compositions are: 1-Ti-rich magnetite; 2-Quartz; 3-Plagioclase; 4-K-feldspar; 5-Augite. b) Merged image of all the individual maps. c-i) Individual X-ray digital maps of major elements in the analogue area shown in (a). The colors intensities are proportional to the element concentration.

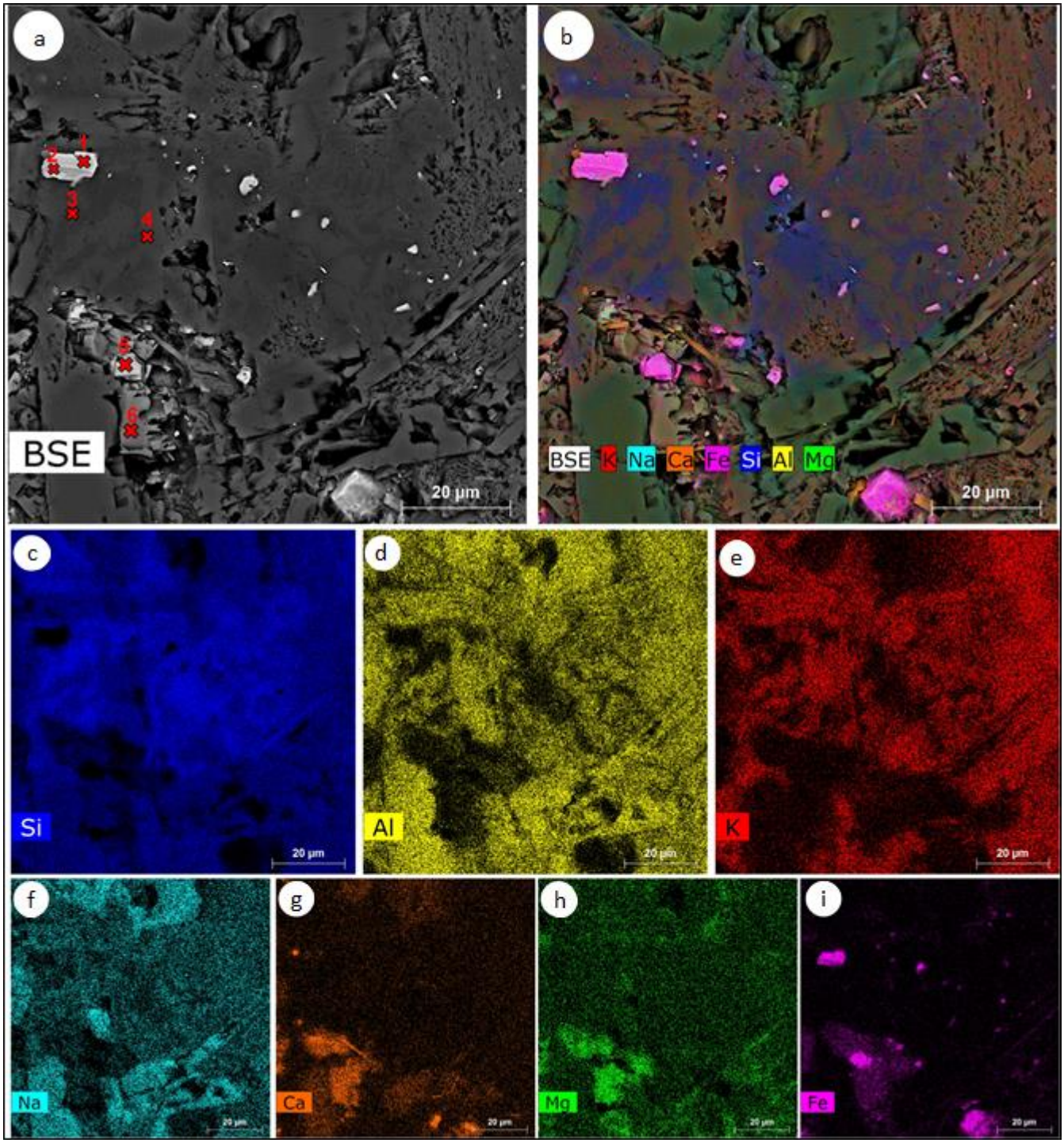

Figure 11 - a) BSE image of a MM and PM (chiefly on the right corner) domains. The red spots and numbers indicate the targets of EDS analyses. The respective compositions are: 1-Magnetite; 2-Ilmenite; 3-Quartz; 4- K-feldspar; 5-Magnetite; 6-Augite. b) Merged image of all the individual maps. c-i) Individual X-ray digital maps of major elements in the analogue area shown in (a). The colors intensities are proportional to the element concentration.

4.5 X-ray Diffraction

Figure 12 shows the X-ray diffraction patterns from both light and dark bands of sample FP-15-15. They have similar mineral composition, with large predominance of plagioclase over quartz and sanidine, and smaller amounts of augite. However, important differences in mineral relative abundance are observed, since the dark band is enriched in quartz and depleted in sanidine relative to the light band (Table 7). Both bands are holocrystaline.

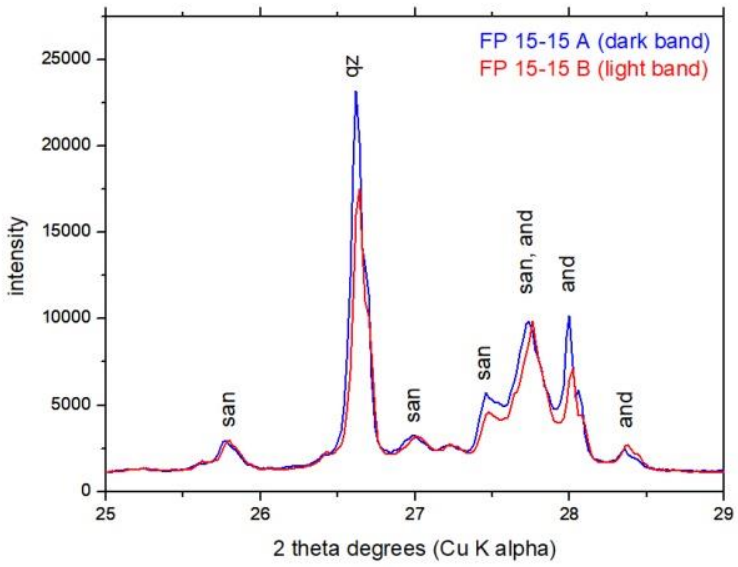

Figure 12 – X-ray diffraction patterns of light and dark bands in blue and red lines, respectively.

Table 7 - Modal mineralogy estimated after Rietveld treatment. Chi-square is a measure of data quality which equals the square of the ratio of the weighted profile R-factor over the expected R-factor.

	FP -15 - 15	
	Dark band	Light band
Quartz	21.5	17.3
Sanidine	24.8	31.7
Andesine	49.6	46.5
Augite	4.1	4.4
chi^2	13.6	8.6

4.6 Crystal Size Distribution

Plagioclase CSD results are shown in Figure 13a. Crystal populations were divided in 11 to 12 size ranges (Table 8). The CSDs have striking similar shapes defining concave-up curves, with a turn-down at classes with smaller crystal sizes. Sample PA-16-21, which was sampled at the contact with the basaltic substrate, shows steeper patterns for the smaller crystal classes (Fig. 13a). Plagioclase crystals were separated in different populations according to a main inflection on the CSD curves represented by separate linear fits (Fig. 13b). We defined phenocrysts and microphenocrysts as being larger and smaller than 3 mm respectively. Except for the fit obtained for sample PA-16-21, the resulting values for slope and intercept of the linear segments are very similar (Table 9). Residence times calculated for microphenocyst and phenocryst populations are shown in Table 9.

Table 8 - Number of crystals per unit area

Sample:	FP-15-15	FP-15-17	PA-16-01	PA-16-04	PA-16-06B	PA-16-07	PA-16-19A	PA-16-21	PA-16-23
Area (mm^2):	6681	7672	6558	6836	7610	6486	6686	6942	6625
Size bin range (mm)									
14.7 - 23.3	1	1	0	3	0	0	5	0	0
9.28 - 14.7	11	6	1	3	2	1	3	3	4
5.85 - 9.28	8	17	10	17	12	6	6	4	17
3.69 - 5.85	39	34	29	42	30	31	47	33	30
2.33 - 3.69	106	80	88	103	105	80	98	93	60
1.47 - 2.33	155	136	127	166	182	174	146	140	105
0.928 - 1.47	190	162	140	202	207	180	189	184	104
0.585 - 0.928	168	183	164	210	259	206	201	231	138
0.369 - 0.585	98	198	167	200	282	219	218	272	144
0.233 - 0.369	14	156	173	101	242	263	239	324	128
0.147 - 0.233	0	70	47	6	79	144	92	126	69
0.0928 - 0.147	0	1	3	0	2	9	9	1	12

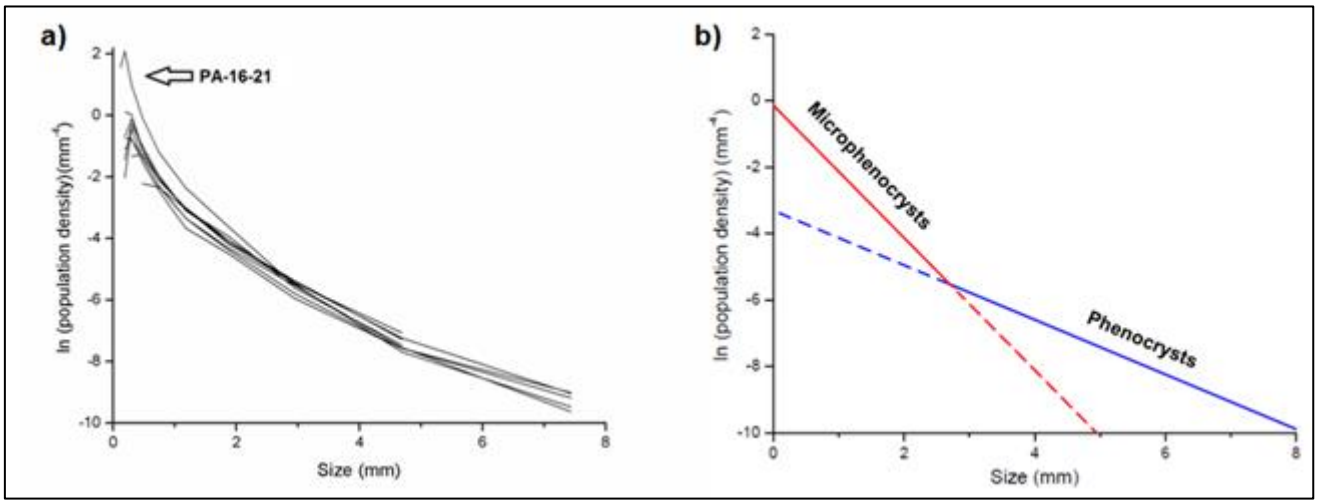

Figure 13 - a) Compilation of crystal size distribution of the nine GAV samples selected for this study. b) Linear best fitting for plagioclase phenocrysts (blue line) and microphenocrysts (red line).

Table 9 – Geometrical parameters and magmatic timescales obtained from microphenocryst and phenocryst populations (Fig. 13b).

	Slope (S)	Intercept (n^0)	R^2	G ($mm.s^{-1}$)	τ (-1/GS)
Phenocrysts	-0.82	-3.31	0.96	10^{-8}	3.9
				10^{-9}	38.6
Microphenocrysts	-1.88	0.44	0.93	10^{-8}	1.7
				10^{-9}	16.8
Microphenocrysts PA-16-21	-2.57	1.45	0.92	10^{-8}	1.2
				10^{-9}	12.3

τ is expressed in years

4.7 Plagioclase Sr isotopes

Sr isotope results obtained on plagioclase crystals are summarized in Figure 14. Obtained ratios vary from 0.70549 to 0.70587 with an average 2σ uncertainty of ± 0.00004 and Rb/Sr under 0.02. Except for sample FP-15-15 which shows $^{87}Sr/^{86}Sr$ ratios overlapping within error, two of the three analyzed crystals in sample PA-16-01, and three of the four analyzed crystals in sample PA-16-21, display intracrystal variations outside analytical error. As a general trend, isotope profiles are marked either by more radiogenic cores overgrown by comparatively primitive rims, referred as A-type profiles (sample PA-16-01) or by more primitive cores overgrown by isotopically evolved rims, referred as U-type profiles (sample PA-16-21). Regardless of isotope zoning fashion, obtained $^{87}Sr/^{86}Sr$ ratios all fall within the isotopic spectrum of the GAV whole rock data (see blue area in Fig. 14; Garland et al., 1995).

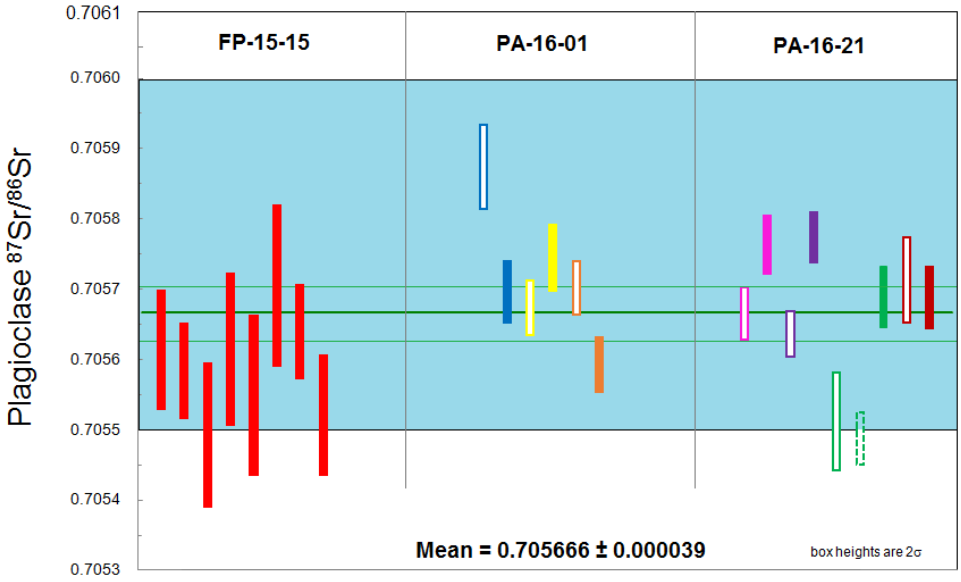

Figure 14 - Plagioclase *in situ* Sr isotope results in 2σ. The mean $^{87}Sr/^{86}Sr$ ratio and its envelopes are shown in thick and thin green lines, respectively. The blue area represents the GAV whole-rock $^{87}Sr/^{86}Sr$ interval (Garland et al., 1995). Bar length represent analytical errors. Sample FP-15-15 (red bars) have no spatial control relative to core-rim distance. On other samples, each color represent a single analyzed crystal. Empty and filled bars represent rims and cores, respectively. One stippled bar in sample PA-16-21 correspond to an intermediate analyzed position.

5 DISCUSSION

5.1 Reliability of *in situ* Sr isotopes

$^{87}Sr/^{86}Sr$ ratios determined via LA-ICP-MS might be hampered by the interference of ^{87}Rb. Thus, the latter must be corrected in order to guarantee reliable Sr isotope ratios. Rb has only one non-radiogenic isotope (^{85}Rb) and mass bias fractionation of Sr might be applied to correct the Rb fractionation. In order to minimize such problems, this technique must be applied for materials bearing very low Rb/Sr ratios (usually <0.05) (Ramos et al., 2004; Vroon et al., 2008). The high Sr signals (average 2.88 V) imply minimum Rb isobaric interference.and reliable $^{87}Sr/^{86}Sr$ ratios determinations.

5.2 Plagioclase CSD Shapes

In igneous rocks, the final texture results from a balance between kinetic, mechanical and equilibrium processes (e.g. Higgins, 2006). Concave-up CSDs have been reported in many natural rocks and attributed to a variety of processes such as physical mixing of distinct magmas (Higgins, 1996; Salisbury et al., 2008), textural coarsening (Higgins, 1998, 2002, 2011a,b), continuous to sudden changes of intensive magmatic variables (Cashman & Marsh, 1988; Armienti, 1994; Marsh, 1998; Ngonge et al., 2013; Preece et al., 2013; Fornaciai et al., 2015), heterogeneous nucleation (Špillar & Dolejš, 2015) or a combination of these processes. Concave-up CSDs were also obtained in run products of experimental studies, reinforcing the ubiquity of this feature in silicate melts (e.g. Burkhard, 2002; Pupier et al., 2008; Brugger & Hammer, 2010). The concave-up CSDs reported in this study display a turn-down to the left of their maximum population density (Fig. 13a). This effect cannot be an artifact due to inadequate spatial resolution as the smallest bin represented on the CSD graph – 0.147 to 0.233 mm – has distinct values among different samples and all of them were obtained following the same procedures. The scarcity of crystals under a critical size might be achieved by textural coarsening, also known as Ostwald ripening (Voorhees, 1992). As smaller crystals have a higher surface/volume ratio than larger ones, they contain a higher surface free energy, which might imply in their dissolution to give way to coarser crystals in melts kept under high temperature, close to the mineral *liquidus* (Higgins, 2011a). As coarsening progresses, the slope of the right side of the CSD decreases. The observation of rounded plagioclase crystals with curved contacts against each other and the relatively scarcity of small crystals associated with the exceptionally high GAV magmatic temperatures (Table 10), are consistent to coarsening as the main mechanism responsible for the concave-up curvature of the plagioclase CSD curves.

5.3 Magmatic Timescales

According to the CSD theory, the slope of the CSD curve is inversely proportional to the product of growth rate (G) and residence time (τ) (Marsh, 1988). However, G is a composition-dependent factor that may show a non-linear relation with cooling rates (e.g. Gibb, 1974; Swanson, 1977; Fenn, 1977). Cashman (1993) showed that increasing cooling rate by 100 will produce an insignificant tenfold increase in G values of plagioclase crystallizing from basaltic melts. This corroborated previous findings that plagioclase G commonly vary no more than one order of magnitude over a broad range of crystallization conditions (Cashman & Marsh, 1988; Cashman, 1990, 1992).

Plagioclase growth rates in acid magmas are still poorly constrained relative to mafic compositions. Estimates based on experimental studies (Geschwind & Rutherford, 1995; Hammer & Rutherford, 2002; Couch, 2003; Larsen, 2005; Brugger & Hammer, 2010), crystal size distribution (Cashman, 1992; Higgins, 1996; Hammer et al., 1999), compositional zoning patterns (McCanta et al., 2007), and in situ secondary ion mass spectrometry depth profiling (Genareau & Clarke, 2010), point to typical values ranging between 10^{-8} and 10^{-9} mm.s^{-1}. Using these growth rates, the obtained timescales are up to a few tens of years (Table 9). We prefer the slower growth rates and respective timescales for the phenocrysts (35-40 years), whereas faster growth rates are preferred for the microphenocryst population (1.5–1.8 years).

5.4 Eruptive Style

Acid lavas with large areal extents and low aspect ratios are rarely observed within intraplate volcanic provinces (Bonnichsen & Kauffman, 1987; Henry et al., 1988; Creaser & White, 1991; Green & Fitz, 1993). This is because acid magma often forms pyroclastic deposits produced by explosive instead of effusive volcanic activity (e.g. Cas & Wright, 1987). Previous studies have proposed textural and field criteria for distinguishing between strongly rheomorphic ignimbrites and extensive silicic lavas (Henry & Wolff, 1992). However, these criteria are often ambiguous, blurring a verdict about the eruptive style (e.g. Henry et al., 1988; Andrews & Branney, 2011).

Most studies regarding the emplacement model of the PMP acid volcanism are concentrated on the southernmost Palmas rocks, where an effusive eruption style seems to predominate (Garland et al., 1995; Waichel et al., 2012; Polo & Janasi, 2014; Polo et al., 2017; Rosseti et al., 2017; Guimarães et al., 2017; Simões et al., 2017; Lima et al., 2018). Similar investigations on the Chapecó-type rocks are much less abundant, but equally point to a predominant effusive emplacement (Garland et al., 1995; Janasi et al., 2007). However, the eruptive style of Palmas and Chapecó rocks is still a matter of debate and rejection is specially based on the acid nature of such rocks (Luchetti et al., 2018a, b).

Literature geothermometric data calculated using different models indicate that the Chapecó-type rocks crystallized from very hot magmas, with temperatures on the order of 950 – 1050°C (see Table

10). GAV magmas water content were estimated by input of whole rock major element composition (Table 2), plagioclase anorthite content (Nardy et al., 2011) and magmatic temperature (Table 10), using to be very low (below 1.5% H_2O, Fig. 17a; Waters & Lange, 2015). Afterwards, viscosity values were calculated by input of 1.5% H_2O, 1000°C and atmospheric pressure was probably close to $10^{4.01}$ Pa.s (Fig. 17b, Giordano et al., 2008). These results are considerably lower than intensive variables calculated for recent well-documented lavas with similar silica contents (59-65% SiO_2) that flowed far from their vents (viscosities ranging from 10^9 - 10^{11} Pa s; MacKay et al., 1998; Navarro-Ochoa et al., 2002; Harris et al., 2004).

Table 10 - Geothermometric data of the Chapecó rocks compiled from the literature. Temperatures are reported in Celsius degrees.

Authors	Mineral	Method	Temperature
Bellieni et al. (1986)	Coexisiting Ca-rich and Ca-poor pyroxene	Kretz (1982)	1130 ± 27
	Pigeonite	Ishii (1975)	1044 ± 15
	Plagioclase	Kudo & Weill (1970)	919 ± 26
	Plagioclase	Mathez (1973)	1018 ± 19
Garland et al. (1995)	Coexisiting Ca-rich and Ca-poor pyroxene	Kretz (1982)	1005 ± 30
	Coexisiting Ca-rich and Ca-poor pyroxene	Lindsley (1983)	1100 ± 50
Janasi et al. (2007)	Coexisiting Ca-rich and Ca-poor pyroxene	Lindsley (1983)	1000
	Plagioclase	Putirka (2005)	995 ± 25
	Zircon	Watson & Harrison (1983)	885 ± 15
	Apatite	Watson & Harrison (1984)	995 ± 15
Nardy et al. (2011)	Clinopyroxene	Putirka et al. (2003)	995 ± 26
	Plagioclase	Putirka (2005)	1033 ± 12
Luchetti et al. (2018b)	Clinopyroxene	Putirka et al. (2003)	969 ± 18
	Plagioclase	Putirka (2005)	1030 ± 4

Luchetti et al. (2018b) found similar viscosity values for the GAV magmas, but instead of an effusive eruptive style, the authors proposed a pyroclastic low fountaining origin for the respective deposits, and stressed the fact that similar or even less viscous magmas could fragment and behave explosively, according to experimental work performed on rhyolite melts of calc-alkaline (10^6 – 10^8 Pa s; Castro & Dingwell, 2009) or pantelleritic (10^4 – 10^6 Pa s; Di Genova et al., 2013; Campagnola et al., 2016; Hughes et al., 2017) compositions. However, we stress that direct comparison of rocks with such distinct compositions and geological settings has to be taken cautiously, because of the intricate relationship between composition and viscosity.

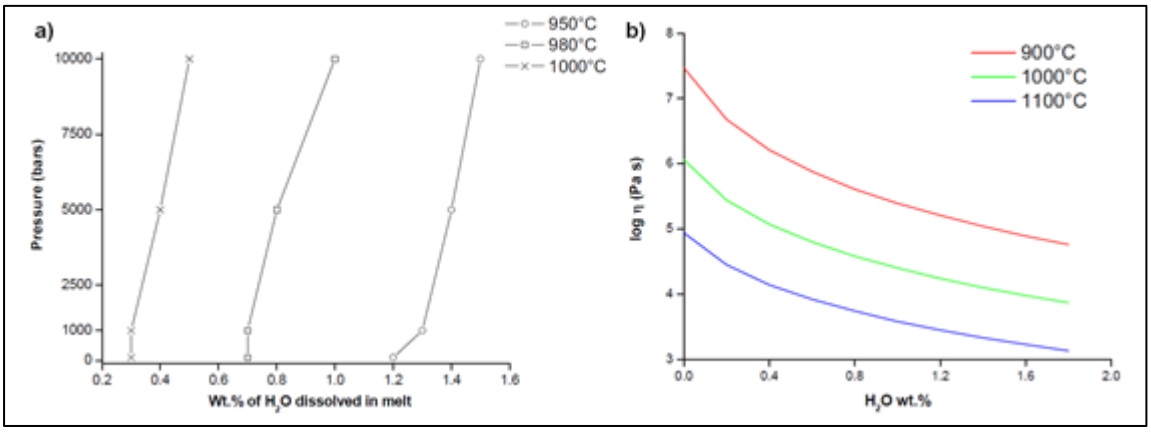

Figure 17 – A) Graph displaying the initial water contents (in weight %) of the GAV melts as a function of feasible temperature and pressure conditions. As there are no published glass/groundmass analyses of the GAV rocks, we considered the whole-rock as the initial melt composition. Above 1000°C the water contents are negligible and were omitted from the graph. Whole-rock compositions and corresponding plagioclase An contents required for the calculations were taken from Garland et al. (1995), Lopes (2008) and Nardy et al. (2011). Hygrometer model by Waters & Lange (2015). B) Graph displaying magmatic viscosities at atmospheric pressure as function of temperature and water dissolved in the GAV melts. Viscosity model by Giordano et al. (2008).

Based on the detailed investigation performed in this contribution, we offer an alternative explanation for the eruptive style of the GAV rocks. The steeper and larger population density of sample PA-16-21 (taken from the contact with the underlying basalts) along with the smaller plagioclase sizes, indicate a faster solidification of the lower border relative to the core of the volcanic body (Fig.13a; Table 9). Such stratigraphic controlled plagioclase size distribution has not been described in ignimbrites. Unfortunately, due to erosion, we did not find an equivalent upper border, but there is no obvious reason to believe it does not existed. Once formed, these fast-solidified borders would act as carapaces preventing further heat loss and reducing cooling rates at the interior of the flow via thermal insulation. Remote imaging of active lava fields has demonstrated how exceptional thermal insulation allow km-scale flowing of highly viscous acid lavas (Harris et al., 2004; Tuffen et al., 2013). The combination of low magmatic viscosities, high eruption rates and thermal insulation would have created a singular condition for an effusive emplacement of the GAV magmas, accounting for their sheet-like geometry. The identification of Chapecó (Ourinhos type; Janasi et al., 2007) and Palmas (Simões et al., 2017; Lima et al., 2018) dykes point to a fissural and shallow feeder system for the acid magmatism of the PEMP, in which such flows would be continuously fed and inflated by these dykes. The lack of basal breccias, typical at the contact of regular lava flows with the substrate due to the large temperature difference, would be explained by flow of the acid lavas over a relatively hot basaltic substrate that could prevent the development of fractures as on the lower portions of the GAV deposits.

5.5 The origin of banded structures

Banding in the acid rocks of the PEMP has been interpreted as a product of bomb coalescence and welding (dark bands, or ´blobs') followed by stretching due to flow-induced rheomorphism in a low-explosivity, fire fountain, eruptive scenario (Luchetti et al., 2018a). The authors did not discuss how such coalescence would produce the alternate colors observed in rocks.

Based on the detailed textural studies conducted in bands with different colors, we offer an alternative explanation for the origin of the banded structure based on: (1) the lack of broken crystals or of any kind of discontinuity observed in the groundmass under the petrographic microscope, CL and SEM images (2) the crosscut relationship between different bands and plagioclase major axis (3) the low viscosities and very low water contents dissolved in the magmas that would allow flowing even considering the high silica contents (4) the isotopic homogeneity recorded in plagioclase (5) the regional scale of the banding occurring through tens of meters thick volcanic deposits.

Magmatic flow banding has been attributed to magma mingling (e.g. Seaman et al., 1995) or repeated fracture and healing events (e.g. Tuffen et al., 2003; Gonnermann & Manga, 2005). However, such mechanisms seem unlikely here once GAV show no evidence of interaction between contrasting magmas and the observed banding is not planar neither shows abrupt contacts, respectively. The complete lack of textural evidence further disproves these hypotheses. Seaman et al. (2009) suggested that heterogeneous distribution of water in a rhyolitic lava flow could led to uneven undercooling rates, textures and colors, resulting in flow banding. Despite the very low water contents of the GAV magmas ($\leq$ 1.5%; Fig. 17), fluids certainly played a role on the eruptive style as indicated by the common presence of vesicles. Feldspar microlites in the massive matrix (MM) domains are commonly characterized by plagioclase cores (possibly andesine) mantled by potassium-rich alkali feldspar rims (see Fig. 10i); compositional pairs which are not in equilibrium (Nekvasil, 1992). This uncommon feature has also been described in the Merapi Dome andesitic lavas, Indonesia, where it was attributed to a sudden change in the melt evolution path over the feldspar ternary diagram, passing from the plagioclase + liquid field to the alkali feldspar + liquid field in response to syn-eruptive degassing, allowing overgrowth of the alkali feldspar over plagioclase (Hammer et al., 2000).

Interstitial quartz crystals in the MM indicate a highly evolved melt and relatively small undercooling rates allowing sluggish nucleation and growth of quartz. Apparently, degassing only occurred in very shallow levels and probably continued up to the surface (Nardy et al., 2011). We suggest that the GAV magmas were originally erupted as a homogeneous mixture of very hot lava carrying a ~15% crystal cargo containing plagioclase + pyroxene + Fe-Ti oxides and minor volatiles. The lack of flow banding and massive aspect of the groundmass on sample PA-16-21 (Figs. 7g, h and i), taken at the contact with the basaltic substrate, reinforce this interpretation, since rapid crystallization would prevent flow and continued growth of the plagioclase microphenocryst population. The high eruption rates and relatively low viscosities enabled a relatively fast outpouring

and spreading of the GAV magmas over the flat and probably hot basaltic paleosurface. Once the MM domains started crystallizing in the inner portions of the body, the exsolved fluids would have diffused away from the anhydrous intergrowth in a self-organized fashion, enriching the residual melt in water and decreasing its viscosity. The fluid might have escaped through open spaces as horizontal cooling cracks (Figs. 7e and f). As this process progressed, multiple discrete zones with contrasting rheology developed, separating high viscosity MM-dominated zones and low viscosity fluid-enriched zones. The driving force for this zonation was probably flow-induced shearing within the lava due to gradual viscosity rise. The same mechanism might explains the sub-horizontal, yet irregular, stretched geometry of the flow bands, parallel to the flow direction. Thus, MM-dominated domains apparently achieved their rheological lock-up early and crystallized to originate the dark bands. The residual fluid-enriched zones remained plastic and developed an interconnected permeable network that allowed open-system degassing, precluding explosive activity. This interpretation is supported by outcrop relationships in which light bands locally cross-cut dark bands. The sinuous and diffusive nature of the contacts between distinct bands are assigned to the very high magmatic temperatures, which enabled healing and interfingering between the two described rheological domains.

The different colors on both bands are probably a late to post-magmatic feature related to different porosities or mineralogical abundances (Fig. 12; Table 7). The awkward "vuggy" aspect of the feldspars in the PM domains could result from an extreme case of non-radiating spherulite crystallization due to very high undercooling rates. We do not discard the possibility of selective hydrothermalism, that would have led to quartz leaching and leaving the vuggy feldspar behind (dequartzification; e.g. Cathelineau, 1986; Petersson & Eliasson, 1997). To our knowledge, none such similar texture has been described to date.

5.6 Petrogenetic Insights

The analyzed rocks show 10-15% of plagioclase macrocrysts without any appreciable optical zoning. The homogeneity in CSD curves indicate that the large plagioclase crystals resided in a deep-seated reservoir under *supersolidus* conditions up to 40 years (Table 9). Plagioclase crystals show remarkably similar textural histories which, together with homogeneous Sr isotope signatures indicate that they shared a common deep reservoir where they grew as true phenocrysts, given that isotope signatures coincide with whole-rock data (Davidson et al., 2007).

We interpret plagioclase + pyroxene clusters described here are interpreted as disrupted mushy margins of the magmatic chamber and, in this sense, represent cumulate fragments or autholits. Similar occurrences have been described in intraplate silicic ignimbrites elsewhere (e.g. Barbey et al., 2005; Ellis & Wolf, 2012; Ellis et al., 2014). Very high magmatic temperatures, high crystallinity and limited interaction with the surrounding melt prevented plagioclase growth and enabled textural

maturation by coarsening of these cumulate fragments, as suggested by lobate and healed contacts. On the other hand, individual euhedral plagioclase crystals seem to have grown with available space, probably in the inner portions of the chamber, in a cogenetic magmatic system to that envisaged for the crystallization of the cumulate fragments, given their coincident chemical and isotopic signatures.

Subtle fluctuations in the $^{87}Sr/^{86}Sr$ ratios in plagioclase suggest protracted melt supply in the magmatic chamber. These recharge/reinjection events by similar cogenetic magma batches would redistribute the cumulate fragments and induce turbulence within the chamber, favoring homogenization. Moreover, it would prevent rapid cooling and provide the heat required for the long-lived crystallization interval of the plagioclase phenocrysts (Table 9).

6 SUMMARY AND CONCLUSIONS

Plagioclase phenocrysts from the trachydacites of the Guarapuava region occur preferably as single euhedral and unzoned crystals. There is a rare but common association of plagioclase in multimineralic clusters containing pyroxene ± Fe-Ti oxides. Combined petrography (via optical microscopy, SEM and CL) and CSD studies enabled the recognition of two distinct environments of plagioclase crystallization: one under deep-seated conditions with local action of coarsening, responsible for the crystallization of plagioclase phenocrysts and cumulate fragments or autholits, and another one at the shallow and/or surface level, responsible for the crystallization of plagioclase microphenocryst population. Magmatic timescales of crystallization of phenocrysts and microphenocrysts varied from a few tens of years (< 40 years; $G = 10^{-9} mm.s^{-1}$) to less than 2 years ($G = 10^{-8} mm.s^{-1}$), respectively. Plagioclase Sr isotopes showed a very subtle inter- and intracrystalline variation, with $^{87}Sr/^{86}Sr$ ratios overlapping with whole-rock isotopy, implying a relatively monogenetic magmatic system throughout GAV evolution.

The irregular flow banding observed in the majority of the GAV outcrops revealed to be defined by sinuous dark and light bands with distinct textures and mineral abundances. This structure formed during syn-eruptive degassing of the GAV magmas and heterogeneous distribution of water within it, leading to discrete zones organized in centimeter scale with distinct rheology. Banding is marked by alternation of porous and massive domains and the first probably result from the self-organized fluid exsolution that might have led to selective hydrotermalism and quartz leaching. Based on the intensive and rheological parameters calculated for the studied rocks, we argument an effusive eruptive style for the rocks outcropping in the Guarapuava region.

7 REFERENCES

ANDERSON, A. T. Probable relations between plagioclase zoning and magma dynamics, Fuego Volcano, Guatemala. **American Mineralogist**, v. 69, n. 7–8, p. 660–676, 1984.

ANDREWS, B. J.; GARDNER, J. E.; HOUSH, T. B. Repeated recharge, assimilation, and hybridization in magmas erupted from El Chichón as recorded by plagioclase and amphibole phenocrysts. **Journal of Volcanology and Geothermal Research**, v. 175, n. 4, p. 415–426, 2008.

ANDREWS, G. D. M. & BRANNEY, M. J. Emplacement and rheomorphic deformation of a large, lava-like rhyolitic ignimbrite: Grey's landing, southern Idaho.**Geological Society of America Bulletin**, v. 123(3), p. 725-743, 2011.

ARMIENTI, P.; PARESCHI, M. T.; INNOCENTI, F.; POMPILIO, M. Effects of magma storage and ascent on the kinetics of crystal growth - The case of the 1991-93 Mt. Etna eruption. **Contributions to Mineralogy and Petrology**, v. 115, n. 4, p. 402–414, 1994.

BAKSI, A. K. Paraná flood basalt volcanism primarily limited to ~1 Myr beginning at 135 Ma: New $^{40}Ar/^{39}Ar$ ages for rocks from Rio Grande do Sul and critical evaluation of published radiometric data. Journal of Volcanology and Geothermal Research. Available on line. 2017.

BARBEY, P.; AYALEW, D.; YIRGU, G. Insight into the origin of gabbro-dioritic cumulophyric aggregates from silicic ignimbrites: Sr and Ba zoning profiles of plagioclase phenocrysts from Oligocene Ethiopian Plateau rhyolites. **Contributions to Mineralogy and Petrology**, v. 149, n. 2, p. 233–245, 2005.

BARRETO, C. J. S.; LAFON, J. M.; LIMA, E. F.; SOMMER, C. A. Geochemical and Sr-Nd-Pb isotopic insight into the low-Ti basalts from southern Paraná Igneous Province, Brazil: The role of crustal contamination. **International Geology Review**, v. 58, n. 11, p. 1324–1349, 2016.

BELLIENI, G.; COMIN-CHIARAMONTI, P.; MARQUES, L. S.; MELFI, A. J.; NARDY, A. J. R.; PAPATRECHAS, C.; PICCIRILLO, E. M.; ROINSENBERG, A.; STOLFA, D. Petrogenetic aspects of acid and basaltic lavas from the Paraná Plateau (Brazil): geological, mineralogical and petrochemical relationships. **Journal of Petrology**, v. 27 (4), p. 915-944, 1986.

BONNICHSEN, B.; KAUFFMAN, D. F. Physical features of rhyolite lava flows in the Snake River Plain volcanic province, Southwest Idaho. **Geological Society of America**, Special Paper 212, 1987.

BROWNE, B. L..; EICHELBERGER, J. C.; PATINO, L.C.; VOGEL, T. A.; UTO, K.; HOSHIZUMI, H. Magma mingling as indicated by texture and Sr / Ba ratios of plagioclase phenocrysts from Unzen volcano, SW Japan. **Journal of Volcanology and Geothermal Research**, v. 154, n. 1–2, p. 103–116, 2006.

BRUGGER, C. R.; HAMMER, J. E. Crystal size distribution analysis of plagioclase in experimentally decompressed hydrous rhyodacite magma. **Earth and Planetary Science Letters**, v. 300, n. 3–4, p. 246–254, 2010.

BRYAN, S. E.; ERNST, R. E. Revised definition of Large Igneous Provinces (LIPs). **Earth-Science Reviews**, v. 86, n. 1–4, p. 175–202, 2008.

BRYAN, S. E.; PEATE, I. U.; PEATE, D. W.; SELF, S.; JERRAM, D. A.; MAWBY, M. R..; MARSH, J.S.; MILLER, J.A. The largest volcanic eruptions on Earth. **Earth-Science Reviews**, v. 102, n. 3–4, p. 207–229, 2010.

CAMPAGNOLA, S.; ROMANO, C.; MASTIN, L. G.; VONA, A. Confort 15 model of conduit dynamics: applications to Pantelleria Green Tuff and Etna 122 BC eruptions. **Contributions to Mineralogy and Petrology**, v. 171, n. 6, 2016.

CAS, R. & WRIGHT, J. 1987. Volcanic Successions – Modern and Ancient. Chapman & Hall. 528 pages.

CASHMAN, K. V. Textural constraints on the kinetics of crystallization of igenous rocks. **Reviews in Mineralogy and Geochemistry**, v. 24(1), p. 259 – 314.,1990.

CASHMAN, K. V. Groundmass crystallization of Mount St. Helens dacite, 1980-1986: a tool for interpreting shallow magmatic processes. **Contributions to Mineralogy and Petrology**, v. 109, n. 4, p. 431–449, 1992.

CASHMAN, K. V. Relationship between plagioclase crystallization and cooling rate in basaltic melts. **Contributions to Mineralogy and Petrology**, v. 113, n. 1, p. 126–142, 1993.

CASHMAN, C. V; MARSH, B. D. Crystal size distribution (CSD) in rocks and the kinetics and dynamics of crystallisation. **Contributions to Mineralogy and Petrology**, v. 99, p. 277–291, 1988.

CASHMAN, K.; BLUNDY, J. Degassing and crystallization of ascending andesite and dacite. **Philosophical Transactions of the Royal Society A: Mathematical, Physical and Engineering Sciences**, v. 358, n. 1770, p. 1487–1513, 2000.

CASTRO, J. M.; DINGWELL, D. B. Rapid ascent of rhyolitic magma at Chaitén volcano, Chile. **Nature**, v. 461, n. 7265, p. 780–783, 2009.

CATHELINEAU, M. The hydrothermal alkali metasomatism effects on granitic rocks: quartz dissolution and related sub-solidus changes. **Journal of Petrology**, v. 27, n. 4, p. 945-965. 1986.

COMIN-CHIARAMONTI, P. & GOMES, C.B. An introduction to the alkaline and alkaline-carbonatitic magmatism in and around the Paraná Basin. In: "The Mesozoic to Cenozoic Alkaline Magmatism in the Brazilian Platform". Comin-Chiaramonti, P. & Gomes, C.B. Editora da Universidade de São Paulo, 2005.

COOTE, A. C.; SHANE, P. Crystal origins and magmatic system beneath Ngauruhoe volcano (New Zealand) revealed by plagioclase textures and compositions. **Lithos**, v. 260, p. 107–119, 2016.

COUCH, S. The Kinetics of Degassing-Induced Crystallization at Soufriere Hills Volcano, Montserrat. **Journal of Petrology**, v. 44, n. 8, p. 1477–1502, 2003.

CREASER R. A.; WHITE, A. J. R. Yardea dacite – Large volume, high temperature felsic volcanism from the middle Proterozoic of South Australia. **Geology**, v. 19, p. 48-51, 1991.

DAVIDSON, J.P.; TEPLEY, F.; PALACZ, Z.; MEFFAN-MAIN, S. Magma recharge, contamination and residence times revealed by in situ laser ablation isotopic analysis of feldspar in volcanic rocks. **Earth and Planetary Science Letters**, v. 184, n. 2, p. 427–442, 2001.

DAVIDSON, J. P.; MORGAN, D. J.; CHARLIER, B. L. A; HARLOU, R.; HORA, J. M. Microsampling and Isotopic Analysis of Igneous Rocks: Implications for the Study of Magmatic Systems. **Annual Review of Earth and Planetary Sciences**, v. 35, n. 1, p. 273–311, 2007.

DAVIDSON, J. P. & TEPLEY, F. J. Recharge in volcanic systems: Evidence from isotope profiles of phenocrysts. **Science**, v. 275, n. 5301, p. 826–829, 1997.

DI GENOVA, D.; ROMANO, C.; HESS, K.U.; VONA, A.; POE, B. T.; GIORDANO, D.; DINGWELL, D. B.; BEHRENS, H. The rheology of peralkaline rhyolites from Pantelleria Island. **Journal of Volcanology and Geothermal Research**, v. 249, p. 201–216, 2013.

DIAS, F. R. A.; POLO, L. A.; JANASI, V. A.; CARVALHO, F .M .S. Volcanic glass in Cretaceous dacites and rhyolites of the Paraná Magmatic Province, southern Brazil: characterization and quantification by XRD- Rietveld. **Journal of Volcanology and Geothermal Research**, available online 26 august, 2017.

ELLIS, B. S.; BACHMANN, O.; WOLFF, J. A. Cumulate fragments in silicic ignimbrites: The case of the Snake River Plain. **Geology**, v. 42, n. 5, p. 431–434, 2014.

ELLIS, B. S.; WOLFF, J. A. Complex storage of rhyolite in the central Snake River Plain. **Journal of Volcanology and Geothermal Research**, v. 211–212, n. June 2017, p. 1–11, 2012.

FENN, P. M. The Nucleation and Growth of Alkati Feldspars From Hydrous Melts. **Canadian Mineralogist**, v. 15, p. 135–161, 1977.

FLORISBAL, L. M.; JANASI, V. A.; BITENCOURT, M. F.; NARDI, L. V. S.; MARTELETO, N. S. Geological, geochemical and isotope diversity of ~134 Ma dykes from the Florianópolis dyke swarm, Paraná Magmatic Province: Geodynamic controls on petrogenesis. **Journal of Volcanology and Geothermal Research**, v. 355, n. 15, p. 181 - 203, 2018.

FORNACIAI, A.; PERINELLI, C.; ARMIENTI, P.; FAVALLI, M. Crystal size distributions of plagioclase in lavas from the July–August 2001 Mount Etna eruption. **Bulletin of Volcanology**, v. 77, n. 8, 2015.

FRANK, H. T.; GOMES, M. E. B.; FORMOSO, M. L. L. Review of the areal extent and the volume of the Serra Geral Formation, paraná Basin, South America. **Pesquisas em Geociencias**, v. 36, n. 1, p. 49–57, 2009.

FREITAS, V.A. A geração de magmas ácidos na Província Magmática do Paraná, região de Piraju-Ourinhos (SP): uma contribuição da geoquímica isotópica e de elementos traços em rochas e minerais. **Unpublished masters thesis**. Universidade de São Paulo, 2009.

GARLAND, F.; HAWKESWORTH, C. J.; MANTOVANI, M. S. M Description and petrogenesis of the Paraná rhyolites, southern Brazil. **Journal of Petrology**, v. 36, p. 1193-1227, 1995.

GAGNEVIN, D.; WAIGHT, T.E.; DALY, J.S; POLI, G.; CONTICELLI, S. Insights into magmatic evolution and recharge history in Capraia Volcano (Italy) from chemical and isotopic zoning in plagioclase phenocrysts. **Journal of Volcanology and Geothermal Research**, v. 168, n. 1–4, p. 28–54, 2007.

GENAREAU, K.; CLARKE, A. B. In situ measurements of plagioclase growth using SIMS depth profiles of $^{7}Li/^{30}Si$: A means to acquire crystallization rates during short-duration decompression events. **American Mineralogist**, v. 95, n. 4, p. 592–601, 2010.

GESCHWIND, C. H.; RUTHERFORD, M. J. Crystallization of microlites during magma ascent: the fluid mechanics of 1980-1986 eruptions at Mount St Helens. **Bulletin of Volcanology**, v. 57, n. 5, p. 356–370, 1995.

GIACOMONI, P. P.; FERLITO, C.; COLTORTI, M.; BONADIMAN, C.; LANZAFAME, G. Plagioclase as archive of magma ascent dynamics on “open conduit” volcanoes: The 2001-2006 eruptive period at Mt. Etna. **Earth-Science Reviews**, v. 138, p. 371–393, 2014.

GIBB, F. G. F. Supercooling and the Crystallization of Plagioclase from a Basaltic Magma. **Mineralogical Magazine**, v. 39, n. 306, p. 641–653, 1974.

GINIBRE, C.; WÖRNER, G.; KRONZ, A. Minor- and trace-element zoning in plagioclase: Implications for magma chamber processes at Parinacota volcano, northern Chile. **Contributions to Mineralogy and Petrology**, v. 143, n. 3, p. 300–315, 2002.

GIORDANO, D.; RUSSELL, J. K.; DINGWELL, D. B. Viscosity of magmatic liquids: A model. **Earth and Planetary Science Letters**, v. 271, n. 1–4, p. 123–134, 2008.

GONNERMANN, H. M.; MANGA, M. Flow banding in obsidian: A record of evolving textural heterogeneity during magma deformation. **Earth and Planetary Science Letters**, v. 236, n. 1–2, p. 135–147, 2005.

GREEN, J. C.; FITZ, T. J. Extensive felsic lavas and rheoignimbrites in the Keweenawan Midcontinent Rift plateau volcanics, Minnesota: petrographic and field recognition. **Journal of Volcanology and Geothermal Research**, v. 54, n. 3–4, p. 177–196, 1993.

GROVE, T. L.; BAKER, M. B.; KINZLER, R. J. Coupled CaAl-NaSi diffusion in plagioclase feldspar: Experiments and applications to cooling rate speedometry. **Geochimica et Cosmochimica Acta**, v. 48, n. 10, p. 2113–2121, 1984.

GUIMARÃES, L. F.; RAPOSO, M .I. B.; JANASI, V. A.; CAÑON-TAPIA, E.; POLO, L. A.. An AMS study of different silicic units from the southern Paraná-Etendeka Magmatic Province in Brazil: Implications for the identification of flow directions and local sources. **Journal of Volcanology and Geothermal Research**, 2017. In press.

GUIMARÃES, L. F.; CAMPOS, C. D.; JANASI, V. A.; LIMA, E. F.; DINGWELL, D. B. Flow and fragmaentation patterns in the silicic feeder system and related deposits in the Paraná-Etendeka Magmatic Province, São Marcos, South Brazil. **Journal of Volcanology Research**, 2018. In press.

HAMMER, J. E.; CASHMAN, K. V.; HOBLITT, R. P.; NEWMAN, S. Degassing and microlite crystallization during pre-climactic events of the 1991 eruption of Mt. Pinatubo, Philippines. **Bulletin of Volcanology**, v. 60, n. 5, p. 355–380, 1999.

HAMMER, J. E.; CASHMAN, K. V.; VOIGHT, B. Magmatic processes revealed by textural and compositional trends in Merapi dome lavas. **Journal of Volcanology and Geothermal Research**, v. 100, n. 1–4, p. 165–192, 2000.

HAMMER, J.; RUTHERFORD, M. J. An experimental study of the kinetics of decompression-induced crystallization in slicic melt. **Journal of Geophysical Research**, v. 107, n. 0, 2002.

HARRIS, C. & MILNER, S. Crustal origin for the Paraná rhyolites: Discussion of 'Description and petrogenesis of the Paraná rhyolites, Southern Brazil' by Garland *et al*. (1995). **Journal of Petrology**, v. 38, n. 2, p. 299-302. 1997.

HARRIS, A. J. L.; FLYNN, L. P.; MATIAS, O.; ROSE, W. I.; CORNEJO, J. The evolution of an active silicic lava flow field: An ETM+ perspective. **Journal of Volcanology and Geothermal Research**, v. 135, n. 1–2, p. 147–168, 2004.

HARRISON, T. M.; WATSON, E. B. The behavior of apatite during crustal anatexis: Equilibrium and kinetic considerations. **Geochimica et Cosmochimica Acta**, v. 48, n. 7, p. 1467–1477, 1984.

HAWKESWORTH, C. J., GALLAGHER, K., KELLEY, S., MANTOVANI, M., PEATE, D.W., REGELOUS, M., ROGERS, N. W. Paraná magmatism and the opening of the south Atlantic ocean. In: Alabaster, A., Pankhurst, R. (Eds.), Magmatism and Causes of Continental Break-up. Geological Society Special Publications, vol. 68, pp. 221-240. London. 1992.

HENRY, C. D.; PRICE G.P.; RUBBIN, J.N.; PARKER, D.F.; WOLFF, J.A.; SELF, S.; FRANKLIN, R.; BARKER, D.S. Widespread, lavalike silicic volcanic rocks of Trans-Pecos Texas. **Geology**, v. 16, n. 6, p. 509–512, 1988.

HIGGINS, M. D. Determination of crystal morphology and size from bulk measurements on thin sections: numerical modelling. **American Mineralogist**, v. 79, n. December, p. 113–119, 1994.

HIGGINS, M. D. Magma dynamics beneath Kameni volcano, Thera, Greece, as revealed by crystal size and shape measurements. **Journal of Volcanology and Geothermal Research**, v. 70, n. 1–2, p. 37–48, 1996.

HIGGINS, M. D. Measurement of crystal size distributions. **American Mineralogist**, v. 85, n. 9, p. 1105–1116, 2000.

HIGGINS, M. D. A crystal size-distribution study of the Kiglapait layered mafic intrusion, Labrador, Canada: Evidence for textural coarsening. **Contributions to Mineralogy and Petrology**, v. 144, n. 3, p. 314–330, 2002.

HIGGINS, M.D. 2006. Quantitative textural measurements in igneous and metamorphic petrology. Cambridge University Press, 276 pages.

HIGGINS, M. D. Textural coarsening in igneous rocks. **International Geology Review**, v. 53, n. 3–4, p. 354–376, 2011a.

HIGGINS, M. D. Quantitative petrological evidence for the origin of K-feldspar megacrysts in dacites from Taapaca volcano, Chile. **Contributions to Mineralogy and Petrology**, v. 162, n. 4, p. 709–723, 2011b.

HODELL, D. A.; MEAD, G. A.; MUELLER, P. A. Variation in the strontium isotopic composition of seawater (8 Ma to present): Implications for chemical weathering rates and dissolved fluxes to the oceans. Chemical **Geology**, v. 80, 1990.

HORST, W.; TAGAI, T.; KOREKAWA, M.; JAGODZINSKI, H. Modulated structure of a plagioclase Angz: Theory and structure determination. **Zeitschrift für Kristallographie**, v. 157, p. 233 – 250. 1981.

HUGHES, E. C.; NEAVE, D. A.; DOBSON, K. J.; WITHERS, P. J.; EDMONDS, M. How to fragment peralkaline rhyolites: Observations on pumice using combined multi-scale 2D and 3D imaging. **Journal of Volcanology and Geothermal Research**, v. 336, p. 179–191, 2017.

ISHII, T. The relations between temperature and composition of pigeonite in some lavas and their application to geothermometry **Mineralogical Journal**, 1975.

JANASI V. A..; MONTANHEIRO, T. J.; FREITAS, V. A.; REIS, P. M.; NEGRI, F. A.; DANTAS, F. A. Geology, petrography and geochemistry of the acid volcanism of the Paraná Magmatic Province in the Piraju-Ourinhos region, SE Brazil. **Revista Brasileira de Geociências**, v. 37(4), p. 745-759, 2007.

JANASI, V. A.; DE FREITAS, V. A.; HEAMAN, L. H. The onset of flood basalt volcanism, Northern Paraná Basin, Brazil: A precise U-Pb baddeleyite/zircon age for a Chapecó-type dacite. **Earth and Planetary Science Letters**, v. 302, n. 1–2, p. 147–153, 2011.

KRETZ, R. Transfer and exchange equilibria in a portion of the pyroxene quadrilateral as deduced from natural and experimental data. **Geochimica et Cosmochimica Acta**, v. 46, n. 3, p. 411–421, 1982.

KUDO, A. M. & WEILL, D. F. An igneous plagioclase thermometer. **Contributions to Mineralogy and Petrology**, v. 25(1), p. 52-65, 1970.

LARSEN, J. F. Experimental study of plagioclase rim growth around anorthite seed crystals in rhyodacitic melt. **American Mineralogist**, v. 90, p. 417-427, 2005.

LIMA, E. F.; WAICHEL, B. L.; ROSSETI, L. M. M.; SOMMER, C. A.; SIMÕES, M. S. Feeder systems of acidic lava flows from the Paraná-Etendeka Igneous Province in southern Brazil and their implications for eruption style. **Journal of South American Earth Sciences**, v. 81, p. 1–9, 2018.

LINDSLEY, D. H. Pyroxene thermometry. **American Mineralogist**, v. 68, n. 5–6, p. 477–493, 1983.

LOFGREN, G. An experimental study of plagioclase crystal morphology: isothermal crystallization. **Journal of Science**, v. 274, p. 243-273, 1980.

LOPES, K. Caracterização morfológica, petrográfica e química dos derrames da Província Magmática do Paraná com ênfase para as rochas aflorantes no município de Guarapuava-PR. **Unpublished masters thesis**. Universidade Federal do Paraná, 2008.

LUCHETTI, A. C. F.; NARDY, A. J. R.; MACHADO, F. B.; MADEIRA, J. E. O.;ARNOSIO, J. M.. New insights on the occurrence of peperites and sedimentary deposits within the silicic volcanic sequences of the Paraná Magmatic Province, Brazil. **Solid Earth**, v. 5, n. 1, p. 121–130, 2014.

LUCHETTI, A. C. F.; GRAVLEY, D.M.; GUALDA, G. A. R.; NARDY, A. J. R. Textural evidence for high-grade ignimbrites formed by low-explosivity eruptions, Paraná Magmatic Province, southern Brazil. **Journal of Volcanology and Geothermal Research**, v. 355, p. 87-97, 2018a.

LUCHETTI, A. C. F.; NARDY, A. J. R.; MADEIRA, J. Silicic, high- to extremely high-grade ignimbrites and associated deposits from the Paraná Magmatic Province, southern Brazil. **Journal of Volcanology and Geothermal Research**, v. 355, p. 270-286, 2018b.

MACKAY, M. E.; ROWLAND, S. K.; MOUGINIS-MARK, P. J.; GARBEIL, H. Thick lava flows of Karisimbi Volcano, Rwanda: Insights from SIR-C interferometric topography. **Bulletin of Volcanology**, v. 60, n. 4, p. 239–251, 1998.

MARSH, B. D. Crystal Size Distribution (CSD) in rocks and the kinetics and dynamics of crystallization. **Contributions to Mineralogy and Petrology**, v. 99(3), p. 277 – 291, 1988.

MARSH, B. D. On the interpretation of crystal size distributions in magmatic systems. **Journal of Petrology**, v. 39, n. 4, p. 553–599, 1998.

MATHEZ, E. A. Refinement of the Kudo-Weill plagioclase thermometer and its application to basaltic rocks. **Contributions to Mineralogy and Petrology**, v. 41(1), p. 61-72, 1973.

MCCANTA, M. C.; RUTHERFORD, M. J.; HAMMER, J. E. Pre-eruptive and syn-eruptive conditions in the Black Butte, California dacite: Insight into crystallization kinetics in a silicic magma system. **Journal of Volcanology and Geothermal Research**, v. 160, n. 3–4, p. 263–284, 2007.

MORA, C. I. & RAMSEYER, K. Cathodoluminescence of coexisting plagioclases, Boehls-Butte anorthosite, CL activators and fluid-flow paths. **American Mineralogist**, V. 77, P. 1258-1265, 1992.

MORGAN, D. J.; JERRAM, D. A.; CHERTKOFF, D. G.; DAVIDSON, J. P.; PEARSON, D. G.; KRONZ, A.; NOWELL, G. M. Combining CSD and isotopic microanalysis: Magma supply and mixing processes at Stromboli Volcano, Aeolian Islands, Italy. **Earth and Planetary Science Letters**, v. 260, n. 3–4, p. 419–431, 2007.

NARDY, A. J. R.; OLIVEIRA, M. A. F.; BETANCOURT, R. H. S.; VERDUGO; D. R. H.; MACHADO, F. B. Geologia e estratigrafia da Formação Serra Geral. **Geociências**, v. 21, p. 15-32, 2002.

NARDY, A. J. R.; MACHADO, F. B.; OLIVEIRA, M. A. F. As rochas vulcânicas mesozóicas ácidas da Bacia do Paraná: litoestratigrafia e considerações geoquímico-estratigráficas. **Revista Brasileira de Geociências**, v. 38, n. 1, p. 178–195, 2008.

NARDY, A. J. R.; ROSA, M.C.; LUCHETTI, A. N. F.; FERREIRA, M. L. C.; MACHADO, F. B.; OLIVEIRA, M. A. F. Parâmetros físicos pré-eruptivos do magmatismo ácido da província magmática do Paraná: Resultados preliminares. **Geociências**, v. 30, n. 4, p. 575–588, 2011.

NEKVASIL, H. Ternary feldspar crystallization in high-temperature felsic magmas. **American Mineralogist**, v. 77, n. 5–6, p. 592–604, 1992.

NGONGE, E. D.; ARCHANJO, C. J.; HOLLANDA, M. H. B. M. Plagioclase crystal size distribution in some tholeiitic mafic dykes in Cabo Frio-Buzios, Rio de Janeiro, Brazil. **Journal of Volcanology and Geothermal Research**, v. 255, n. APRIL 2013, p. 26–42, 2013.

NIXON, G. T.; PEARCE, T. H. Laser-interferometry study of oscillatory zoning in plagioclase: The record of magma mixing and phenocryst recycling in calc-alkaline magma chambers, Iztaccihuatl volcano, Mexico. **American Mineralogist**, v. 72, p. 1144, 1987.

PAGEL, M.; BARBIN, V.; BLANC, P.; OHNENSTETTER, D. 2000. Cathodoluminescence in Geosciences. Springer, Berlin.

PEARCE, N. J. G.; PERKINS, W. T.; WESTGATE, J. A.; GORTON, M.P.; JACKSON, S.E.; NEAL, C. R.; CHENEREY, S. P.. A compilation of new and published major and trace element data for NIST SRM 610 and NIST SRM 612 glass reference materials. **Geostandards Newsletter**, v. 21, n. 1, p. 115–144, 1997.

PEATE, D. W. The Parana-Etendeka Province. In: Large Igneous Provinces: continental, oceanic, planetay flood volcanism. Geophysical Monography, 100, American Geophysical Union, 438 p., 1997.

PEATE, D. W.; HAWKESWORTH, C. J.; MANTOVANI, M. S. M. Chemical stratigraphy of the Paraná lavas, South America: classification of magma types and their spatial distribution. **Bulletin of Volcanology**, v.55, p. 119-139, 1992.

PETERSSON, J. & ELIASSON, T. Mineral evolution and element mobility during episyenitization (dequartzification) and albitization in the postkinematic Bohus granite, southwest Sweden. **Lithos**, v. 42, p. 123-146. 1997.

PINTO, V. M.; HARTMANN, L. A.; SANTOS, J .A. S.; MCNAUGHTON, N. J.; WILDNER, W. Zircon U-Pb geochronology from the Paraná bimodal volcanic province support a brief eruptive cycle at ~135Ma. **Chemical Geology**, v. 281, n. 1–2, p. 93–102, 2011.

PIOCHI, M.; MASTROLORENZO, G.; PAPPALARDO, L. Magma ascent and eruptive processes from textural and compositional features of Monte Nuovo pyroclastic products, Campi Flegrei, Italy. **Bulletin of Volcanology**, v. 67, n. 7, p. 663–678, 2005.

POLO, L. A. & JANASI, V. DE A. Volcanic stratigraphy of intermediate to acidic rocks in southern Paraná Magmatic Province, Brazil. **Geologia USP. Série Científica**, v. 14, n. 2, p. 83–100, 2014.

POLO, L. A.; JANASI, V. A.; GIORDANO, D.; LIMA, E. F.; CAÑON-TAPIA, E.;ROVERATO, M. Effusive silicic volcanism in the Paraná Magmatic Province, South Brazil: Physico-chemical conditions of storage and eruption and considerations on the rheological behavior during emplacement. **Journal of Volcanology and Geothermal Research**, 2017.

PUPIER, E.; DUCHENE, S.; TOPLIS, M. J. Experimental quantification of plagioclase crystal size distribution during cooling of a basaltic liquid. **Contributions to Mineralogy and Petrology**, v. 155, n. 5, p. 555–570, 2008.

PUTIRKA, K. D. Igneous thermometers and barometers based on plagioclase + liquid equilibria: Tests of some existing models and new calibrations. **American Mineralogist**, v. 90, n. 2–3, p. 336–346, 2005.

PUTIRKA, K. D.; MIKAELIAN, H.; RYERSON, F.; SHAW, H. New clinopyroxene-liquid thermobarometers for mafic, evolved, and volatile-bearing lava compositions, with applications to lavas from Tibet and the Snake River Plain, Idaho. **American Mineralogist**, v. 88, p. 1542-1554, 2003.

RAMOS, F. C.; WOLFF, J. A.; TOLLSTRUP, D. L. Measuring $^{87}Sr/^{86}Sr$ variations in minerals and groundmass from basalts using LA-MC-ICPMS. **Chemical Geology**, v. 211, n. 1–2, p. 135–158, 2004.

RAMOS, F. C.; TEPLEY, F. J. Inter- and Intracrystalline Isotopic Disequilibria: Techniques and Applications. **Reviews in Mineralogy and Geochemistry**, v. 69, n. 1, p. 403–443, 2008.

RANDOLPH, A.D. & LARSON, M.A., 1971. Theory of particulate processes. *Academic Press*, New York, 251 p.

RASBAND, W.S. 2010. ImageJ. U.S. National Institute of Health, Bethesda, Maryland, USA. http://www.rsb.info.nih.gov/ij/

RENNE, P.; ERNESTO, M;, PACCA, I. G; COE, R. S.; GLEN, J. M., PREVÓT, M., PERRIN, M. The age of the Paraná flood volcanism, rifting and Gondwanaland, and the Jurassic-Cretaceous boundary. **Science**, v. 258, p. 975-979, 1992.

RENNE, P. R.; DECKART, K.; ERNESTO, M.; FÉRAUD, G.; PICCIRILLO, E.M. Age of the Ponta Grossa dike swarm (Brazil), and implications to Paraná flood volcanism. **Earth and Planetary Science Letters**, v. 144, n. 1–2, p. 199–211, 1996.

ROCHA-JÚNIOR, E. R. V; MARQUES, L. S.; BABINSKY, M.; NARDY, A. J. R.; FIGUEIREDO, A. M. G.; MACHADO, F. B. Sr-Nd-Pb isotopic constraints on the nature of the mantle sources involved in the genesis of the high-Ti tholeiites from northern Paraná Continental Flood Basalts (Brazil). **Journal of South American Earth Sciences**, v. 46, p. 9–25, 2013.

ROSSETTI, L.; LIMA, E. F.; WAICHEL, B. L.; HOLE, M. J.; SIMÕES, M. S.; SCHERER, C. M. S. Lithostratigraphy and volcanology of the Serra Geral Group, Paraná-Etendeka Igneous Province in Southern Brazil: Towards a formal stratigraphical framework. **Journal of Volcanology and Geothermal Research**, p. 1–17, 2016.

RUPRECHT, P.; WÖRNER, G. Variable regimes in magma systems documented in plagioclase zoning patterns: El Misti stratovolcano and Andahua monogenetic cones. **Journal of Volcanology and Geothermal Research**, v. 165, n. 3–4, p. 142–162, 2007.

SALISBURY, M. J.; BOHRSON, W. A.; CLYNNE, M. A.; RAMOS, F. C.; HOSKIN, P. Multiple plagioclase crystal populations identified by crystal size distribution and in situ chemical data: Implications for timescales of magma chamber processes associated with the 1915 eruption of Lassen Peak, CA. **Journal of Petrology**, v. 49, n. 10, p. 1755–1780, 2008.

SEAMAN, S. J.; SCHERER, E. E.; STANDISH, J. J. Multistage magma mingling and the origin of the flow banding in the Aliso lava dome, Tumacacori Mountains, South Arizona.Journal of Geophysical Research, v. 100, p. 8381 – 8398, 1995.

SEAMAN, S. J.; DYAR, M. D.; MARINKOVIC, N. The effects of heterogeneity in magma water concentration on the development of flow banding and spherulites in rhyolitic lava. **Journal of Volcanology and Geothermal Research**, v. 183, n. 3–4, p. 157–169, 2009.

SHANE, P. Contrasting plagioclase textures and geochemistry in response to magma dynamics in an intra-caldera rhyolite system, Okataina volcano. **Journal of Volcanology and Geothermal Research**, v. 297, p. 1–10, 2015.

SIMÕES, M. S. et al. Structures and lithofacies of inferred silicic conduits in the Paraná-Etendeka LIP, southernmost Brazil. **Journal of Volcanology and Geothermal Research**, 2017. In press.

SINGER, B. S.; DUNGAN, M. A.; LAYNE, G. D. Textures and Sr, Ba, Mg, Fe, K, and Ti compositional profiles in volcanic plagioclase: clues to the dynamics of calc-alkaline magma chambers. **American Mineralogist**, v. 80, n. 7–8, p. 776–798, 1995.

ŠPILLAR, V.; DOLEJŠ, D. Heterogeneous nucleation as the predominant mode of crystallization in natural magmas: numerical model and implications for crystal–melt interaction. **Contributions to Mineralogy and Petrology**, v. 169, n. 1, 2015.

SWANSON, S. E. Relation of nucleation and crystal-growth rate to the development of granitic textures. **American Mineralogist**, v. 62, p. 966–978, 1977.

SYLVESTER, P. J. 2008. Laser ablation-ICP-MS in the earth sciences: Current practices and outstanding issues. Mineralogical Association of Canda, 348 pages.

THIEDE, D. S. & VASCONCELOS, P. M. Paraná flood basalts: Rapid extrusion hypothesis confirmed by new $^{40}Ar/^{39}Ar$ results. **Geology**, v. 38, p. 747-750, 2010.

TUFFEN, H.; DINGWELL, D. B.; PINKERTON, H. Repeated fracture and healing of silicic magma generate flow banding and earthquakes? **Geology**, v. 31, n. 12, p. 1089–1092, 2003.

TUFFEN, H.; JAMES, M. R.; CASTRO, J. M.; SCHIPPER, C. I. Exceptional mobility of an advancing rhyolitic obsidian flow at Cordón Caulle volcano in Chile. **Nature Communications**, v. 4, p. 1–7, 2013.

VICCARO, M.; GIACOMINI, P.P.; FERLITO, C.; CRISTOFOLINI, R.. Dynamics of magma supply at Mt. Etna volcano (Southern Italy) as revealed by textural and compositional features of plagioclase phenocrysts. **Lithos**, v. 116, n. 1–2, p. 77–91, 2010.

VOORHESS, P.W. Ostwald ripening of two-phases mixtures. **Annual Review of Materials Science**, v. 22, p. 197-215, 1992.

VROON, P. Z. et al. Problems in obtaining precise and accurate Sr isotope analysis from geological materials using laser ablation MC-ICPMS. **Analytical and Bioanalytical Chemistry**, v. 390, n. 2, p. 465–476, 2008.

WAICHEL, B. L.; LIMA, E.F.; VIANA, A.R.; SCHERER, C.M.; BUENO, G.V.; DUTRA, G. Stratigraphy and volcanic facies architecture of the Torres Syncline, Southern Brazil, and its role in understanding the Paraná-Etendeka Continental Flood Basalt Province. **Journal of Volcanology and Geothermal Research**, v. 215–216, p. 74–82, 2012.

WATERS, L. E. & LANGE, R. A. An updated calibration of the plagioclase-liquid hygrometer-thermometer applicable to basalts through rhyolites. **American Mineralogist**, v. 100, n. 10, p. 2172–2184, 2015.

WATSON, E. B. & HARRISON, T. M. Zircon saturation revisited: temperature and composition effects in a variety of crustal magma types. **Earth and Planetary Science Letters**, v. 64, n. 2, p. 295–304, 1983.

8 APPENDIX

8.1 CSD files

FP-15-15

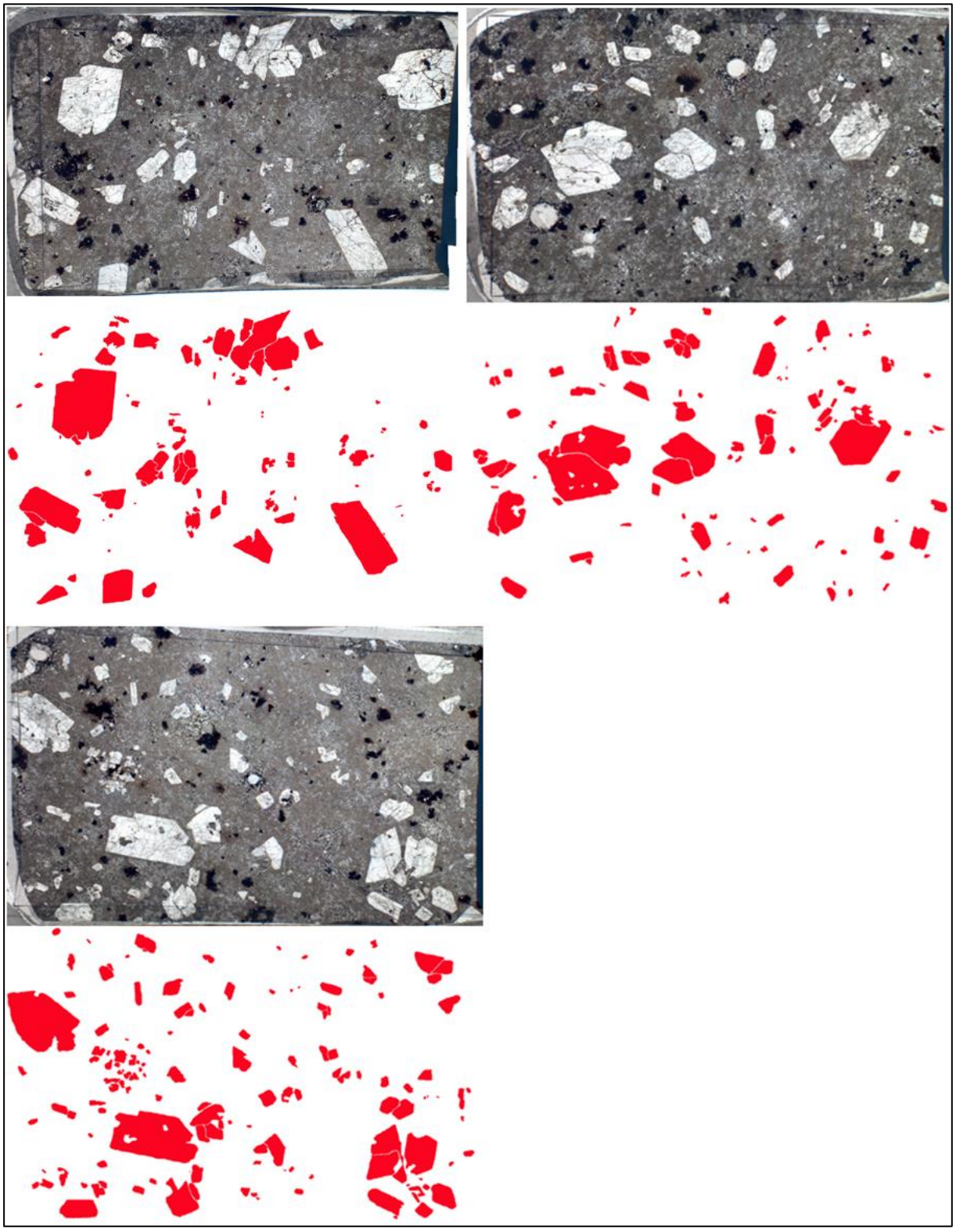

FP-15-15

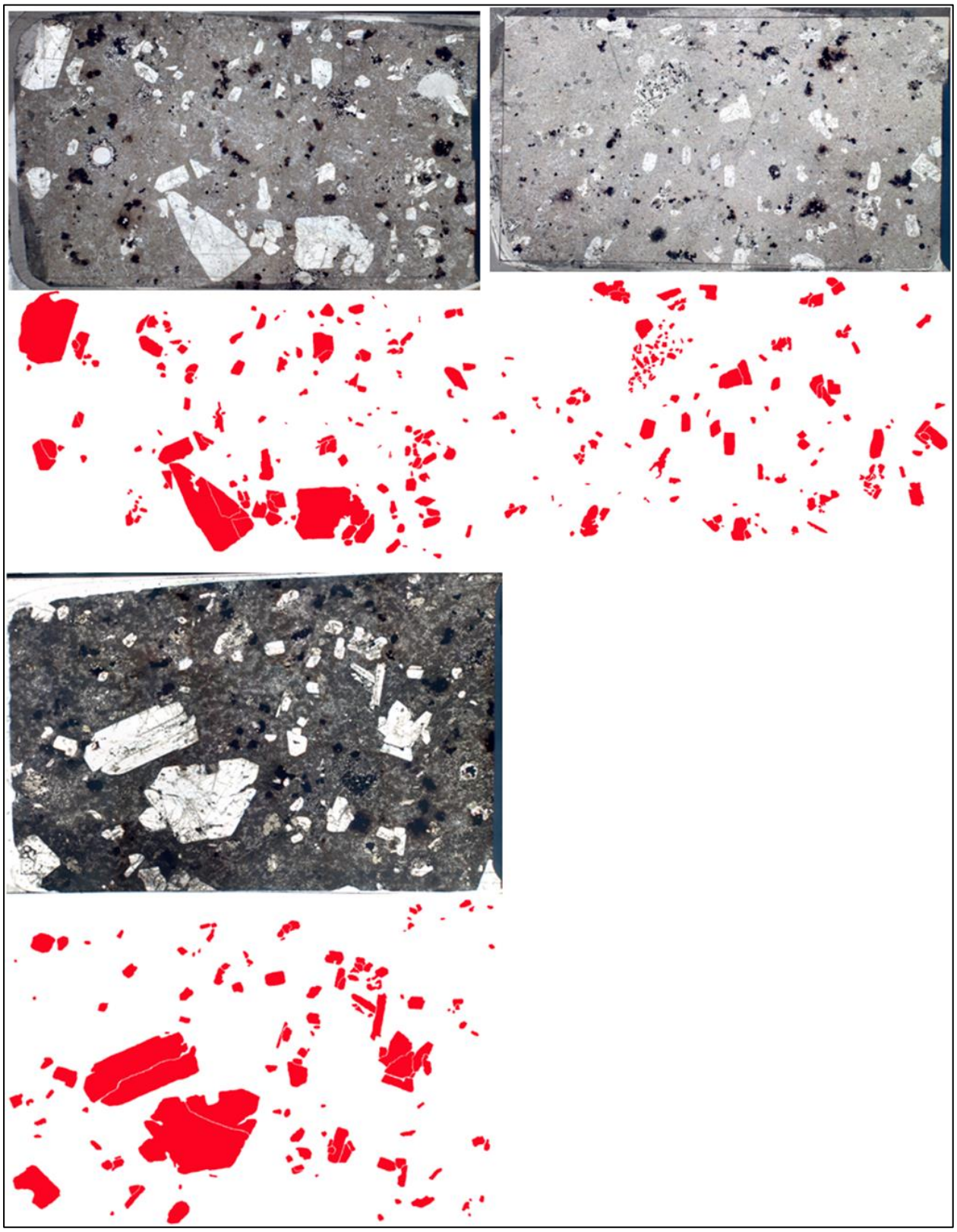

FP-15-17

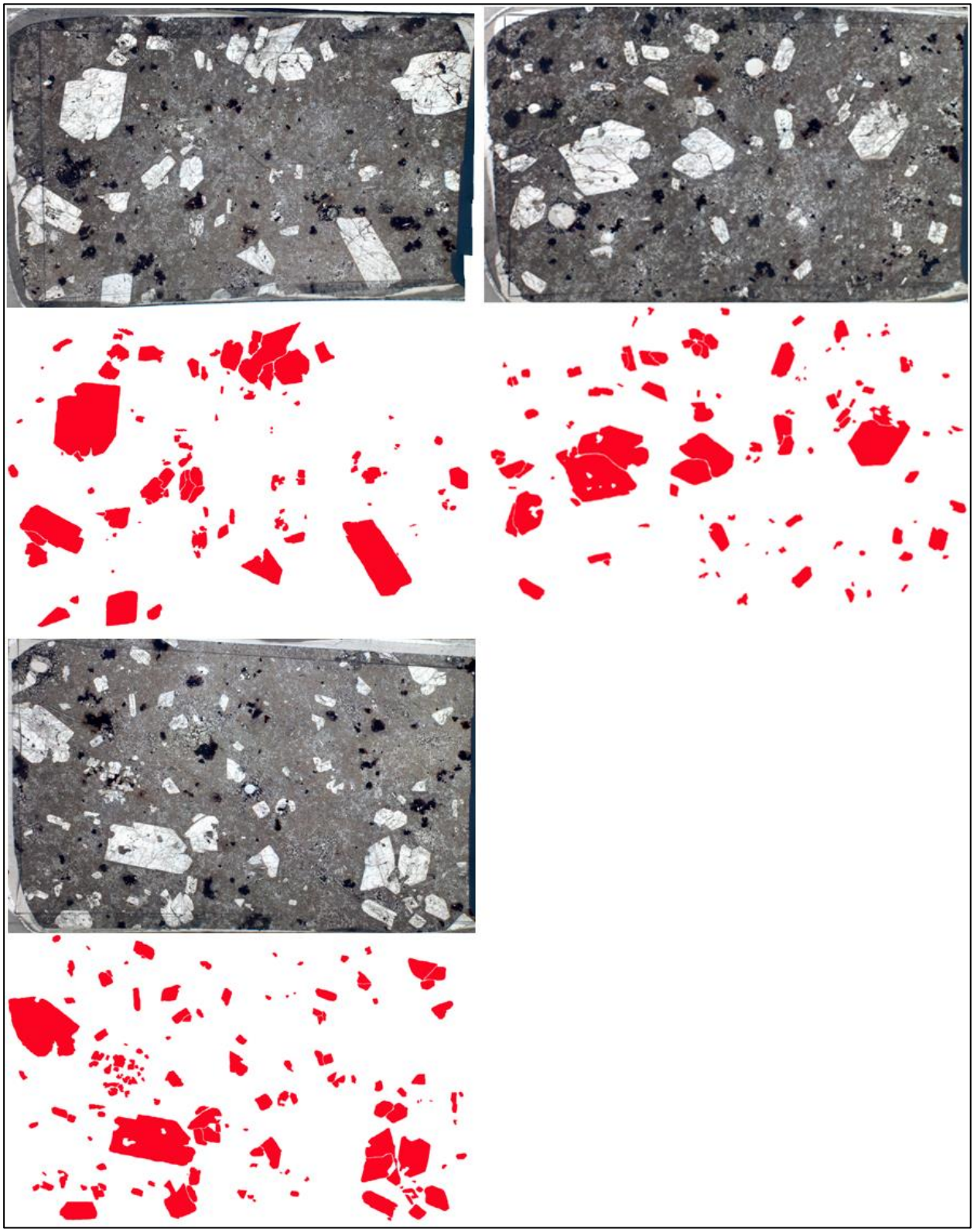

FP-15-17

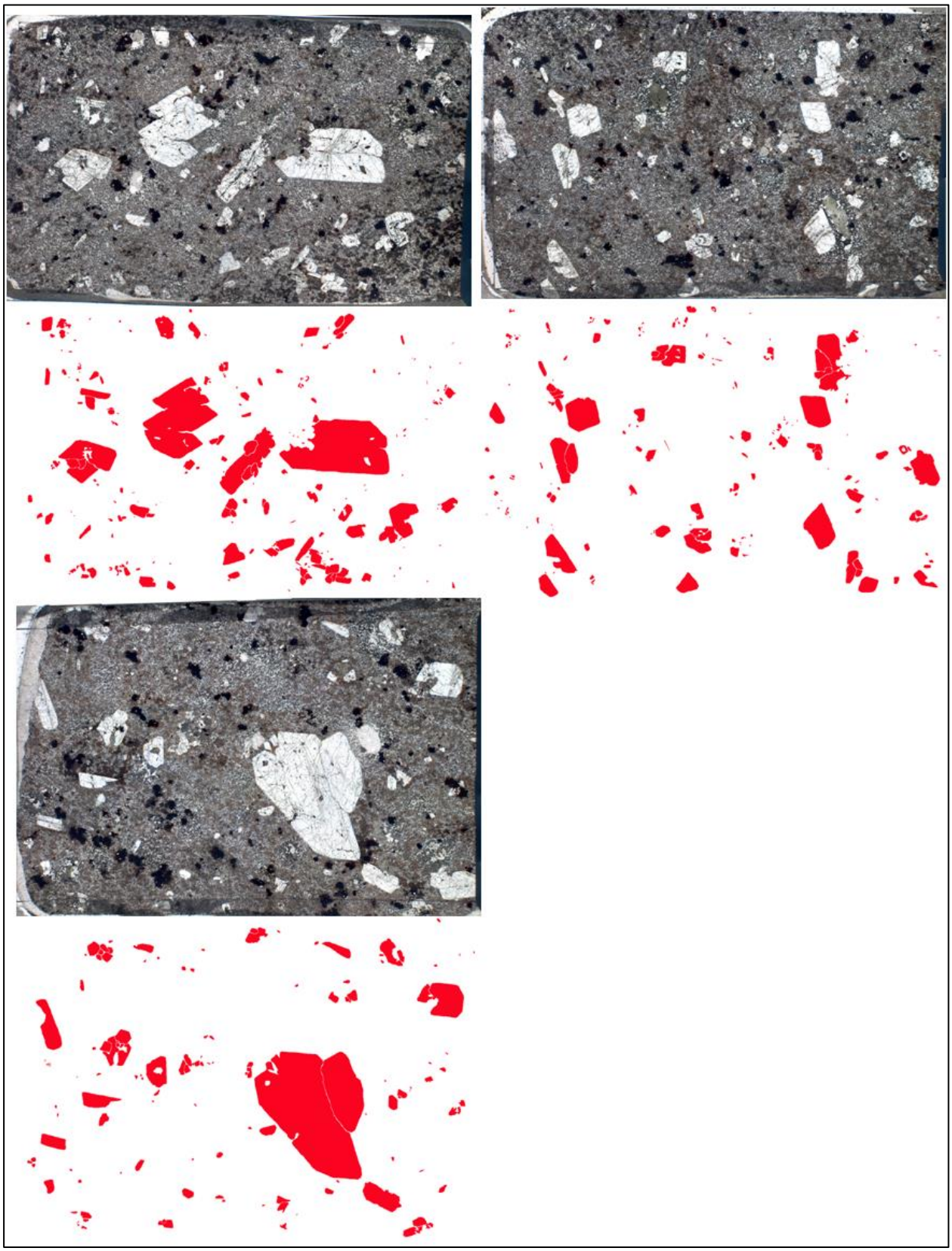

PA-16-01

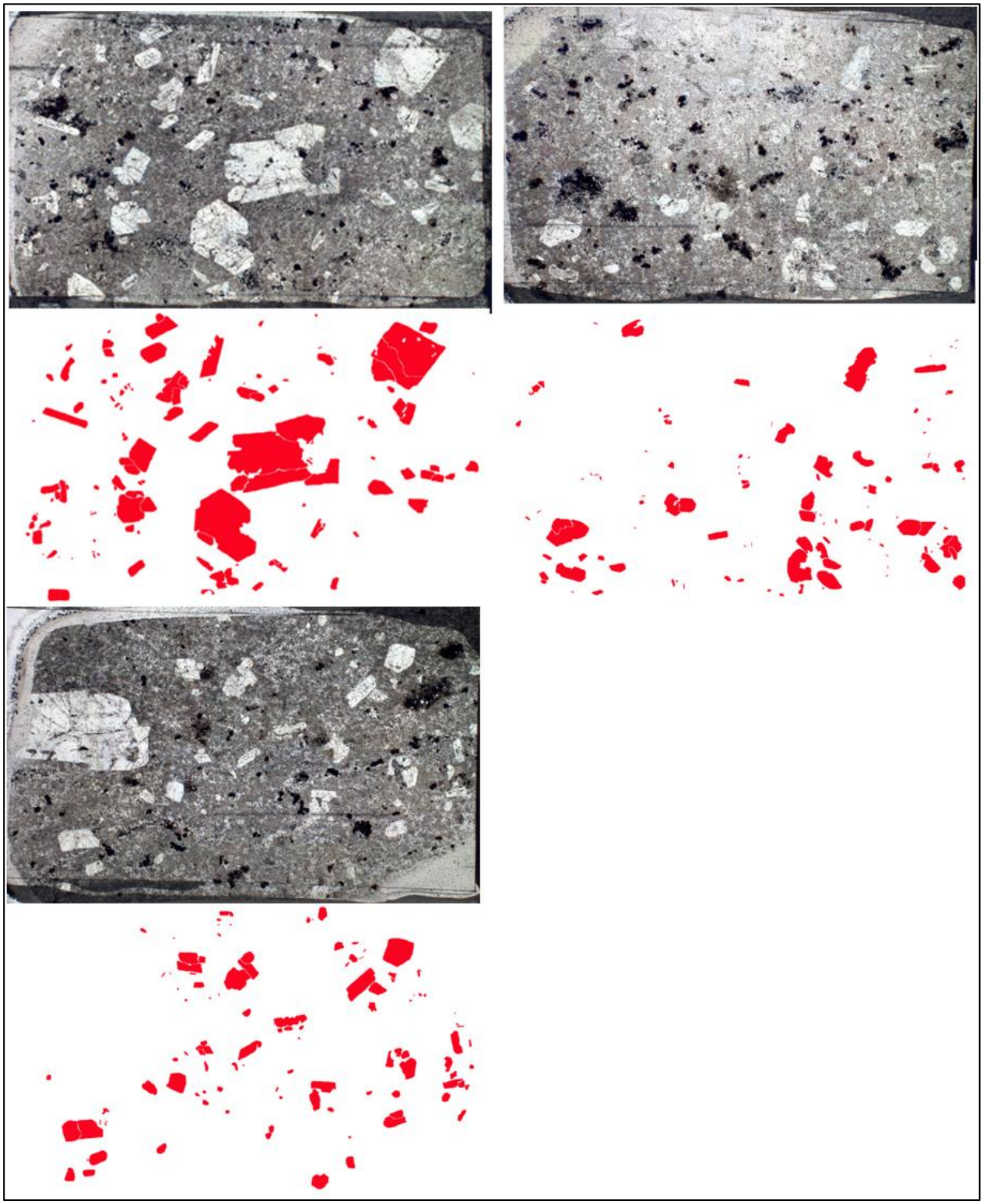

PA-16-01

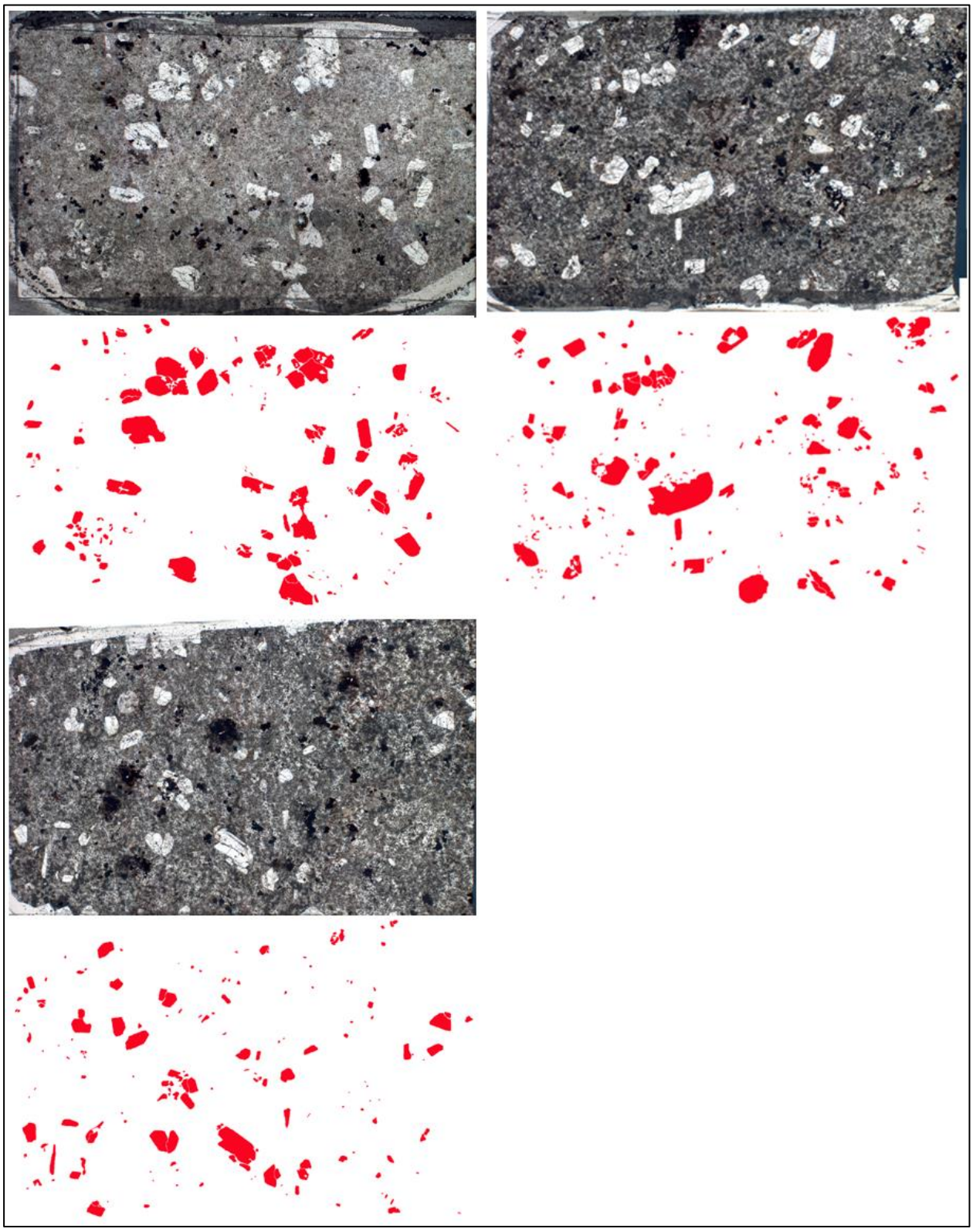

PA-16-04

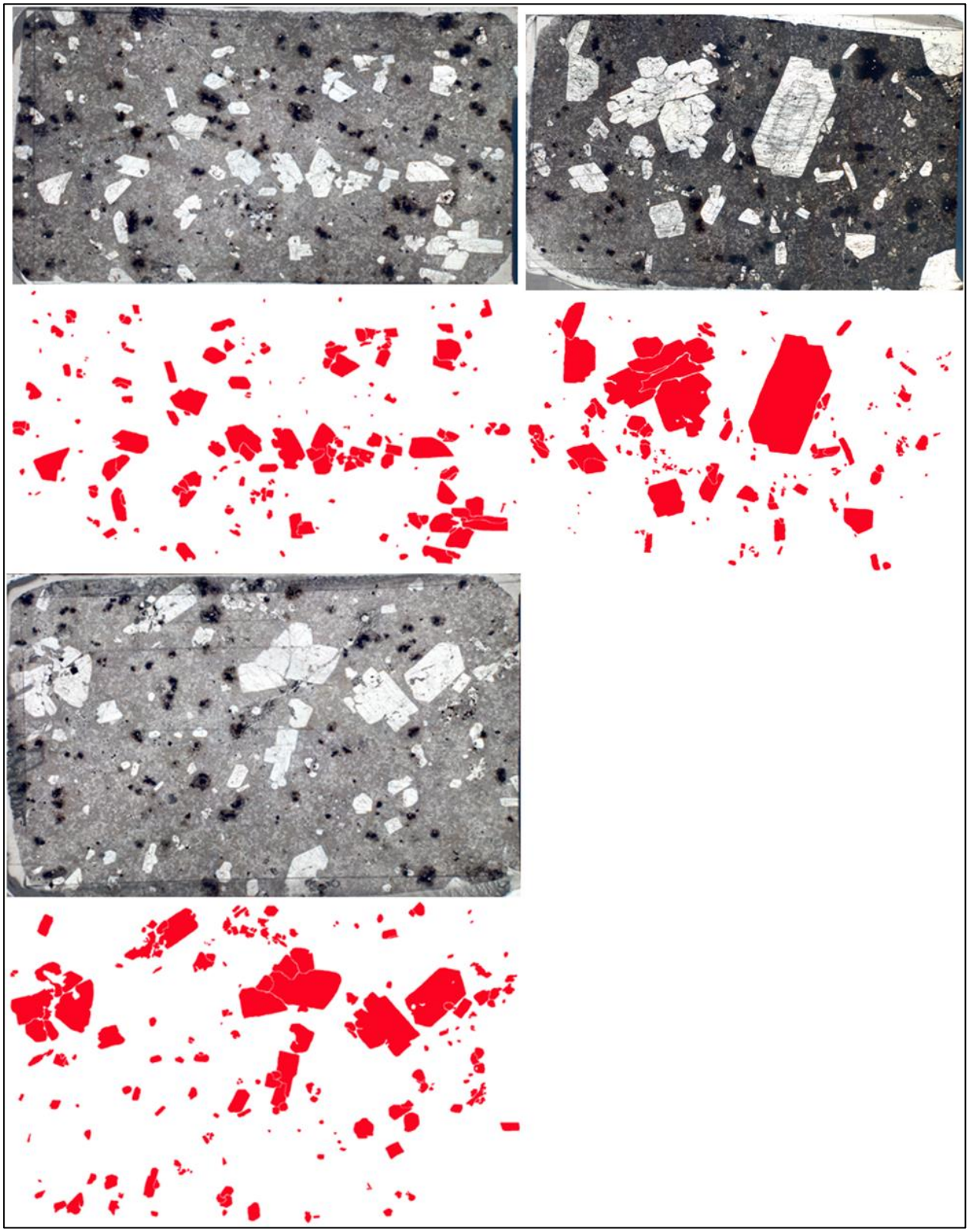

PA-16-04

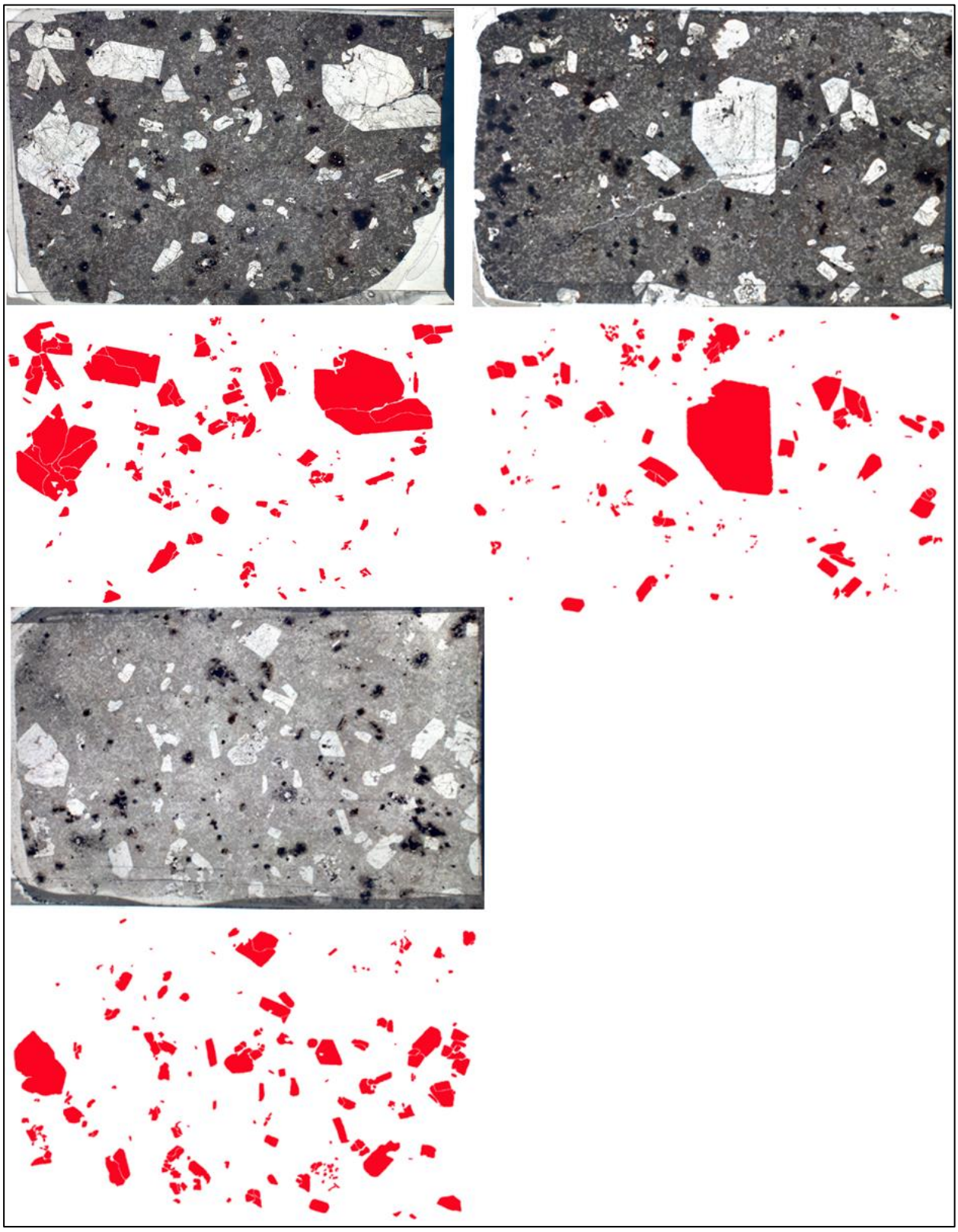

PA-16-06B

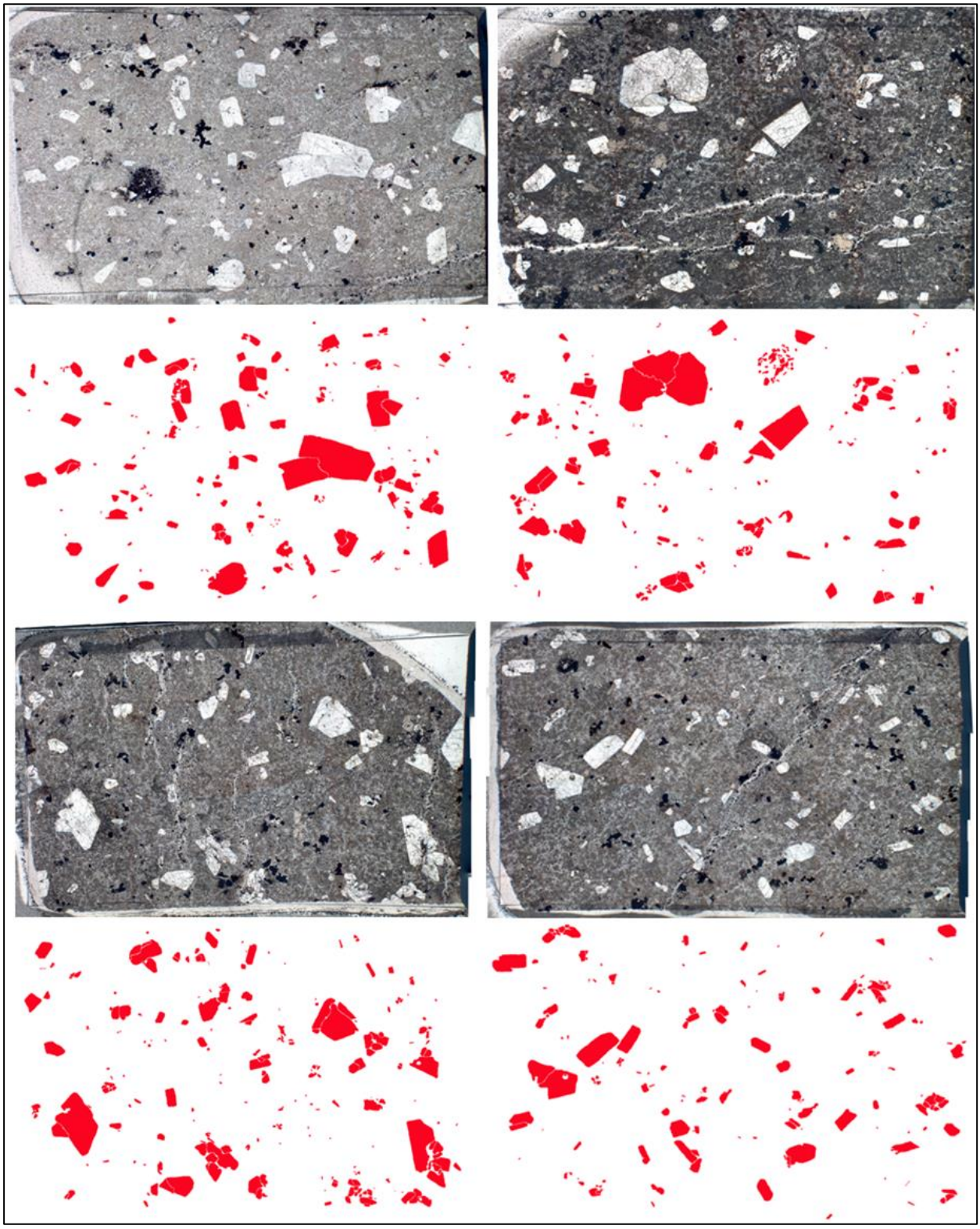

PA-16-06B

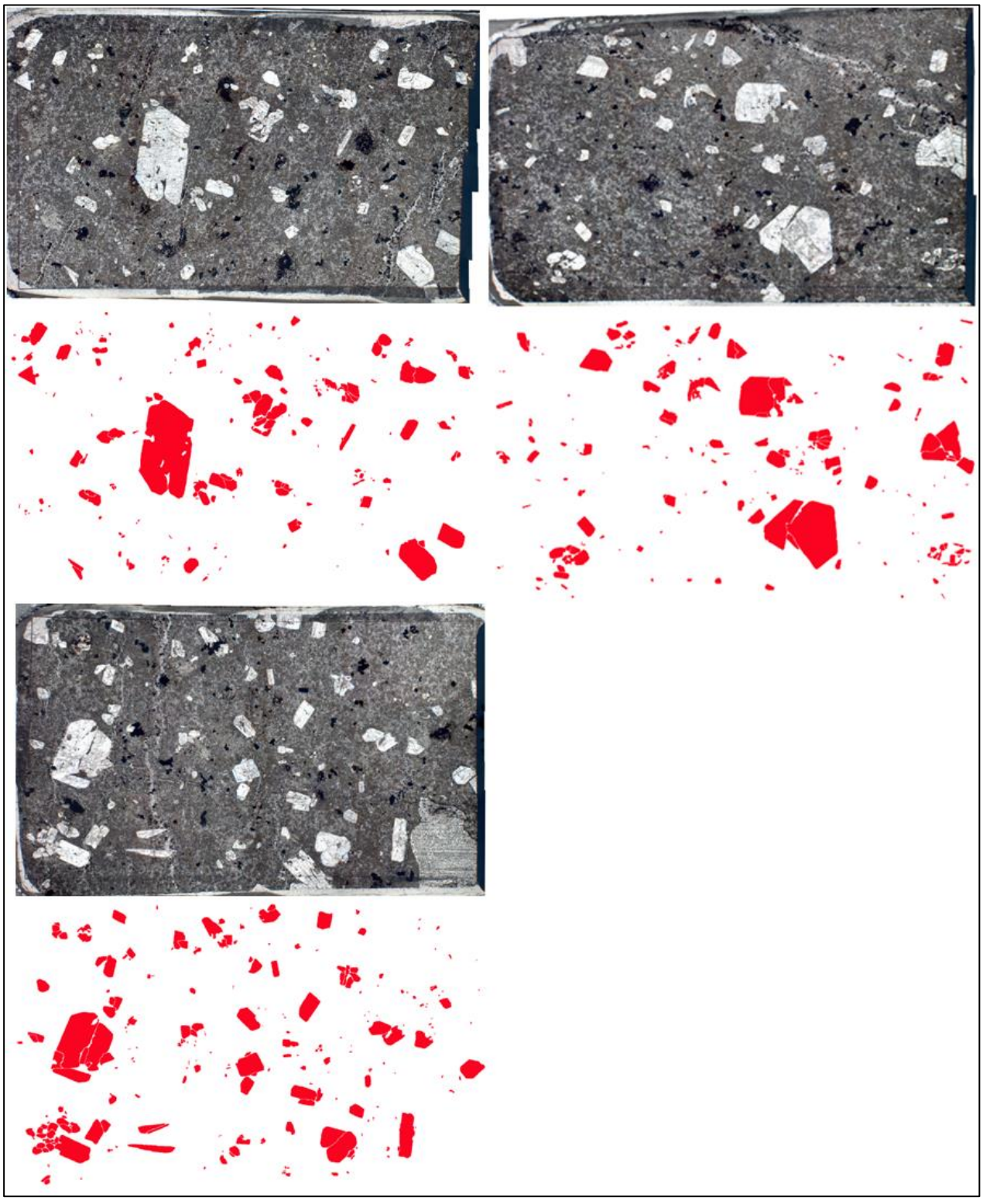

PA-16-07

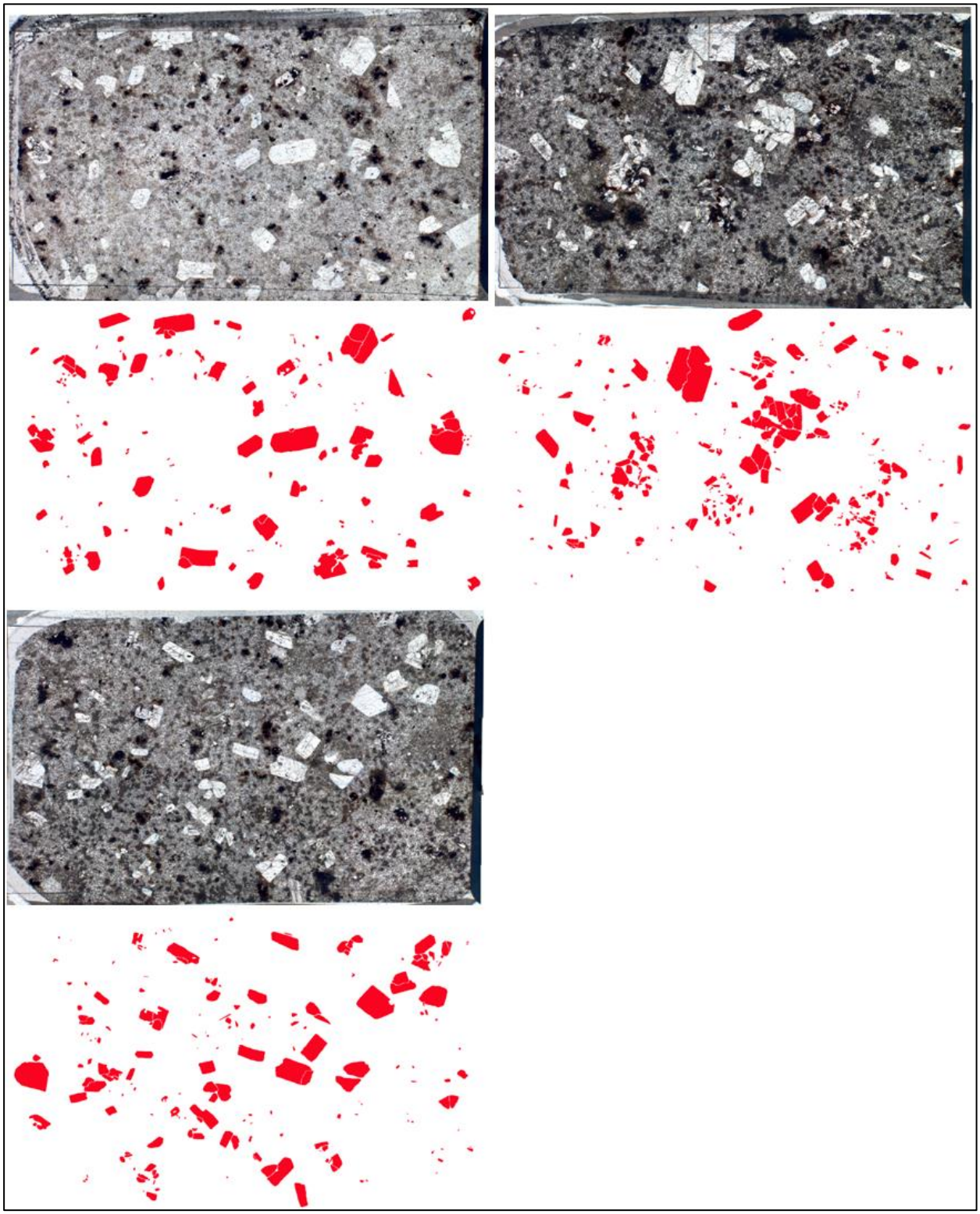

PA-16-07

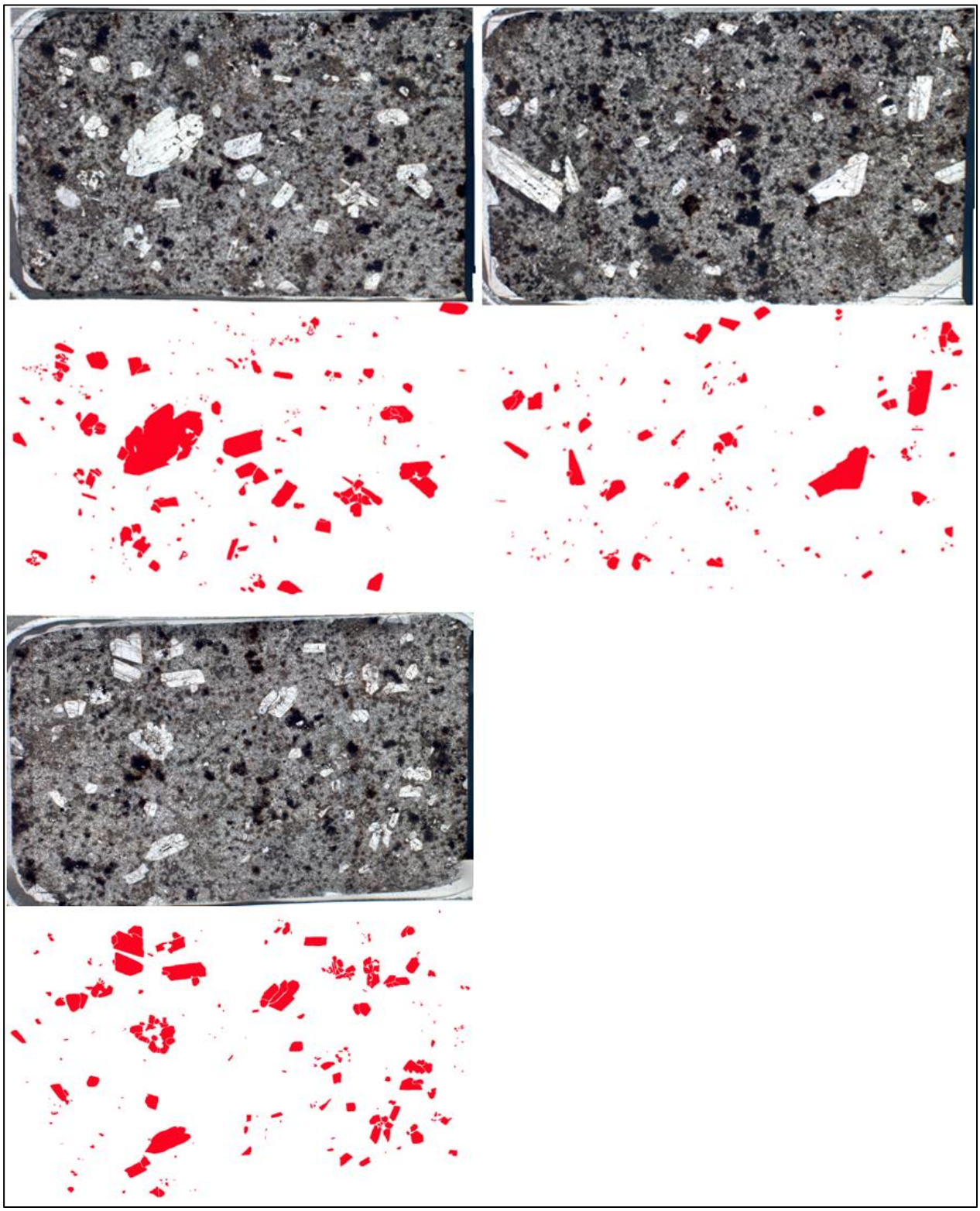

PA-16-19

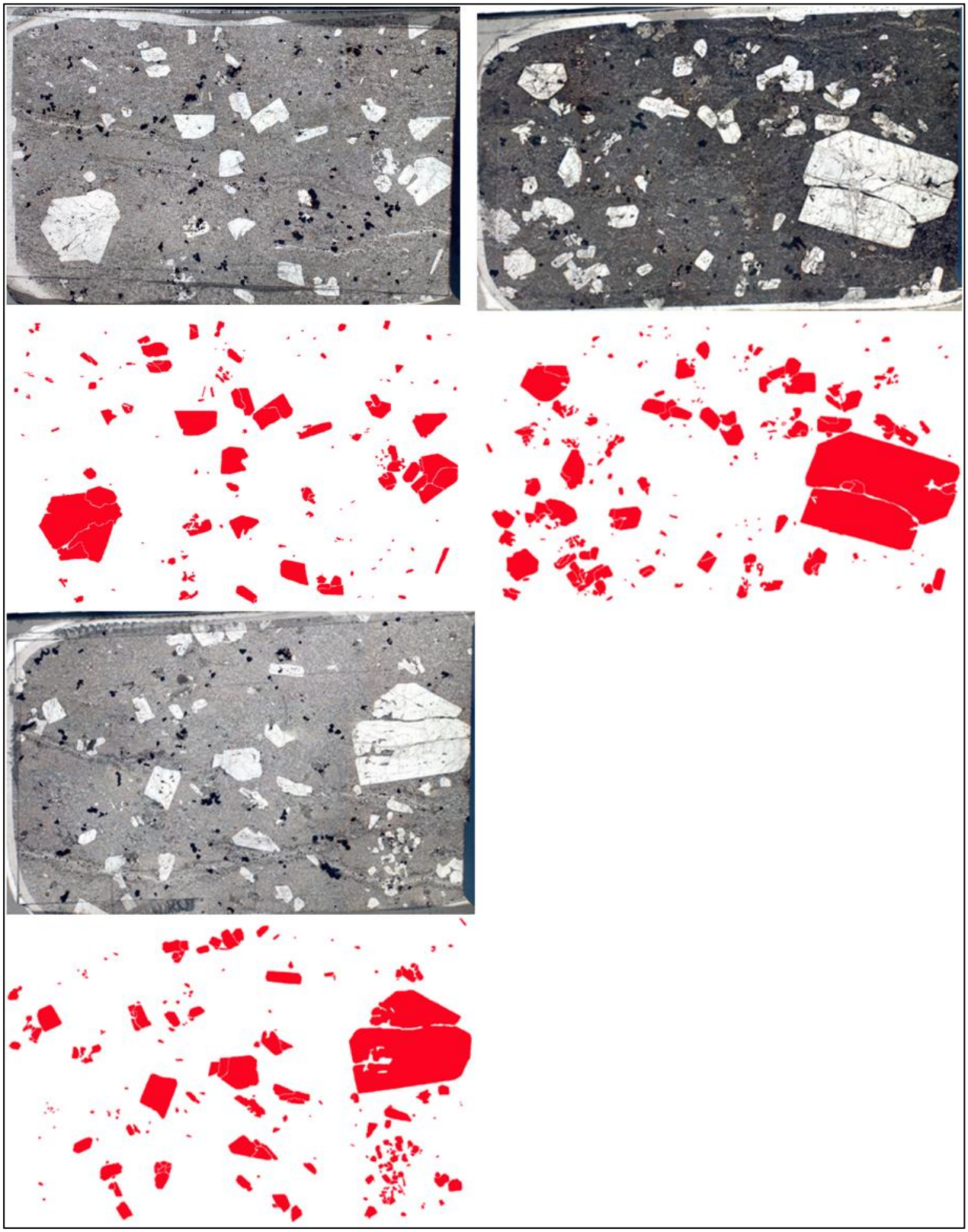

PA-16-19

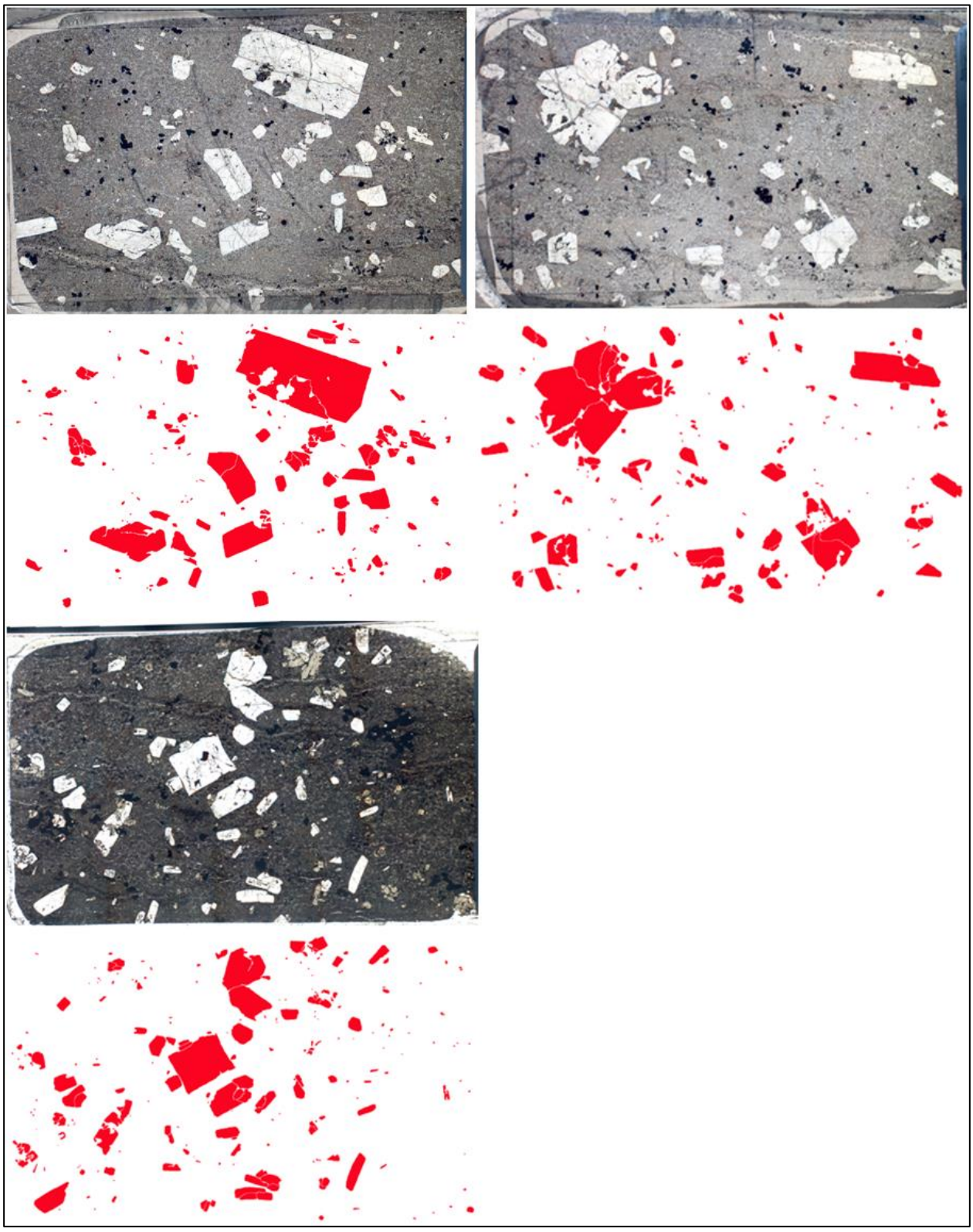

PA-16-21

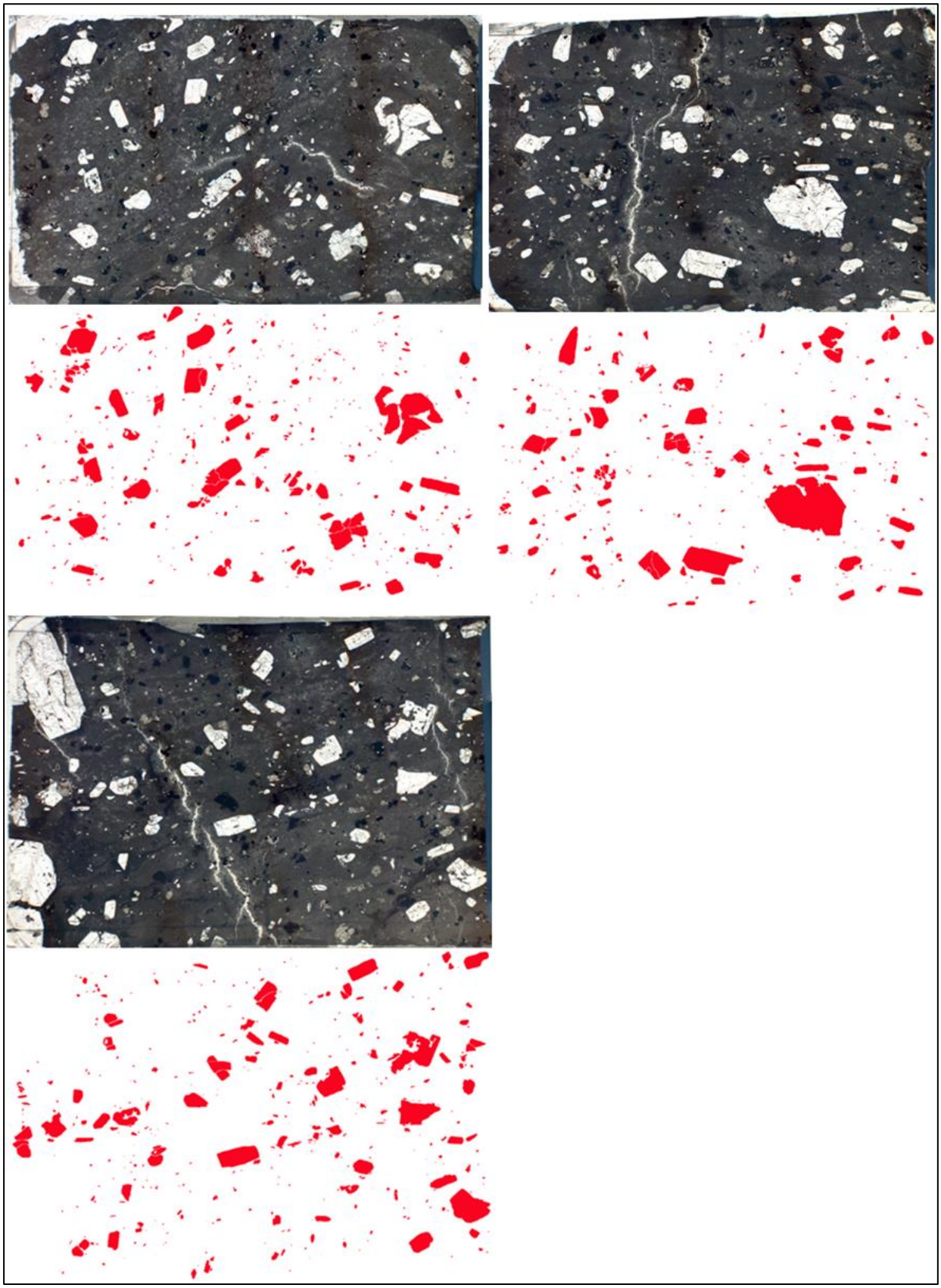

PA-16-21

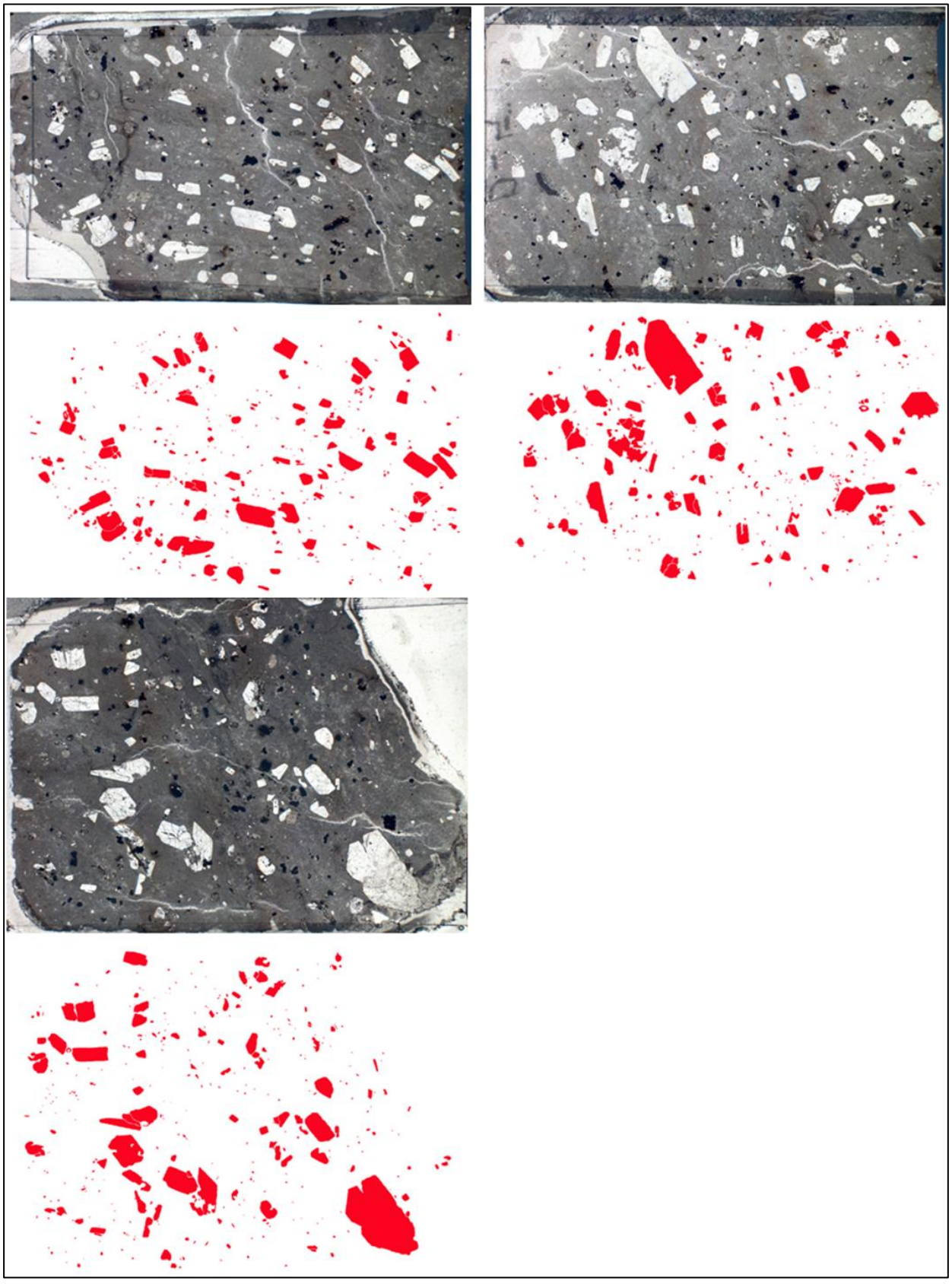

PA-16-23

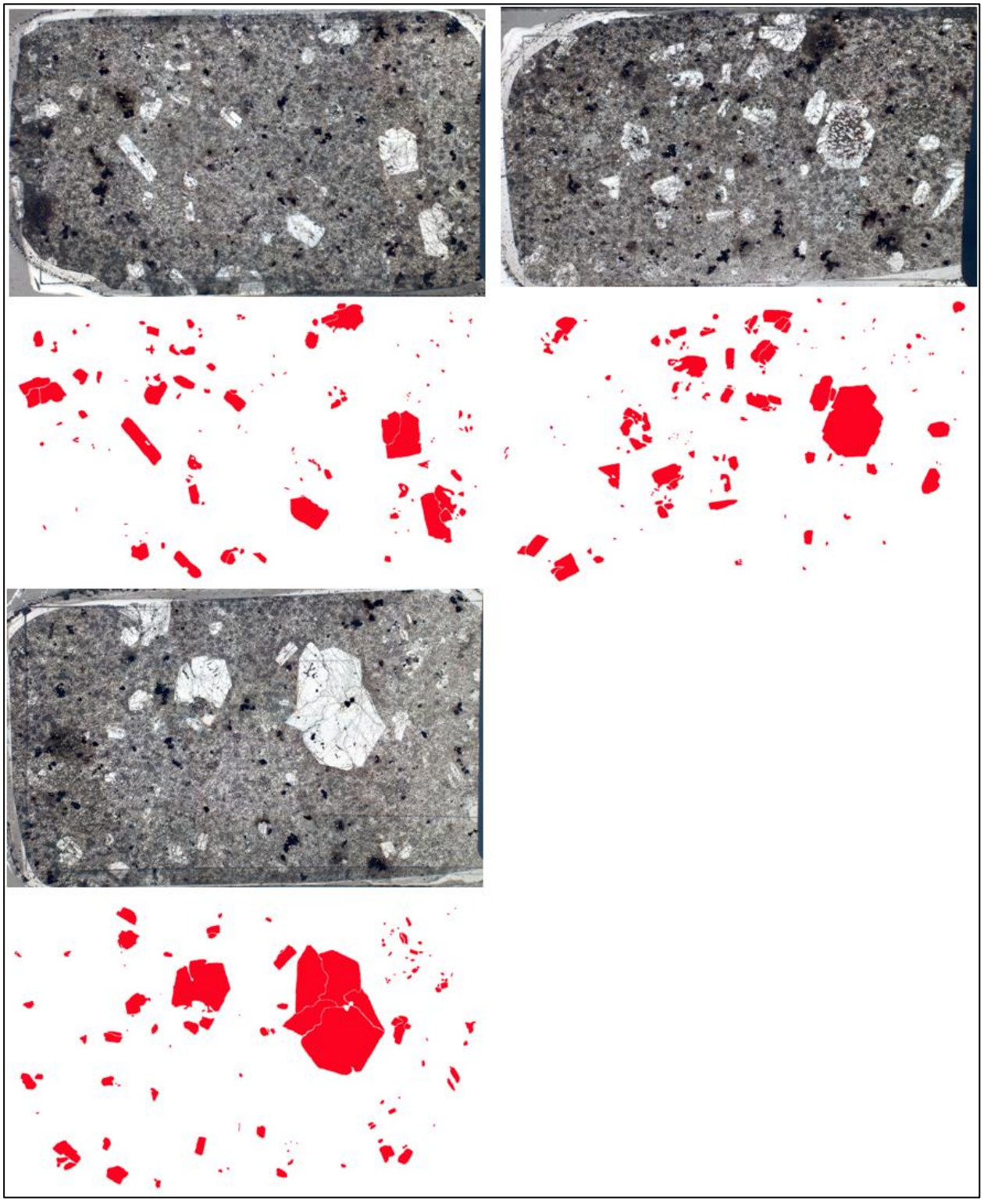

PA-16-23

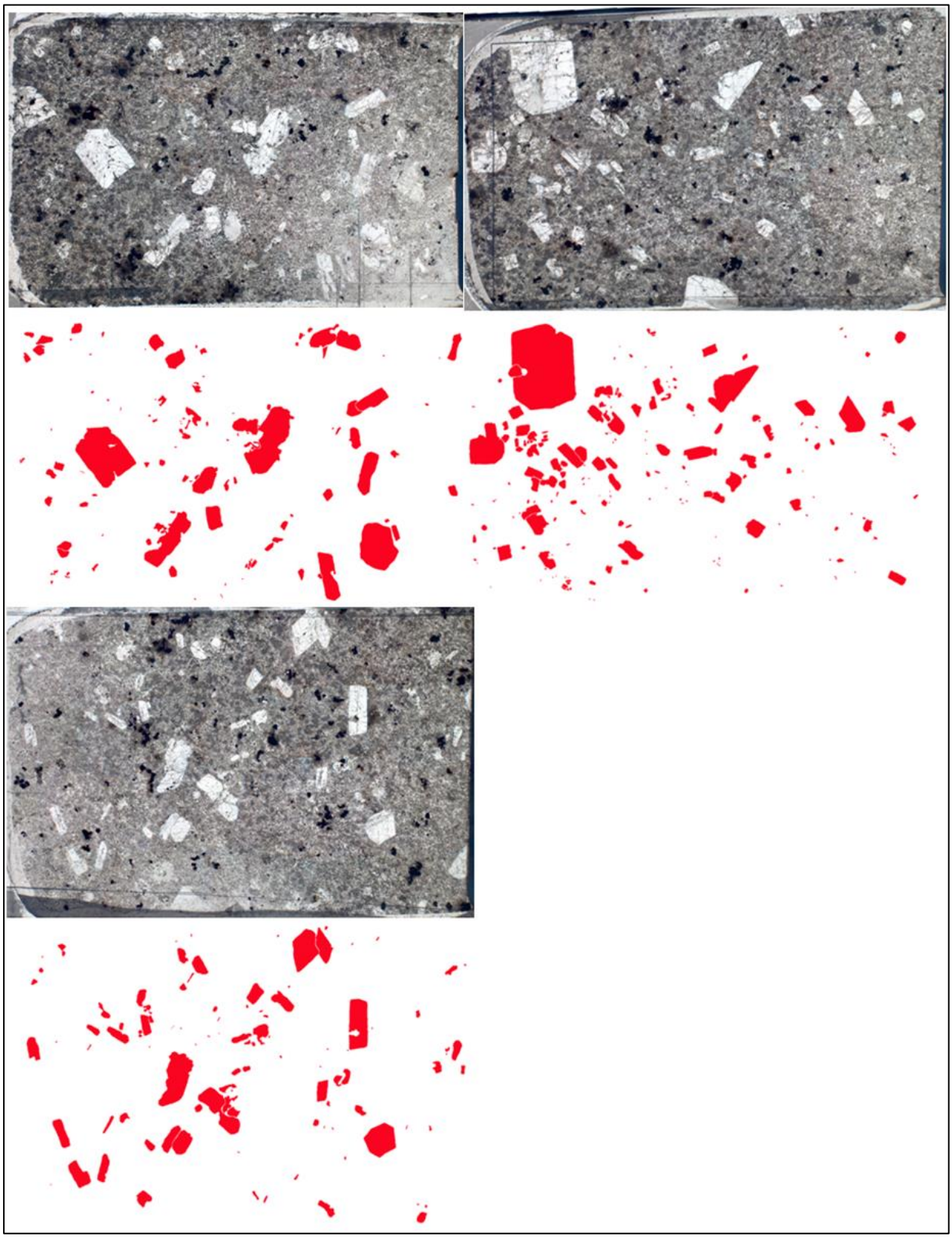

8.2 EDS analyzes

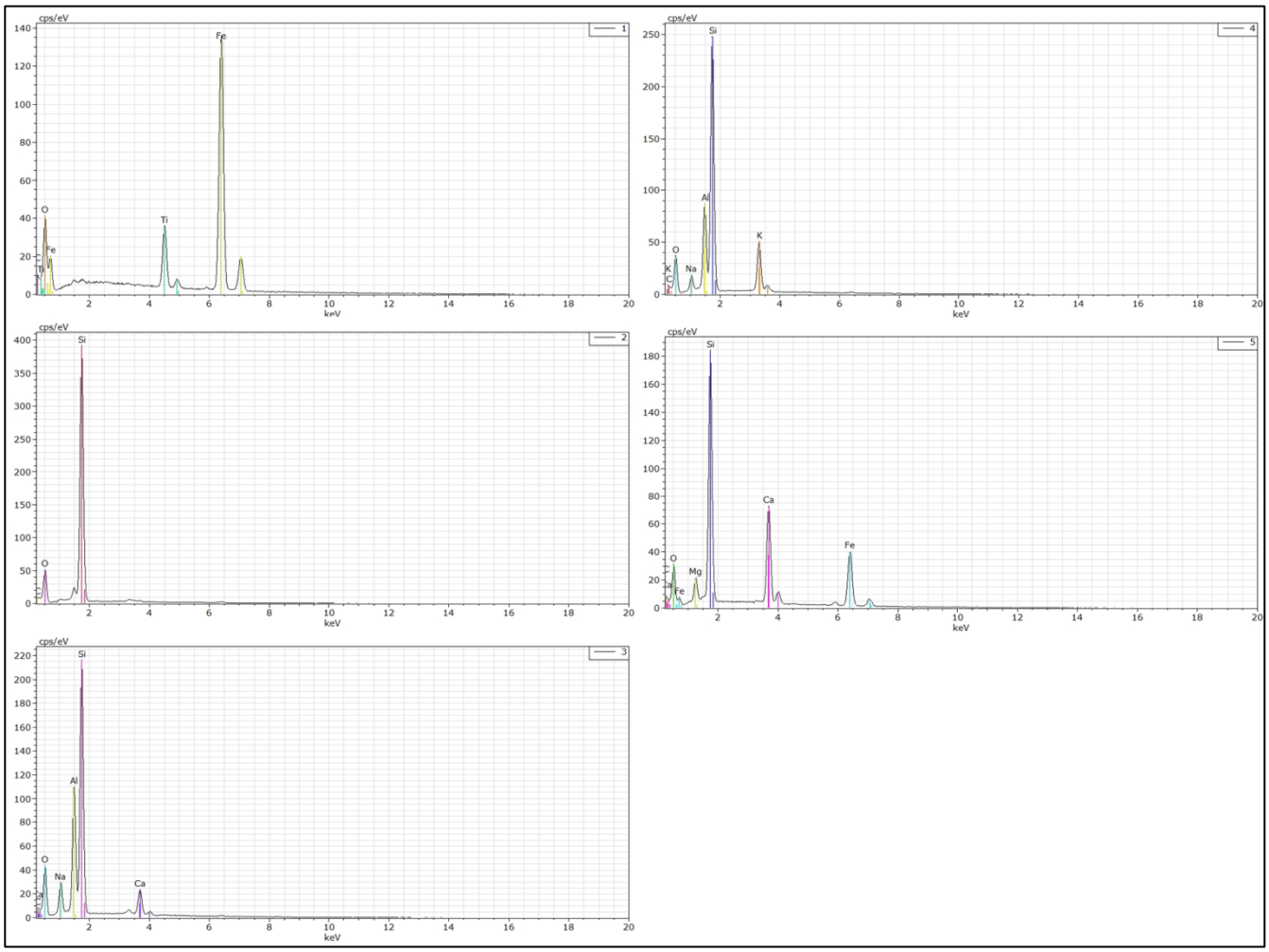

EDS analyses graphs on the respective spots indicated in Figure 10a.

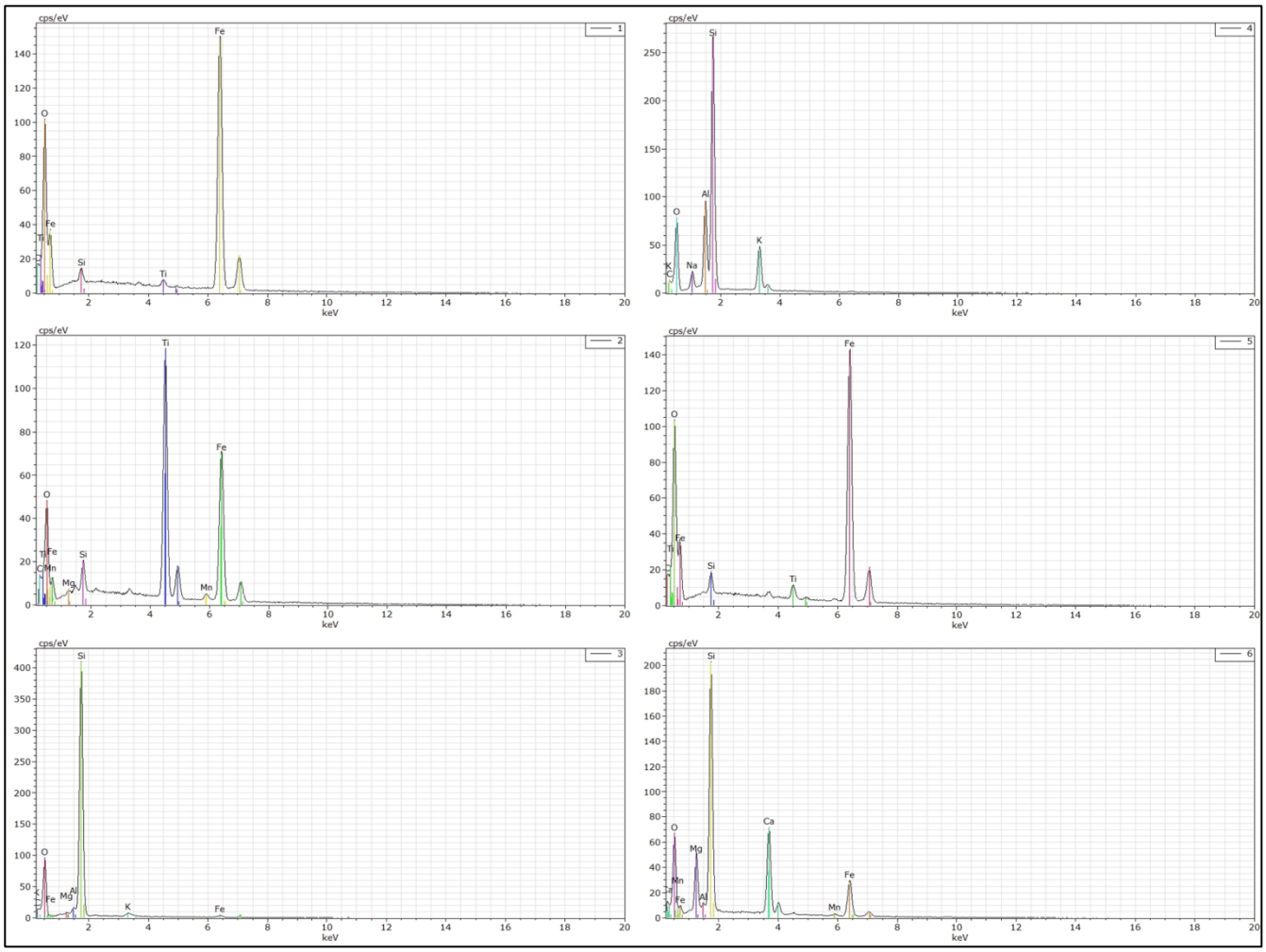

EDS analyses graphs on the respective spots indicated in Figure 11a.